PLOS | COMPUTATIONAL BIOLOGY

RESEARCH ARTICLE

A Quantitative Model of the GIRK1/2 Channel Reveals That Its Basal and Evoked Activities Are Controlled by Unequal Stoichiometry of Gα and Gβγ

Daniel Yakubovich[1☯], Shai Berlin[1☯¤a], Uri Kahanovitch[1☯], Moran Rubinstein[1], Isabella Farhy-Tselnicker[1¤b], Boaz Styr[1], Tal Keren-Raifman[1], Carmen W. Dessauer[2], Nathan Dascal[1]*

1 Department of Physiology and Pharmacology and Sagol School of Neuroscience, Tel Aviv University, Tel Aviv, Israel, **2** Department of Integrative Biology and Pharmacology, University of Texas Health Science Center, Houston, Texas, United States of America

☯ These authors contributed equally to this work.
¤a Current address: Department of Molecular and Cell Biology, University of California, Berkeley, Berkeley, California, United States of America
¤b Current address: Molecular Neurobiology Laboratory, Salk Institute for Biological Studies, La Jolla, California, United States of America
* dascaln@tauex.tau.ac.il

CrossMark
click for updates

OPEN ACCESS

Citation: Yakubovich D, Berlin S, Kahanovitch U, Rubinstein M, Farhy-Tselnicker I, Styr B, et al. (2015) A Quantitative Model of the GIRK1/2 Channel Reveals That Its Basal and Evoked Activities Are Controlled by Unequal Stoichiometry of Gα and Gβγ. PLoS Comput Biol 11(11): e1004598. doi:10.1371/journal.pcbi.1004598

Editor: Dirk Gillespie, Rush University Medical Center, UNITED STATES

Received: May 27, 2015

Accepted: October 13, 2015

Published: November 6, 2015

Copyright: © 2015 Yakubovich et al. This is an open access article distributed under the terms of the Creative Commons Attribution License, which permits unrestricted use, distribution, and reproduction in any medium, provided the original author and source are credited.

Data Availability Statement: All relevant data are within the paper and its Supporting Information files.

Funding: This work was supported by the US-Israel Binational Science Foundation (http://www.bsf.org.il/), grants no. 2009255 and 2013230; and by Israeli Science Foundation, http://www.isf.org.il/, grants no. 49/08 and 436/14. The funders had no role in study design, data collection and analysis, decision to publish, or preparation of the manuscript.

Abstract

G protein-gated K^+ channels (GIRK; Kir3), activated by Gβγ subunits derived from $G_{i/o}$ proteins, regulate heartbeat and neuronal excitability and plasticity. Both neurotransmitter-evoked (I_{evoked}) and neurotransmitter-independent basal (I_{basal}) GIRK activities are physiologically important, but mechanisms of I_{basal} and its relation to I_{evoked} are unclear. We have previously shown for heterologously expressed neuronal GIRK1/2, and now show for native GIRK in hippocampal neurons, that I_{basal} and I_{evoked} are interrelated: the extent of activation by neurotransmitter (activation index, R_a) is inversely related to I_{basal}. To unveil the underlying mechanisms, we have developed a quantitative model of GIRK1/2 function. We characterized single-channel and macroscopic GIRK1/2 currents, and surface densities of GIRK1/2 and Gβγ expressed in *Xenopus* oocytes. Based on experimental results, we constructed a mathematical model of GIRK1/2 activity under steady-state conditions before and after activation by neurotransmitter. Our model accurately recapitulates I_{basal} and I_{evoked} in *Xenopus* oocytes, HEK293 cells and hippocampal neurons; correctly predicts the dose-dependent activation of GIRK1/2 by coexpressed Gβγ and fully accounts for the inverse I_{basal}-R_a correlation. Modeling indicates that, under all conditions and at different channel expression levels, between 3 and 4 Gβγ dimers are available for each GIRK1/2 channel. In contrast, available $G\alpha_{i/o}$ decreases from ~2 to less than one Gα per channel as GIRK1/2's density increases. The persistent Gβγ/channel (but not Gα/channel) ratio support a strong association of GIRK1/2 with Gβγ, consistent with recruitment to the cell surface of Gβγ, but not Gα, by GIRK1/2. Our analysis suggests a maximal stoichiometry of 4 Gβγ but only 2 $G\alpha_{i/o}$ per one GIRK1/2 channel. The unique, unequal association of GIRK1/2 with G protein subunits,

Competing Interests: The authors have declared that no competing interests exist.

and the cooperative nature of GIRK gating by Gβγ, underlie the complex pattern of basal and agonist-evoked activities and allow GIRK1/2 to act as a sensitive bidirectional detector of both Gβγ and Gα.

Author Summary

Many neurotransmitters and hormones inhibit the electric activity of excitable cells (such as cardiac cells and neurons) by activating a K^+ channel, GIRK (**G** protein-gated **I**nwardly **R**ectifying $\mathbf{K}^+$ channel). GIRK channels also possess constitutive "basal" activity which contributes to regulation of neuronal and cardiac excitability and certain disorders, but the mechanism of this activity and its interrelation with the neurotransmitter-evoked activity are poorly understood. In this work we show that key features of basal and neurotransmitter-evoked activities are similar in cultured hippocampal neurons and in two model systems (mammalian HEK293 cells and *Xenopus* oocytes). Using experimental data of the neuronal GIRK1/2 channel function upon changes in GIRK and G protein concentrations, we constructed a mathematical model that quantitatively accounts for basal and evoked activity, and for the inverse correlation between the two. Our analysis suggests a novel and unexpected mechanism of interaction of GIRK1/2 with the G protein subunits, where the tetrameric GIRK channel can assemble with 4 molecules of the Gβγ subunits but only 2 molecules of Gα. GIRK is a prototypical effector of Gβγ, and the unequal stoichiometry of interaction with G protein subunits may have general implications for G protein signaling.

Introduction

G proteins and the linked G protein-coupled receptors (GPCRs) are prominent regulators of excitability, which activate or inhibit ion channels by a variety of mechanisms [1]. This paper focuses on the quantitative analysis of the classical GPCR-initiated signaling cascade that culminates in the activation of GIRK channels (G protein-gated K^+ channel; Kir3). GIRKs are important transducers of inhibitory neurotransmitter effects in heart and brain. They regulate heartbeat, neuronal excitability and plasticity, analgesia, alcohol and drug effects, and are implicated in a number of disorders such as epilepsy, Down syndrome, bipolar disorder, atrial fibrillation and primary aldosteronism [2,3,4,5,6]. GIRK is also the first-discovered effector of Gβγ [7] and a prototypical model of membrane-delimited G protein signaling. In the now classical scheme, the agonist-bound GPCR catalyzes GDP/GTP exchange at Gα and the separation of $G\alpha_{i/o}{}^{GTP}$ from Gβγ; Gβγ directly binds to GIRK and triggers channel opening [8,9,10,11].

Mammalian GIRKs are usually heterotetramers of GIRK1 with one of the other subunits (GIRK2, GIRK3 and GIRK4). GIRK1/2 is predominant in mammalian brain, but heterotetrameric GIRK1/3, GIRK2/3 and homotetrameric GIRK2 are also abundant in certain brain regions [2]. A GIRK channel is activated by direct binding of up to 4 molecules of Gβγ, but partial activation is achieved by binding of 1–3 Gβγ molecules [12,13,14,15,16]. NMR studies [17], crystal structure [18] and docking models [19] of GIRK-Gβγ complexes have confirmed the 4:1 Gβγ:GIRK stoichiometry, showing binding of one Gβγ to each interface between adjacent GIRK subunits. Further, a strong association of GIRKs with Gβγ has been suggested by co-immunoprecipitation and Förster/Bioluminescence Resonance Energy Transfer (FRET/BRET, respectively) [20,21,22,23,24]. In support, in *Xenopus* oocytes, GIRK1-containing channels

recruit Gβγ to the plasma membrane (PM) [25]. GIRK also binds $G\alpha_{i/o}$ subunits which regulate the channel's basal activity, specificity and kinetics of signaling [26,27,28,29,30,31,32,33,34], but the mechanisms are poorly understood. No FRET between GIRK subunits and $G\alpha_{i/o}$ could be detected in the PM [24,35,36]; GIRK1 does not recruit $G\alpha_i$ to the PM [25] and binds $G\alpha_{i/o}$ *in vitro* less strongly than Gβγ [36]. The stoichiometry of Gα-GIRK interaction is unknown.

Traditionally, GIRKs have been regarded as inhibitory devices operated exclusively by inhibitory neurotransmitters which elicit the GIRK's evoked response (I_{evoked}). However, recent studies revealed that neuronal GIRKs also have a substantial basal activity, I_{basal} [37,38,39]. GIRK's basal activity and the balance between I_{basal} and I_{evoked} are important determinants of neuronal excitability [39,40], bistability of neuronal networks [41], neuronal plasticity [42,43,44], dendritic integration [45], atrial arrhythmia and remodeling [46], and have recently been proposed to be related to effects of Li^+, a drug used in the treatment of bipolar disorder [47]. Thus, changes in I_{basal} and its relation to I_{evoked} are physiologically relevant and need to be understood.

The molecular mechanisms of I_{basal} and I_{evoked} have been extensively studied in heterologous model systems, mainly *Xenopus* oocytes and human embryonic kidney (HEK) cells (e.g. [48,49]). We discovered that, for the neuronal GIRK1/2, I_{basal} and I_{evoked} are coupled. Incremental expression of GIRK1/2 in *Xenopus* oocytes revealed an inverse correlation between I_{basal} and the extent of activation by transmitter. The higher I_{basal}, the smaller the index of activation by the transmitter (R_a) and by coexpressed Gβγ ($R_{\beta\gamma}$) [30]. The I_{basal}-I_{evoked} coupling was regulated by $G\alpha_i$: coexpression of $G\alpha_{i3}$ reduced I_{basal}, increased agonist- and Gβγ-induced GIRK currents (a phenomenon we dubbed "priming" by $G\alpha_{i/o}$"), and eliminated the inverse correlation between I_{basal} and R_a [30,31,50,51]. These findings compelled an unusual explanation of the underlying mechanism. We proposed that Gβγ available for GIRK regulation is in excess over $G\alpha_{i/o}$, thus the high I_{basal} of GIRK1/2. We suggested that the magnitude of I_{basal} and its relation to I_{evoked} are crucially regulated by the availability of $G\alpha_{i/o}$ [30,31,50]. Here we demonstrate that cultured hippocampal neurons show the same inverse relation between I_{basal} and R_a as previously found in oocytes and HEK cells. This prompted us to further use these heterologous systems to address the coupling between GIRK's basal and evoked activity.

In the present work we have developed a quantitative model for I_{basal} and I_{evoked} of GIRK1/2, which uses experimentally determined micro- and macroscopic parameters of GIRK1/2 currents and surface densities and accurately simulates and predicts macroscopic GIRK1/2 currents under a variety of conditions. Furthermore, modeling allowed to assess the apparent molar ratios of Gα and Gβγ available for GIRK, which we term “functional stoichiometry”. Our analysis reveals that, in *Xenopus* oocytes, HEK cells, and hippocampal neurons, 3 to 4 Gβγ molecules are available for the activation of GIRK1/2 channel over a wide range of surface densities of the channel, even when no exogenous Gβγ is coexpressed with GIRK. Calculations in *Xenopus* oocytes suggest a substantial increase in total concentration of Gβγ in the PM when large amounts of GIRK1/2 are expressed, corroborating the proposed mechanism of recruitment of Gβγ by GIRK1 to the PM [25]. In contrast, modeling shows that at most two Gα molecules are available for channel’s activation, even after overexpression of $G\alpha_{i3}$. Furthermore, the Gα/GIRK ratio decreases with increasing channel density. The unequal and variable stoichiometry of GIRK1/2-associated Gα and Gβγ qualitatively and quantitatively explains the inverse R_a-I_{basal} relation. Our results indicate a significant extent of association between GIRK1/2 and Gβγ, and support the notion that Gα is a non-obligatory partner in the GIRK-G protein signaling complex [50], but $G\alpha^{GDP}$ plays a crucial role in regulating basal activity and, consequently, the magnitude of agonist response.

Results

Extent of agonist activation is inversely related to I_{basal} in hippocampal neurons

First, we wanted to characterize the relation between GIRK's I_{basal} and I_{evoked} in hippocampal neurons, known to preferentially express GIRK1/2 [2]. I_{basal} and I_{evoked} were measured using standard experimental paradigms ([39,47]; Fig 1A). Baclofen was used to activate the endogenous $GABA_B$ receptor and to generate I_{evoked} [52]. Net GIRK's I_{basal} was revealed as shown in Fig 1A (see also S1 Fig), by adding 100–120 nM tertiapin-Q (TPNQ), which selectively blocks >90% of GIRK currents in hippocampal neurons [39,43,53].

To characterize the relation between I_{basal} and I_{evoked}, we utilized the activation index R_a, defined as I_{total}/I_{basal} (where I_{total} is the total GIRK current; see Fig 1 and S1 Fig) [51]. GIRK currents of cultured hippocampal neurons showed considerable variability: I_{basal}, 0.2–26 pA/pF, I_{evoked}, 1–65 pA/pF (n = 65). Strikingly, there was a strong inverse correlation between R_a and I_{basal} (Fig 1B, closed triangles), which was similar to that observed in oocytes expressing GIRK1/2 (open circles). The strength of the correlation indicates that it may be driven by a distinct molecular mechanism of potential physiological importance. The similarity of this distinctive phenomenon in hippocampal neurons and GIRK1/2-expressing oocytes encouraged us to further investigate it in the *Xenopus* oocyte expression system. The oocyte is particularly suitable for accurate control of protein expression (by titrating the injected RNA) and for current measurements, which are essential for quantitative modeling of I_{basal} and I_{evoked} of GIRK1/2.

Modeling the steady-state gating of GIRK1/2 by Gβγ

Gβγ is well-established as the main gating agent for GIRK's I_{evoked} [8,9]. This is also true for I_{basal} of heterologously expressed GIRK1/2, which is suppressed by up to 80–90% by the expression of Gβγ-binding proteins such as C-terminus of β-adrenergic kinase, phosducin or Gα, both in *Xenopus* oocytes [30,31,50] and HEK293 cells [28]. In this work, we did not manipulate

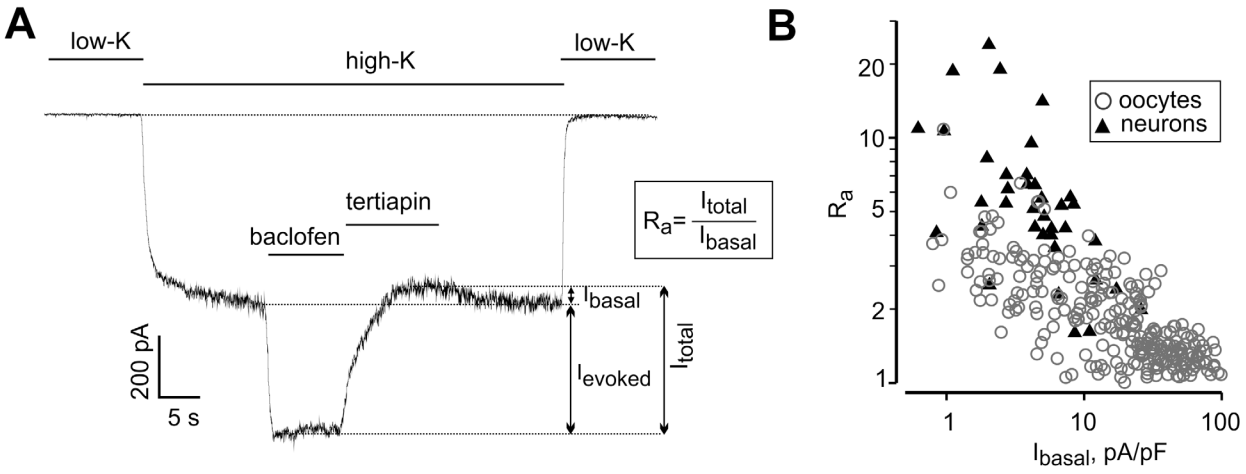

Fig 1. Basal and agonist-evoked GIRK currents in neurons and oocytes are inversely related. (**A**) A representative whole-recording of GIRK current in a neuron. Switching from low-K^+ extracellular solution to a high-K^+ solution led to the development of a large inward current probably carried by several ion channel types. Addition of baclofen elicited I_{evoked}. Arrows show the amplitudes of I_{basal}, I_{evoked} and I_{total}. Extent of activation, R_a, is defined as I_{total}/I_{basal}. (**B**) Inverse correlation between I_{basal} and R_a in oocytes and neurons. To allow direct comparison of I_{basal} in oocytes and neurons, currents in neurons were corrected for the 10 mV difference in holding potential, which was -70 mV in neurons and -80 mV in oocytes (see Methods). The correlation between R_a and I_{basal} was highly significant, p = 0.000000028 (neurons; n = 60; correlation coefficient = -0.633) and p = 0.0000002 (oocytes; n = 272; correlation coefficient = -0.728) by Spearman correlation test.

doi:10.1371/journal.pcbi.1004598.g001

cellular levels of phosphatidylinositol diphosphate (PIP_2), and used healthy cells which always showed robust GIRK currents, indicating levels of PIP_2 sufficient for channel activation [54]. Thus, under the conditions used in this work, Gβγ was the main gating factor determining the steady-state macroscopic GIRK current (I).

In a general form, I is described [1] by:

$$I = I_{single} \cdot P_o \cdot N, \quad (1)$$

where I_{single} is the single-channel current, N is the number of functional channels in the PM, and P_o is the channel's open probability. In a heterologous expression system, the channel's surface density (N/S, where S is the surface area of the cell) can be experimentally manipulated and measured. I_{single} of GIRK channels is an activation-independent parameter; P_o is the gating parameter that changes as a function of the concentration of Gβγ available for GIRK activation by agonist or added Gβγ [9,11].

We start the development of the model by considering how Gβγ, available for activation of GIRK, can be derived from heterotrimeric Gαβγ (Fig 2A). In the absence of GPCR-activated G protein cycle, a small fraction of G proteins dissociates into free $G\alpha^{GDP}$ and Gβγ due to finite affinity of their interaction [55,56] (the left branch of the reaction in Fig 2A). This free Gβγ can contribute to I_{basal} [57,58]. Addition of agonist activates the GPCR and promotes GDP-GTP exchange at Gα and full or partial separation of $G\alpha^{GTP}$ from Gβγ (the right branch of the reaction in Fig 2A; [59,60,61]). In our experiments in *Xenopus* oocytes and HEK293 cells, we coexpressed the muscarinic receptor 2 (m2R) which couples to $G_{i/o}$, and used acetylcholine (ACh)

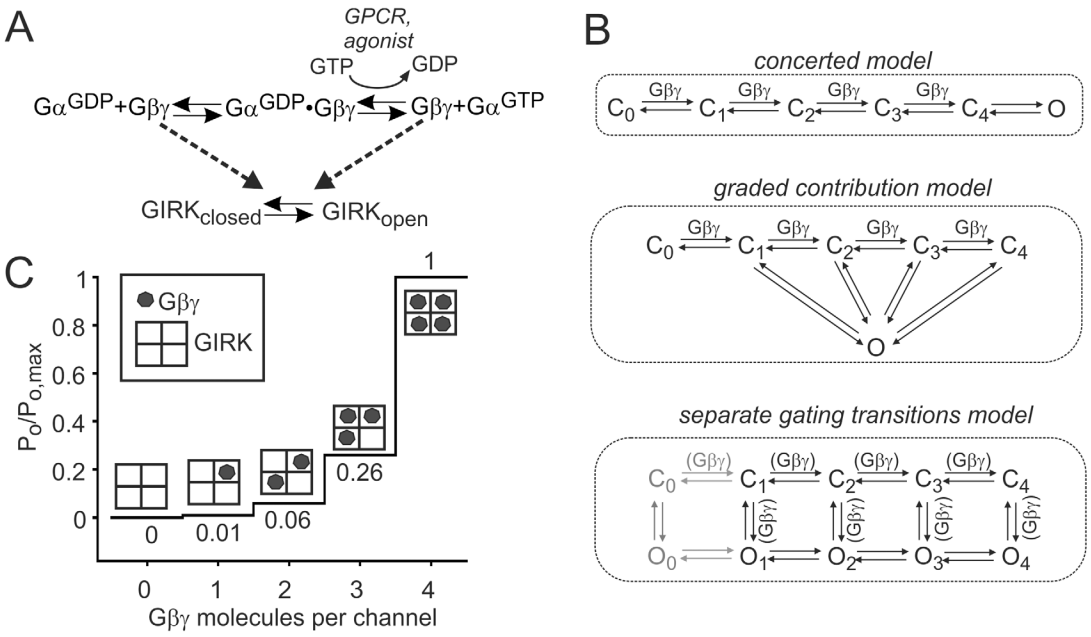

Fig 2. Gating of GIRK1/2 by Gβγ. (**A**) Sources of Gβγ for GIRK activation. $G\alpha^{GDP}$•Gβγ is the undissociated G protein heterotrimer. Note that, in isolated Xenopus oocytes or HEK cells, in the absence of added agonist the right, GPCR-dependent branch of the reaction of Fig 2A does not significantly contribute to I_{basal}, because there are no known $G\alpha_{i/o}$-coupled GPCRs or ambient agonists that can "basally" activate the GTPase cycle (discussed in [51]). (**B**) The schemes of "concerted", "graded contribution" and "separate gating transitions" models of channel activation. (**C**) Graded contribution of the four Gβγ-occupied GIRK states to P_o. Fractional P_o for each state was calculated by normalizing published P_o values [13] of each of the four modes (corresponding to 1–4 Gβγ occupied state) to $P_{o,max}$ (corresponding to 4 Gβγ occupied channel). Almost identical values have been obtained from fractional activation ratios for engineered GIRK channels having 1 to 4 Gβγ binding sites [14].

doi:10.1371/journal.pcbi.1004598.g002

at supramaximal doses [62], 2–10 μM, in order to achieve a complete separation/rearrangement between $G\alpha^{GTP}$ and Gβγ [63,64].

There are two existing models of GIRK gating by Gβγ. The allosteric kinetic model of Kurachi and colleagues, developed for cardiac GIRK1/4 [65,66,67], adequately describes the kinetics and magnitude of agonist- and GTPγS-evoked currents and the effect of RGS proteins. However, this model does not address I_{basal}, does not include an explicit Gβγ binding step (Gβγ acts catalytically) and assumes very high surface densities of G proteins, in the order of 56 mM, which are incompatible with our measurements or those of others (see below and Discussion). It would be difficult to adjust this model for our purposes and to adequately describe I_{basal}, or to implement the Gβγ recruitment phenomenon.

The second model, termed here "concerted model", was previously developed by us to describe the G protein-dependent activation of GIRK by Na^+ (Fig 2B) [58]. The model included a description of I_{basal} and an explicit Gβγ-GIRK binding step, but not the $G\alpha^{GTP}$-Gβγ dissociation step or I_{evoked}. Further, it assumed opening of the channel only when all four Gβγ binding sites are occupied (Fig 2B), which does not concur with the experimental findings that suggest a graded contribution of each bound Gβγ molecule [13,14,68].

Therefore, in the present work, we have developed a "graded contribution" model (Fig 2B and 2C), where each Gβγ-occupied state can contribute to channel opening and thus to P_o [13,14,68]. To date it is not known whether Gβγ binding to GIRK is truly cooperative (i.e. whether Gβγ occupancy at one binding site increases the affinity of Gβγ binding at another site). Therefore, for simplicity, in the graded contribution model we assume that Gβγ binding to GIRK is sequential and the affinity of each Gβγ-binding site is independent of the occupancy of other sites. However, overall the process of gating is cooperative, since occupancy of each additional Gβγ-binding site increases P_o in a more-than-additive manner (Fig 2C). The relative contributions of each Gβγ-occupied channel state to P_o are adopted from published data for the homologous GIRK1/4 channel [13,14]. Thus, one bound Gβγ causes channel opening with a P_o which is 1% of the maximal P_o, $P_{o,max}$; two Gβγ give 6%, three Gβγ 26%, and four Gβγ 100% of $P_{o,max}$ (Fig 2C). This approach is applicable only to steady-state calculations of macroscopic currents since it omits the kinetic details, but it allows to bypass the need to determine (or assume) a large number of unknown parameters: state-dependent changes in channel's affinity to Gβγ, rates of closed-open transitions from different Gβγ-bound states, and the contributions of several potential open states. Once the channel achieved a state with n Gβγ bound, its fractional P_o is known and does not depend on the pathway by which the channel opens. For simplicity, in calculating the steady-state P_o for each Gβγ-occupied state, all open states (usually 2 are reported for GIRKs; [69,70,71,72]) were pooled into a single one (see Fig 2B).

We have also considered a more general model with 4 separate closed states, in which each closed subunit can open independently of other subunits and the opening is promoted by Gβγ binding, giving rise to four open states (the "separate gating transitions model", Fig 2B). The scheme shown also describes an alternative case in which subsequent closed states C_1-C_4 arise from the Gβγ-free closed state C_0, the transitions between closed states are driven by Gβγ binding, and there are 5 separate C-O transitions. In both cases, it can be shown that, utilizing the approach based on graded contributions of each Gβγ-occupied channel state to P_o, the derivation of P_o converges to the same lead equation (eq 6) as for the graded contribution model (see Supplemental Discussion, S2 Text). Therefore, in this study we implemented the graded contribution model to simplify calculations. Throughout this work we also used an extended version of the concerted model, with the inclusion of the GPCR-induced dissociation of $G\alpha^{GTP}$ from Gβγ, to cross-check the conclusions of the graded contribution model.

Quantitative description and modeling of signaling cascades require the evaluation of amounts, stoichiometry, and affinities of interactions of participating proteins [73,74,75,76,77].

We took an approach that rests as much as possible on experimentally determined parameters. The data necessary for simulation by the model (eqs 5–13 in Methods) are the surface density of GIRKs and G proteins in *Xenopus* oocytes, macroscopic parameters of GIRK1/2 gating (whole-cell I_{basal}, I_{evoked} and the current induced by coexpression of Gβγ, $I_{\beta\gamma}$, see S2 Fig) at different channel densities, and I_{single} and $P_{o,max}$. Other parameters were experimentally determined in other works.

Single-channel currents and $P_{o,max}$ of GIRK1/2

To estimate single-channel current (I_{single}) and P_o of Gβγ- and agonist-activated GIRK1/2, we expressed the channels at low density with m2R and recorded channel activity in cell-attached patches (Fig 3A and 3B). I_{single} was determined from amplitude distribution histograms (Fig 3A and 3B; right panels). The Gaussian fits to these histograms showed one main conductance level, suggesting that subconductance states, if any, did not significantly contribute to P_o. The average I_{single} was identical for ACh and Gβγ activation (Fig 3C), ~2.8 pA.

P_o was estimated from patches containing 1 to 3 channels (see Methods). When channels were activated by Gβγ expressed at a saturating dose with no agonist present, P_o was 0.105 ±0.018 (Fig 3D). The Gβγ RNA dose used (5 ng Gβ RNA, 1 ng Gγ RNA) consistently produced maximal macroscopic activation (see below, for example S8 Fig), and ACh generated negligible whole-cell I_{evoked} which was ~10% of I_{basal} (Ra = 1.1 ± 0.02, n = 14). Thus, free endogenous $G\alpha^{GTP}$ produced upon activation of m2R did not substantially affect the GIRK1/2 current evoked by saturating Gβγ. We therefore conclude that the P_o measured in oocytes expressing saturating Gβγ is the $P_{o,max}$ of GIRK1/2, within a possible ~10% error. In comparison, when GIRK1/2 was activated via the coexpressed m2R (no Gα or Gβγ were coexpressed) with 2–5 μM ACh in the pipette, P_o was 0.037±0.008, less than half of $P_{o,max}$. (Fig 3B and 3D). (The actual P_o could be higher because of the desensitization observed with ACh but not with Gβγ; see Methods).

Initial estimation of functional GIRK1/2:Gβγ stoichiometry from macroscopic currents

For further analysis and modeling of whole-cell I_{basal} and I_{evoked}, we varied the surface density of GIRK1/2. The design was to obtain low, intermediate and high densities of GIRK1/2 by injecting 25, 100–200 or 1000–2000 pg RNA of each subunit per oocyte. The cells expressed 1 or 2 ng of m2R RNA which did not affect I_{basal} (S2C Fig and ref. [78]) but could always produce the maximal I_{evoked} [78]. I_{evoked} was elicited by ACh at 10 μM, a saturating dose. Under these conditions, all $G\alpha_{i/o}$ should convert to $G\alpha^{GTP}$, so that all available Gβγ can bind to the channel and activate it. The data are summarized in Table 1; main findings are also briefly highlighted in Fig 3E and 3F. We measured I_{basal}, I_{evoked} and I_{total} in each oocyte (set 1 in Table 1, S2A Fig). In separate groups of oocytes expressing saturating Gβγ, where channel's P_o reached $P_{o,max}$, we measured $I_{\beta\gamma}$ (set 2 in Table 1, S2B Fig).

It is noteworthy that in oocytes, at all channel densities, $I_{\beta\gamma}$ was 1.6–2 fold greater than I_{total}, the total GIRK current (I_{basal} + I_{evoked}) without coexpressed Gβγ (Table 1). A similar $I_{\beta\gamma}/I_{total}$ ratio of 1.66 was observed in HEK293 cells (Table 2), where all data have been pooled together (because GIRK1/2 expression levels have not been monitored). Similarly, $I_{\beta\gamma}/I_{total}$ ratio of ~2.2 for GIRK1/2 expressed in HEK cells can be estimated from the data of Wydeven et al. [79] who activated GIRK with baclofen via $GABA_B$ receptors (I_{evoked} ~40 pA/pF, $I_{\beta\gamma}$ ~ 90 pA/pF). The inverse value, $I_{total}/I_{\beta\gamma}$, ranged 0.5–0.62 at different channel densities (Fig 3F, left panel). Since GIRK1/2 was maximally activated by the doses of Gβγ used in these experiments, $I_{total}/I_{\beta\gamma}$ is equal to the fraction of maximal activation after GPCR activation, $P_o/P_{o,max}$. Note that the

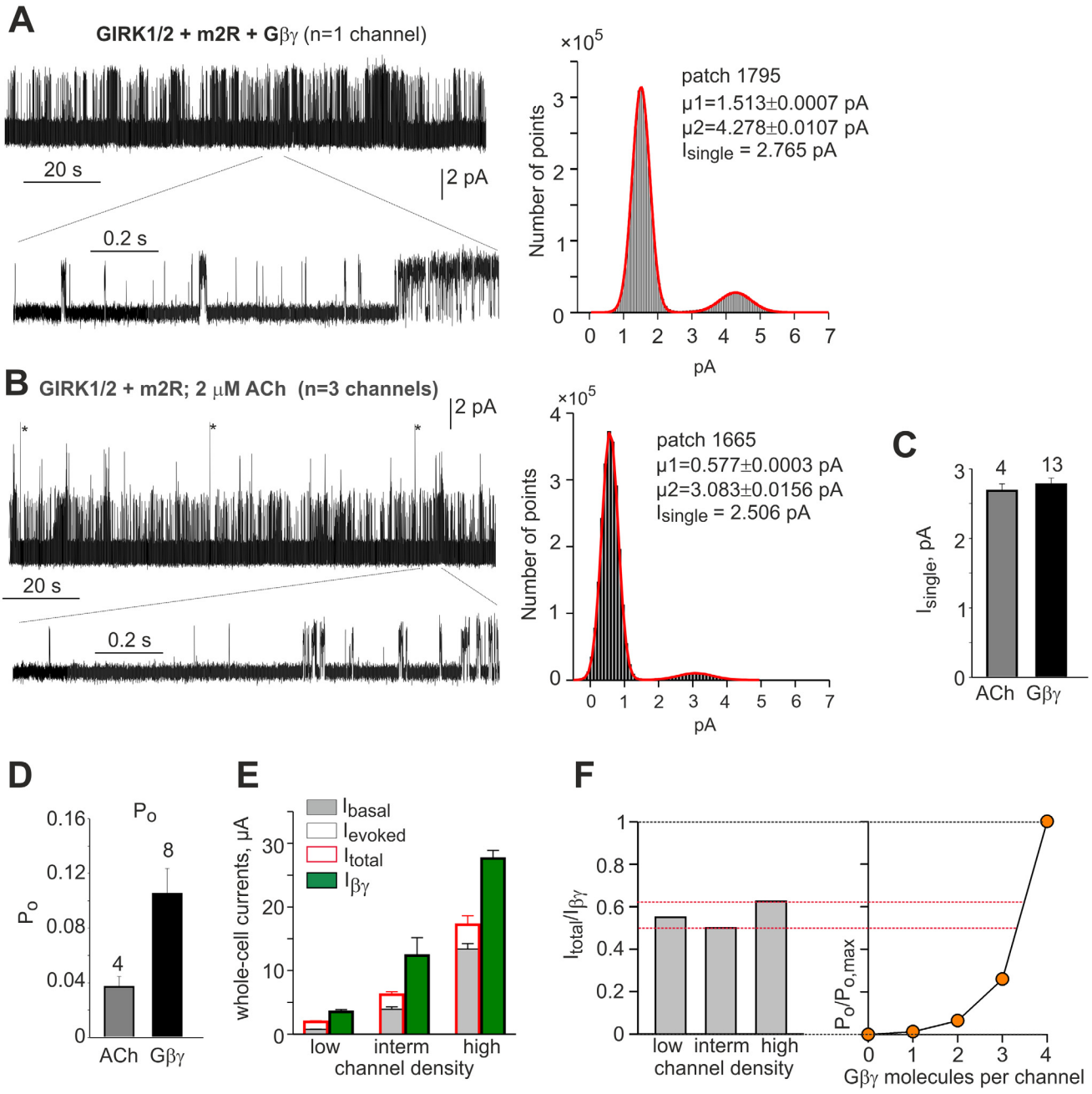

Fig 3. Single channel and whole-cell data reveal incomplete activation of GIRK1/2 by agonist compared to Gβγ. (A) Activity of GIRK1/2 in a cell-attached patch of an oocyte expressing the channel, m2R and Gβγ, without an agonist in the pipette. Right panel shows a 2 minutes segment of record, with zoom (below) on a shorter segment. The amplitude distribution histogram of the same 2 min-segment is shown on the right. Red line shows a two-component Gaussian fit. I_{single} was determined as the difference between the fitted midpoints (μ) of the GIRK current peak on the right (μ2) and the left peak which corresponds to noise (μ1). **(B)** Activity of GIRK1/2 channels in a cell-attached patch of an oocyte expressing the channel and m2R and activated by 2 μM ACh present in the patch pipette. (Asterisks denote artifacts produced by capacity discharges of patch clamp headstage). The corresponding amplitude histogram of the 2 min-segment of the record is shown on the right. In A and B, GIRK1/2 was expressed at low densities (GIRK1, 10–50 pg RNA; GIRK2, 7–17 pg RNA) whereas RNAs of m2R (1–2 ng/oocyte) and Gβγ (5:1 ng/oocyte) were chosen to produce saturating concentrations of these proteins. Inward K^+ currents are shown as upward deflections from zero level. In the traces shown, acquisition was at 20 KHz with 5 KHz analog filter. Very similar values of I_{single} were obtained with 2 KHz filtering (not shown). **(C)** Single channel currents (left plot) are identical with either ACh or Gβγ. **(D)** P_o is lower with ACh than with Gβγ ($p = 0.029$). Bars in C and D show mean±SEM, number of patches is shown above the bars. **(E)** Summary of whole-cell GIRK1/2 currents at three expression levels (densities). See Table 1 for details. **(F)** Left panel shows the $I_{total}/I_{βγ}$ ratios at three channel densities, calculated from data of Table 1. The right panel shows the fractional open probabilities of channels occupied by 0–4 Gβγ, same as in Fig 2C but in a simple graphic form. The red dotted lines are drawn to allow direct comparison of the experimental data from the left panel with the estimates of fractional P_o from the right panel.

doi:10.1371/journal.pcbi.1004598.g003

Table 1. Whole-cell currents of GIRK1/2, the calculated surface density and $I_{\beta\gamma}/I_{total}$ in *Xenopus* oocytes.

Group (channel density)	ng RNA GIRK1, GIRK2	Set 1: experiments with agonist			Set 2: experiments with no agonist		calculated density (channels/μm^2)	$I_{\beta\gamma}/I_{total}$
		I_{basal} (μA)	I_{evoked} (μA)	I_{total} (μA)	No Gβγ I_{basal} (μA)	Gβγ expressed $I_{\beta\gamma}$ (μA)		
Low	0.025	0.73±0.065 (51)	1.19±0.09 (51)	1.92±0.14 (51)	1.06±0.13 (18)	3.49±0.37 (14)	2.74±0.29	1.82
Intermediate	0.1–02	3.9±0.36 (55)	2.3±0.2 (55)	6.2±0.45 (55)	3.77±0.55 (28)	12.34±2.82 (26)	9.7±2.2	2
High	1–2	13.36±0.87 (10)	3.84±0.81 (10)	17.2±1.42 (10)	15±0.84 (75)	27.6±1.3 (77)	21.7±1	1.6

Data are shown as mean±SEM (except $I_{\beta\gamma}/I_{total}$), number of cells is shown in parentheses. Data for each entry were collected from at least 2 independent experiments. The Table summarizes separate sets of experiments: those where I_{basal}, I_{evoked} and I_{total} were measured (in each oocyte); and those where Gβγ was coexpressed and $I_{\beta\gamma}$ was measured. In addition, in Set 2, I_{basal} was measured in each experiment in a separate group of oocytes not injected with Gβγ RNA. For the low density group in oocytes, there was ~30% difference ($p = 0.017$) for I_{basal} between the two sets of experiments, probably because of variability among oocyte batches. In intermediate and high density groups I_{basal} was not different ($p>0.4$) for both sets of experiments.

doi:10.1371/journal.pcbi.1004598.t001

single-channel data (Fig 3D) show less than 40% activation with saturating ACh (although, as noted above, this is probably an underestimate because of desensitization). In all, in oocytes and HEK cells, when the channel is activated by an agonist, only 40–60% of maximal P_o is achieved.

From the data of Fig 3, one can approximately estimate the amount of Gβγ molecules that are bound to the channel after maximal activation by agonist. This is done by comparing between measured values of $I_{total}/I_{\beta\gamma}$ (Fig 3F, left panel) and the expected $P_o/P_{o,max}$ [13,14] from Fig 2C. To facilitate the comparison, we have redrawn the plot of Fig 2C in a simple graphic form (Fig 3F, right panel), and projected the values of $I_{total}/I_{\beta\gamma}$ onto the $P_o/P_{o,max}$ plot (red dashed lines). For 3 bound Gβγ, the expected $P_o/P_{o,max}$ is 0.26, and for 4 Gβγ it is 1. Thus, with $I_{total}/I_{\beta\gamma}$ of 0.4–0.6, we estimate that, even without coexpression of Gβγ, between 3 and 4 Gβγ are available for activation of a single GIRK channel at all channel densities.

Expression-dependent changes in surface levels of GIRK1/2

For saturating Gβγ, Eq 1 for $I_{\beta\gamma}$ takes the form:

$$I_{\beta\gamma} = I_{single} \cdot P_{o,max} \cdot N. \quad (2)$$

From here, we calculated the total number of functional channels in the PM (N) and the corresponding channel density per μm^2 of the PM. As shown in Table 1, our "low", "intermediate" and "high" expression levels correspond to approximately 2.7, 9.7 and 21.7 channels/μm^2,

Table 2. Whole-cell currents of GIRK1/2 and $I_{\beta\gamma}/I_{total}$ in HEK293 cells.

Set 1: experiments with agonist			Set 2: Gβγ expression	$I_{\beta\gamma}/I_{total}$
I_{basal} (pA/pF)	I_{evoked} (pA/pF)	I_{total} (pA/pF)	$I_{\beta\gamma}$ (pA/pF)	
19.1±4.4 (25)	30.6±6.7 (25)	49.7±10.5 (25)	82.6±25.6 (6)	1.66

Data are shown as mean±SEM (except $I_{\beta\gamma}/I_{total}$), number of cells is shown in parentheses. Data for each entry were collected from at least 2 independent experiments, except $I_{\beta\gamma}$ which was measured in one experiment. Raw data of Set 1 were reported in [51].

doi:10.1371/journal.pcbi.1004598.t002

respectively. In the following, the data of Table 1 served as the basis for testing the predictions of the model and for calculating Gα and Gβγ available for channel activation.

Surface levels of GIRK1/2 are confirmed by quantitative immunochemistry

To obtain an independent estimate of the density of GIRK1/2 in the PM, we used quantitative immunochemistry of GIRK1 in cytosol-free, manually separated plasma membranes of *Xenopus* oocytes (Fig 4A and 4B) [80,81]. GIRK1 was coexpressed with GIRK2 at high density, and GIRK1 was probed with a C-terminally directed antibody. Western blots of manually separated PM and of the rest of the cells without the nucleus ("cytosol") showed the presence of two forms of GIRK1. A double band of about 55–58 KDa was always observed, and an additional

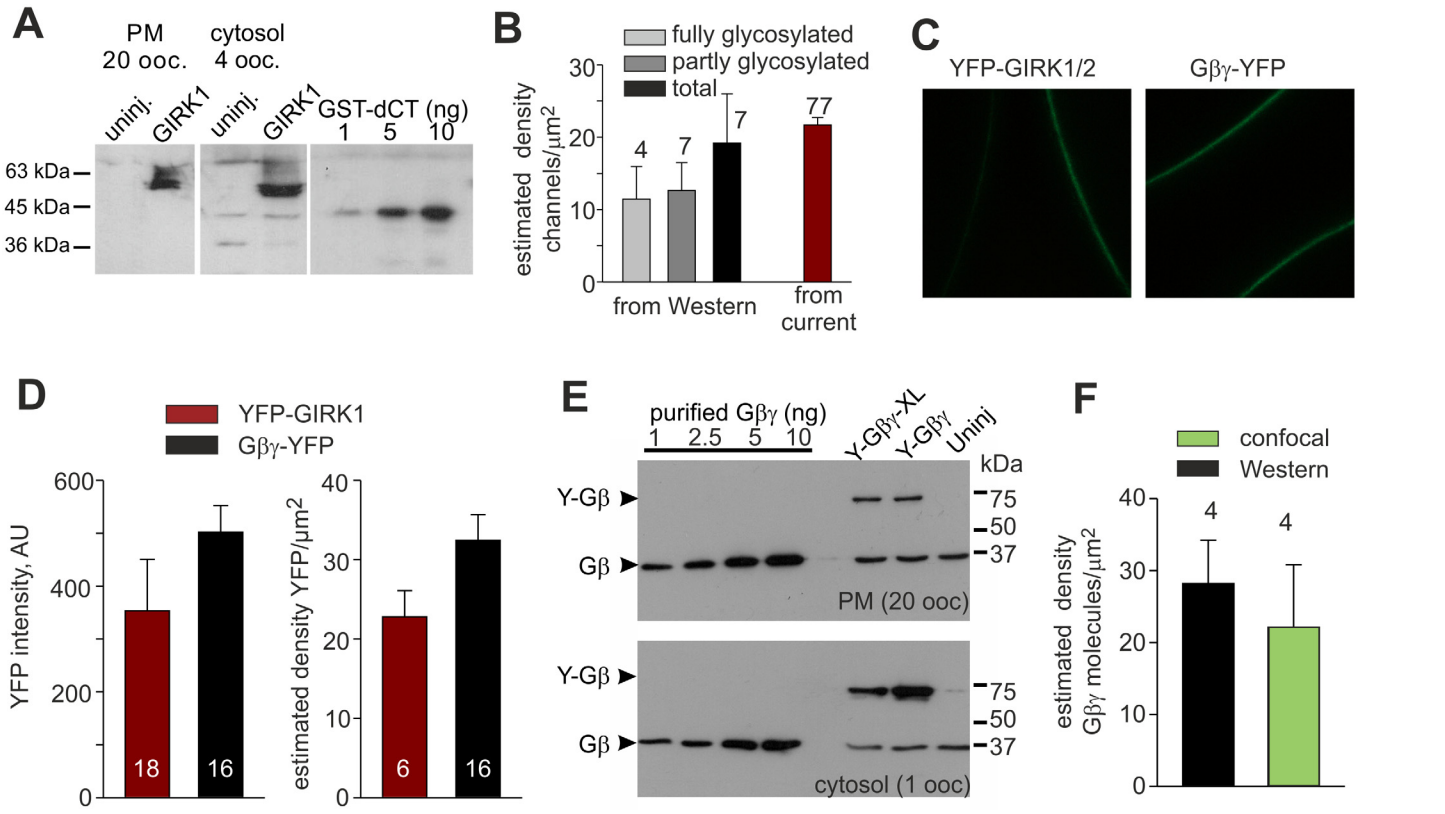

Fig 4. Measuring the surface density of GIRK1/2 and Gβγ in *Xenopus* oocytes. (A) Immunochemical estimation of the amount of GIRK1 in manually separated plasma membranes of *Xenopus* oocytes injected with 1 or 2 ng of GIRK RNA. Shown is a Western blot of 20 manually separated plasma membranes and 4 cytosols, and variable known amounts of the GST-fused distal C-terminus of GIRK1 (the antibody's epitope) used for calibration of the antibody-produced signal. There was a non-specific band at ~75 KDa in cytosols but not PM of uninjected oocytes ("uninj"). **(B)** Summary of quantitative analysis of GIRK1 in PM from Western blots of 7 separate experiments. The fully glycosylated band was observed in 4 out of 7 blots. Molar amounts of protein and PM densities from Western blots were calculated as detailed in Methods. The dark red bar is the GIRK1/2 surface density in the high-density group estimated from $I_{\beta\gamma}$ (see Table 1), shown for comparison. **(C)** Examples of confocal images of oocytes expressing YFP-GIRK1/2 (5 ng RNA) and Gβγ-YFP (5 ng RNA). **(D)** Estimating YFP molecules density in PM using YFP-GIRK1/2 as molecular ruler. A representative experiment is shown. The left plot shows the measured intensities of YFP-GIRK1/2 and YFP-Gβ coexpressed with wt Gγ in a separate group of oocytes (5:1 ng RNA). The right plot shows the PM densities of YFP in the YFP-GIRK1/2 oocytes, calculated as follows: $I_{\beta\gamma}$ was 14.5±2.1 μA (n = 6), corresponding to 11.4±1.6 channels/μm^2, or 22.8±3.3 YFP molecules/μm^2. The density of YFP in the YFP-Gβγ expressing oocytes was calculated based on relative intensities from the left plot. **(E)** Estimating the amount of endogenous Gβ and expressed YFP-Gβ or YFP-Gβ-XL (5 ng RNA) coexpressed with wt-Gγ, in manually separated plasma membranes. Protocol was similar to Fig 4A; wt purified recombinant Gβγ was used for calibration. In parallel to biochemical measurements, we also measured GIRK currents and YFP intensity in 5–15 oocytes expressing either YFP-GIRK1/2-Gβγ or YFP-Gβγ, as explained in D. **(F)** Summary of YFP-Gβγ surface density measurements in 4 experiments by the two methods, quantitative Westerns and confocal imaging with YFP-GIRK1/2 as the molecular ruler.

doi:10.1371/journal.pcbi.1004598.g004

higher diffuse band was seen in four out of seven experiments (Fig 4A and 4B). These bands correspond to partly and fully glycosylated channels, respectively [82,83]. Three oocyte batches showed only partly glycosylated bands in the PM. Since oocytes injected with 2 ng RNA always had large GIRK1/2 currents, it is likely that both partly and fully glycosylated channels are functional at the PM, in agreement with [83]. Notably, the main fraction of the channel was found in the cytosolic fraction (most likely endoplasmic reticulum and Golgi), largely in a partly-glycosylated form (Fig 4A). This is not unexpected, because in *Xenopus* oocytes the PM constitutes only a very small fraction of the cell's total mass [81].

Next, molar amounts of GIRK in the PM fraction were calculated, taking into account the presence of two GIRK1 subunits in each channel. Calibration of antibody-produced signal was done with known amounts of the GST-fused distal C-terminus of GIRK1 which contains the epitope for the antibody. Note that this method yields channel levels in concentration units (e.g. mole/L). Both GIRK and Gβγ are associated with the PM (Gβγ is membrane-anchored by a lipid moiety [84]), and the interaction between GIRK's cytosolic domain and Gβγ takes place within the submembrane space. Therefore, to compare data with GIRK1/2 surface densities obtained by channel counting from currents (Table 1), and for further modeling, we have converted two-dimensional protein densities to protein concentrations within the interaction space as previously described (e.g. [58,85,86,87]; see Supplemental Discussion, S2 Text), according to

$$C = N/(W \cdot S \cdot A), \quad (3)$$

where C is the concentration of protein in the submembrane space, N is the number of protein molecules in the membrane, S is a membrane area, A is Avogadro number and W is the width of the interaction space. For calculations, we used $S_{oocyte} = 2\times10^7$ μm^2 (deduced from an oocyte's capacitance of 200 nF [88] and specific capacitance of plasma membrane of 1 μF/cm^2), and W was assumed to be 10 nm. The latter roughly corresponds to the molecular size of the complex of Gβγ and the cytosolic part of GIRK [18]. The influence of this parameter on the conclusions of the model was tested later (see below, S6 Fig, panels D and E). Consequently, the standard conversion factor between channel density (number of channels/μm^2) and channel concentration (nM) is 1 channel/μm^2 = 166 nM.

Conversion of channel concentrations determined in Fig 4 into surface densities using Eq 3 gave ~12–14 channels/μm^2 for both partly and fully glycosylated channels in the PM, and the average total amount of GIRK1/2 in PM (with partly + fully glycosylated GIRK1) was 19.1±6.8 channels/μm^2 (Fig 4B). This is in good agreement with the independent assessment of ~22 channels/μm^2 obtained from measurements of $I_{\beta\gamma}$ for the high GIRK1/2 expression group (Table 1). To note, the latter was calculated using Eq 2 with $P_{o,max}$ measured at low channel densities. If $P_{o,max}$ were different at high GIRK1/2 expression levels, the densities calculated from $I_{\beta\gamma}$ and immunochemistry would not match. The close correspondence between the two independent approaches indicates that $P_{o,max}$ is preserved at the high expression level.

We conclude that the total surface density of GIRK1/2 channels in the PM can be satisfactorily estimated from whole-cell currents (Eq 2, Table 1). Such measurements are calibration-independent and accurate [1], and therefore GIRK1/2 can be used as a "molecular ruler". In this procedure, the fluorescently labeled GIRK1/2, with its surface density calculated from $I_{\beta\gamma}$, will serve as a reference for estimating PM densities of other fluorescently labeled proteins. To use GIRK1/2 as a molecular ruler, we expressed YFP-GIRK1 (GIRK1 with Yellow Fluorescent Protein (YFP) fused to the N-terminus). Single channel analysis of Gβγ-activated YFP-GIRK1 coexpressed with GIRK2, YFP-GIRK1/2, showed the same $P_{o,max}$ and I_{single} as in wild-type

GIRK1/2 (S3 Fig), allowing the use of this construct for calibration purposes. To obtain high current levels of YFP-GIRK1/2 we usually had to inject 5 ng/oocyte of channel's RNA.

Surface levels of Gβγ

To estimate the expression levels of Gβγ using YFP-GIRK1/2 as molecular ruler, we expressed YFP-GIRK1/2 and, in separate oocytes of the same batch, Gβγ in which either Gβ or Gγ was labeled with YFP. Expression of YFP was monitored from fluorescence intensity in the PM (Fig 4C). In addition, $I_{\beta\gamma}$ was measured and the surface density of YFP-GIRK1/2 was calculated. The amount of YFP molecules per μm^2 was calculated assuming a 2:2 GIRK1:GIRK2 stoichiometry in a heterotetramer [89] (See also Supplemental Discussion, S2 Text). The surface density of Gβγ-YFP was then calculated based on intensity ratios of YFP-GIRK1 and Gβγ-YFP. A typical experiment is shown and explained in Fig 4D.

To validate the estimates of Gβγ expression, in four experiments as in Fig 4D we also measured the levels of Gβ-YFP (coexpressed with unlabeled Gγ) by quantitative immunochemistry in manually separated plasma membranes. We used purified Gβγ to calibrate the signal produced by the Gβ antibody (Fig 4E). We also constructed and expressed an YFP-fused construct corresponding to *Xenopus laevis* Gβ1, YFP-Gβ-XL (see Methods). Western blots showed a prominent ~36 KDa band of the endogenous Gβ, and ~70 KDa bands corresponding to the expressed YFP-Gβ or YFP-Gβ-XL (Fig 4E). The surface density of the expressed YFP-Gβγ assessed by the quantitative immunochemical method was 28±6 molecules/μm^2, close to the estimate of 22.1±8.7 molecules/μm^2 obtained in the same experiments from measurements of fluorescence using YFP-GIRK1 as "molecular ruler" (Fig 4F; 53 oocytes, n = 4 experiments; P = 0.295). These results demonstrate the feasibility of the molecular ruler methodology and provide a good estimate of the expressed Gβγ-YFP. In several sets of experiments (see also below) we consistently found that, with 5 ng RNA of Gβγ, its surface density ranged between 20 and 30 molecules/μm^2.

We next utilized YFP-Gβ-XL as a caliper for the endogenous oocyte's Gβ. Results of 4 experiments showed that, in Western blots, Gβ antibody used here gave similar signal with Gβ-XL as with bovine $G\beta_1$ (S3 Fig, panels C, D). We then estimated the surface density of the endogenous Gβ (the 37 kDa band in Fig 4E) to be 24±4.6 molecules/μm^2 (n = 4). We have also estimated the concentrations of total and cytosolic endogenous Gβγ from the 4 experiments of Fig 4E, assuming an oocyte's water volume of 0.5 μl [88]. The total Gβγ concentration was 173±44 nM, the concentration of Gβγ in the cytosolic fraction was 171±44 nM.

Estimation of functional stoichiometry of GIRK1/2, Gβγ and Gα

We define the molar amounts of proteins physically available for the function of the cascade as functional stoichiometry. It can change depending on availability of a protein, in contrast to limiting (maximal) stoichiometry which reflects the maximal molar ratios of interacting proteins. For example, if one GIRK channel can interact with at most 4 Gβγ and 4 Gα molecules, then the limiting GIRK:Gβγ:Gα stoichiometry is 1:4:4.

Having determined the $P_{o,max}$ and surface densities of GIRK1/2 and endogenous Gβγ, we were now able to simulate macroscopic GIRK currents in oocytes and to assess the functional stoichiometry of GIRK1/2-Gα-Gβγ. We initially assumed that all of the I_{basal} in oocytes was Gβγ-dependent. The affinities of GIRK-Gβγ and Gα-Gβγ interactions were adopted from published work: K_D = 1.86 nM for $G\alpha^{GDP}$-Gβγ binding [56], and K_D = 50 nM for the GIRK-Gβγ interaction, as estimated by biochemical methods [90]. Simulations were done using eqs 5–16 as explained in the Methods section. Simulated data were compared to experimental measurements of GIRK1/2 activity for the three GIRK1/2 surface density groups (Table 1 and Fig 3E).

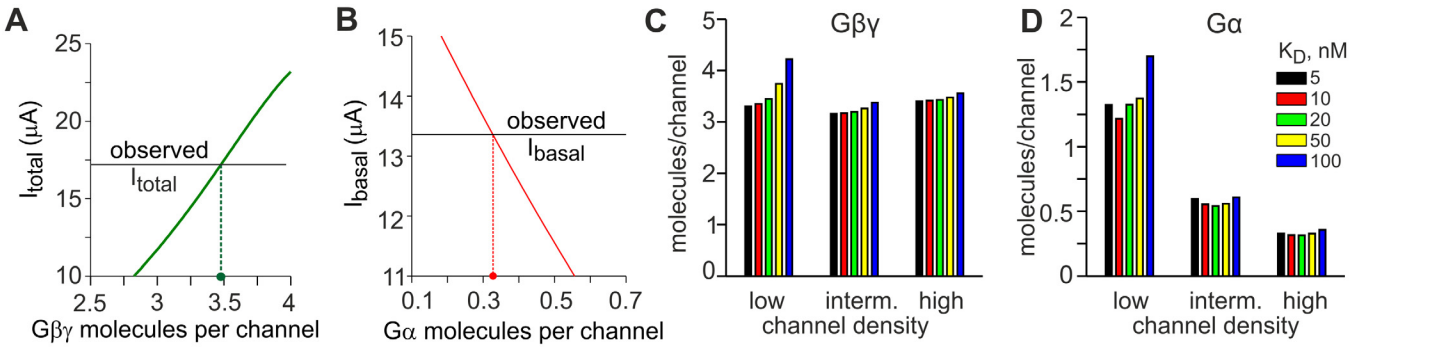

Fig 5. Estimation of Gβγ and Gα available for GIRK1/2 activation from macroscopic currents. (**A, B**) The method of estimation of number of Gβγ and Gα molecules per channel is exemplified for the high channel density group of Table 1. The same procedure has been applied to the low and intermediate density groups (Table 3). **(A)** Estimation of Gβγ available for channel activation utilizing I_{total}. Simulated I_{total} (green line) was calculated for a range of Gβγ surface densities using eqs 5–12, and compared with the experimentally observed I_{total}. **(B)** Estimation of $G\alpha_{i/o}$ available for interaction with the channel. Simulated I_{basal} (red line) was calculated using eqs 5–16 for a range of Gα surface densities, using the Gβγ density calculated in (A), and compared with the experimentally observed I_{basal}. (**C, D**) The estimates of Gβγ:GIRK (C) and Gα:GIRK (D) ratios are stable in a wide range of GIRK-Gβγ interaction affinities, from K_D = 5 nM to 100 nM. Simulations were done with the graded contribution model separately for the low-, intermediate- and high density groups from Table 1 (2.74, 9.7 and 21.7 channels/μm^2, respectively).

doi:10.1371/journal.pcbi.1004598.g005

Note that GIRK densities were calculated from $I_{\beta\gamma}$ but simulations were done for the separately measured I_{basal} and I_{evoked}, avoiding circular reasoning.

We first tried to simulate the experimental data by assuming that only endogenous Gαβγ is available for the activation of GIRK1/2 (S4A Fig). However, no satisfactory description of data can be obtained under this assumption. Simulations that assumed recruitment of 3–4 Gβγ with GIRK, without Gα, gave a better approximation to the data (S4 Fig, panels B, C).

Next, we turned to a more accurate assessment of functional GIRK1/2:Gβγ:Gα stoichiometry. Our model allows to calculate the amounts of Gα and Gβγ available for GIRK1/2 without any prior knowledge or assumption about the G protein concentrations in the cell, directly from experimental data. This idea is illustrated graphically in Fig 5 for the high GIRK1/2 surface density group of Table 1. The procedure consists of two steps. First, because all Gβγ available for GIRK is free to activate the channel after addition of agonist, the total GIRK-available Gβγ can be calculated from I_{total}, as shown in Fig 5A. Here, the solid green line presents the simulated I_{total} for a range of GIRK-available Gβγ densities, normalized to channel density (Gβγ:GIRK ratio). The intercept of simulated I_{total} and the experimentally observed I_{total} produces the estimate of the Gβγ:GIRK ratio. The numeric calculation of Gβγ density from experimental I_{total} can also be done by substituting the channel density and I_{total} into the eqs 5–13 and 16 (see Supplemental Methods (S1 Text) for Matlab routines).

Next, the estimate of Gβγ is used to calculate the available Gα from I_{basal}. I_{basal} is determined by "free" Gβγ that is not bound to $G\alpha^{GDP}$ in the absence of agonist. The calculation is done by substituting channel density, I_{basal} and the estimated value of available Gβγ into the eqs 5–16 (see Supplemental Methods, S1 Text); a graphical illustration is shown in Fig 5B. The summary of calculations, made with our standard assumption of K_D = 50 nM for the GIRK-Gβγ interaction, is presented in Table 3 and Fig 5C and 5D. These calculations show that there are ~3–4 Gβγ, but less than 2 Gα, available for each channel. Moreover, while Gβγ:GIRK ratio remains relatively constant throughout the range of analyzed channel densities, there is a sharp decrease in Gα:GIRK ratio with the increase in channel density (Table 3; see also below and S6 Fig).

The estimate of K_D for the GIRK-Gβγ interaction varies depending on the method used, from K_D = 4–10 nM determined in excised patches [91,92,93] to ~50 nM in direct biochemical measurements [90]. To check for model's stability regarding this parameter, we calculated the

Table 3. Calculation of Gβγ and Gα available for channel activation in *Xenopus* oocytes (without coexpressing Gβγ). K_D for channel-Gβγ interaction was taken as 50 nM. For calculations with other K_D values, see Fig 5 and S5 Fig.

Channel density group	channels/μm² (from Table 1)	Graded contribution model				Concerted model			
		total available Gα and Gβγ, molecules/μm²		Gβγ:GIRK and Gα:GIRK ratios		total available Gα and Gβγ, molecules/μm²		Gβγ:GIRK and Gα:GIRK ratios	
		Gβγ	Gα	Gβγ: GIRK	Gα: GIRK	Gβγ	Gα	Gβγ: GIRK	Gα: GIRK
Low	2.74	10.2	3.75	3.74	1.37	11.3	3.3	4.14	1.22
Intermediate	9.7	31.6	5.4	3.26	0.56	34.2	4.3	3.53	0.44
High	21.7	75.5	7.2	3.48	0.33	79.6	5.6	3.67	0.26

doi:10.1371/journal.pcbi.1004598.t003

available Gβγ and Gα for a range of K_D from 5 to 100 nM. As shown in Fig 5C and 5D, the estimates of Gβγ:GIRK and Gα:GIRK ratios, and the trend in their changes as a function of channel density, remain highly stable within the examined range of K_D. Similar conclusions were attained using the concerted model (Table 3 and S5 Fig). The latter does not involve any assumptions for fractional Gβγ contributions to total P_o. Similarity of conclusion of the two models alleviates concerns regarding the use of values for fractional Gβγ contributions, adopted from GIRK1/4 studies, to simulate GIRK1/2.

Table 3 also shows the total Gβγ and Gα available for GIRK in PM, in molecules/μm², calculated for each of the three channel densities. It is easy to see that, at intermediate and high channel densities, the endogenous Gβγ, 24 molecules/μm² (that was present in the PM before the expression of GIRK) cannot account for the observed GIRK1/2 activation. In contrast, estimates of total Gα available for GIRK1/2 remain within the limits of endogenous Gα. As mentioned before, the calculations have been made without any assumption regarding the presence or amount of endogenous Gαβγ, and made no specific *a priori* assumptions regarding recruitment of Gβγ or Gα. Hence, modeling independently predicts the necessity for GIRK1/2-related increase in PM density of Gβγ, corroborating the experimentally observed recruitment of Gβγ, but not Gα, by GIRK1/2 [25].

Next, we addressed the possible contribution of intrinsic, Gβγ-independent activity to I_{basal}. About 10–20% of I_{basal} of GIRK1/2 in *Xenopus* oocytes [30,31,50] and HEK293 cells [28] persists after expression of Gβγ scavengers or Gα. Whereas the residual I_{basal} may reflect incomplete Gβγ chelation, a genuine Gβγ-independent fraction of I_{basal} cannot be discarded. In the extreme case it may contribute up to 20% of GIRK1/2 I_{basal}. This may account for up to 10% of $P_{o,max}$ (because I_{basal} can reach at most half of $I_{\beta\gamma}$, which is the indicator of $P_{o,max}$; Tables 1 and 2).

We have therefore extended the model to include the contribution of a hypothetical intrinsic Gβγ-independent channel activity. We assume that the intrinsic basal P_o of a channel ($P_{o,intrinsic}$) is an inherent, density-independent property of a single channel, best described as a fraction of $P_{o,max}$. We thus repeated our calculations of GIRK1/2-available Gα and Gβγ assuming a $P_{o,intrinsic}$ in the range between 1% and 10% of $P_{o,max}$ (S6 Fig, panels A, B). For these calculations, Eq 6 (Methods) was modified in the following way:

$$I = i_{single} \cdot N \cdot P_{o,max} \cdot (\phi \cdot \sum_{1}^{4} f_{p,x} \cdot \phi_x + (1 - \phi)) \quad , \tag{4}$$

where Φ is the fraction of $P_{o,max}$ which is Gβγ-dependent (see Eqs 6 and 7 in the Methods for definitions of other parameters). In the whole range of $P_{o,intrinsic}$ tested, the estimation of 3–4 Gβγ per channel remained highly stable (S6 Fig). The estimate of less than 2 Gα per channel

also persisted except at the highest $P_{o,intrinsic}$ and low GIRK1/2 density, where Gα:GIRK ratio slightly exceeded 2 (S6B Fig, low surface density, black bar). Interestingly, for a significant Gβγ-independent intrinsic activity (10% of $P_{o,max}$), up to ~60% of macroscopic I_{basal} could be Gβγ-independent, especially at low channel densities which are common in native cells (S6C Fig). This finding may be relevant to some cells. For instance, coexpression of the Gβγ scavenger phosducin did not significantly reduce I_{basal} in atrial cardiomyocytes [94], where the predominant channel is GIRK1/4.

Finally, we considered the possible impact of variation in the presumed width (W) of the submembrane space within which the GIRK-Gβγ interactions occur. S6D and S6E Fig) shows that the main conclusions regarding the functional stoichiometry of GIRK, Gα and Gβγ remained largely unchanged over a wide range of W, 1–20 nm.

Activation of GIRK1/2 by coexpression of Gβγ: experiment and simulation

We next tested the ability of the model to predict a new result: the dose dependency of activation by Gβγ, using the estimates of available Gα and Gβγ calculated from basal and agonist-evoked currents. We injected increasing amounts of wt-Gβγ mRNA into oocytes expressing GIRK1/2 at a constant density, and monitored both GIRK currents and Gβγ expression.

Relative levels of Gβγ in the PM were directly measured in giant membrane patches of the oocytes [30,95] (Fig 6A) using the anti-Gβ antibody. Absolute surface densities of the expressed Gβγ (X axis in Fig 6C) were calculated assuming that 5 ng mRNA of Gβγ gives 30±4 molecules/μm^2 (n = 47 oocytes). This density was calculated based on 3 experiments performed during the same period as the experiments of Fig 6 and S8 Fig, with wt-Gβ and YFP-Gγ, and using YFP-GIRK1/2 as the molecular ruler.

As shown in Fig 6B, expression levels of Gβγ in the PM (grey bars) reached maximum at 5 ng RNA/oocyte. $I_{\beta\gamma}$ (red circles) reached maximum already at 1 ng Gβγ RNA. Thus, maximal activation of GIRK1/2 has been attained already at submaximal expression levels of Gβγ (see also S8 Fig). Channel density of 13.75 channels/μm^2 was calculated based on $I_{\beta\gamma}$ measured after expression of 5 ng RNA of exogenous Gβγ. Gβγ and Gα available to GIRK without the coexpression of exogenous Gβγ were calculated from I_{basal} and I_{total} (as in Fig 5), yielding ~43 molecules of Gβγ and 10 molecules Gα per μm^2. We remind that the high density of available "endogenous" Gβγ in the presence of GIRK1/2 is due to Gβγ recruitment, explaining the high I_{basal} and the relatively low index of activation of GIRK by Gβγ in a given oocyte, $R_{\beta\gamma}$. ($R_{\beta\gamma}$ was defined as $I_{\beta\gamma}$/[average I_{basal}], where average I_{basal} was determined in a group of oocytes of the same experiment which expressed the channel without Gβγ. The definitions are as in [51]. See S2 Fig for definition of $R_{\beta\gamma}$).

Using the calculated GIRK1/2 density and the amounts of available Gα and Gβγ before coexpression of Gβγ, we next calculated the predicted $I_{\beta\gamma}$ and $R_{\beta\gamma}$ for a range of doses (surface densities) of exogenously coexpressed Gβγ (Fig 6C). The predicted dose-dependencies of $I_{\beta\gamma}$ and $R_{\beta\gamma}$ (blue lines) are in agreement with experimental data (red circles). Assuming that 5 ng/oocyte of Gβ RNA gives either less (20 Gβγ/μm^2) or more (44 Gβγ/μm^2) molecules of coexpressed Gβγ instead of 30 Gβγ/μm^2 produced similar predictions, still in good agreement with experiment (S7 Fig). Thus, the results of the simulations are relatively insensitive to a 50% variation in our estimate of coexpressed Gβγ. Further, very similar results were obtained in a separate experiment using a different experimental design, where we expressed increasing doses of Gβγ-YFP and calibrated Gβγ-YFP density using YFP-GIRK1/2 as molecular ruler (S8 Fig).

We note that, because channel's density is estimated from $I_{\beta\gamma}$ obtained with a saturating dose of Gβγ, the good agreement between measured and predicted $I_{\beta\gamma}$ at this RNA dose might

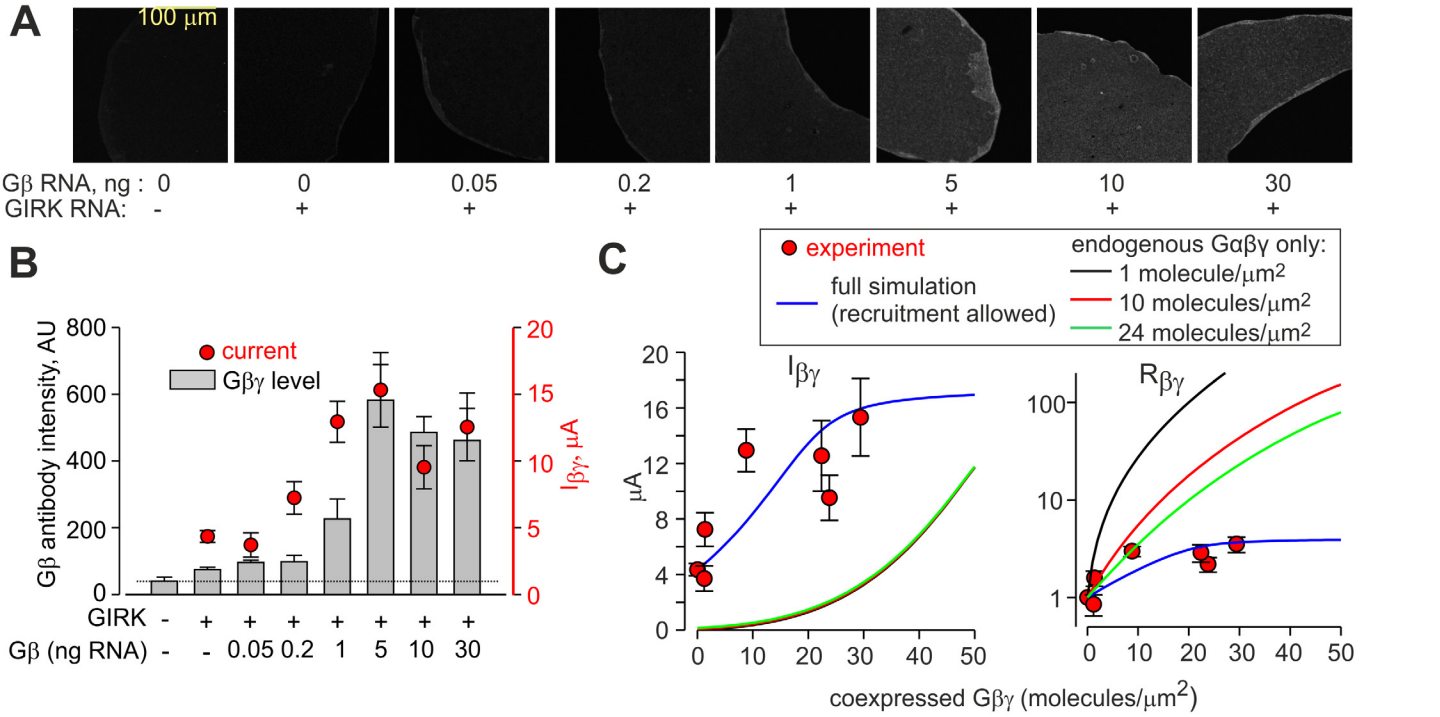

Fig 6. Dose-dependent activation of GIRK1/2 by coexpressed Gβγ: experiment and simulation. GIRK1/2 was expressed at 0.2 ng RNA. All data are mean ± SEM from one experiment. **(A)** Confocal images of Gβγ in giant excised plasma membranes stained with the anti-Gβ antibody. The intensity of all images was increased equally for a better viewing in this figure, but not in the process of image analysis. **(B)** Dose-dependence of Gβγ levels and $I_{βγ}$ in oocytes injected with incrementing amounts of wt Gβγ RNA (0.05–30 ng per oocyte). Gβγ expression in the PM (grey bars) was measured from images shown in A, in 4–8 oocyte membranes, and $I_{βγ}$ currents (red circles; right Y-axis) were measured in 12–16 oocytes. The dashed line shows the basal level of fluorescence, arising from the endogenous Gβγ. Note that, unlike in Western blots, in immunocytochemistry the antibody poorly recognized the endogenous Gβγ compared to the expressed bovine Gβγ. **(C)** Comparison of measured $I_{βγ}$ and $R_{βγ}$ (red circles) and simulated currents (curves). The relative Gβγ levels (from grey bars in B) have been converted into surface densities assuming that 5 ng Gβγ gives 30 molecules Gβγ/μm^2. The blue line presents the simulation using graded contribution model and amounts of Gα and Gβγ (prior to coexpression of Gβγ) calculated using the methods described above: channel density was calculated from $I_{βγ}$ (13.75 channels/μm^2 with 5 ng Gβγ RNA in this experiment), and Gβγ and Gα were estimated from I_{total} and I_{basal}, giving 3.16 and 0.73 Gβγ:GIRK and Gα:GIRK ratios, respectively. For simulation with endogenous G proteins only and no Gβγ recruitment allowed (red, black and green lines), the channel density was the same and 1, 10 or 24 endogenous Gαβγ were assumed to be available for GIRK1/2.

doi:10.1371/journal.pcbi.1004598.g006

be expected. However, the densities of Gα and Gβγ available to GIRK before coexpression of exogenous Gβγ (0 point on X-axis in Fig 6C) are calculated from I_{basal} and I_{evoked}. Therefore, in both experiments (Fig 6 and S8 Fig), the satisfactory predictions of $I_{βγ}$ and $R_{βγ}$ at intermediate Gβγ doses, or the shape of the dose-response curves of $I_{βγ}$ and $R_{βγ}$ vs. Gβγ density, do not result from circular reasoning and are not trivial. This is illustrated by showing simulations that assume equal amounts of endogenous Gα and Gβγ (1, 10 or 24 molecules/μm^2) available for GIRK1/2, and no Gβγ recruitment. The use of these "classical" assumptions failed to reproduce the experimental data (black, red and green lines in Fig 6C and S7 Fig). In particular, saturation of $R_{βγ}$ was predicted to happen at much higher doses of coexpressed Gβγ than in the experiment, obviously because the presumed initial basal level of Gβγ available to the channels was too low, thus requiring expression of more additional Gβγ.

Application of the model to the HEK293 expression system and hippocampal neurons

We next evaluated the model's applicability to another expression system (HEK293 cells), and also to hippocampal neurons that natively express GIRK1/2 channels. We re-grouped raw data

Table 4. GIRK currents in mouse hippocampal neurons and in GIRK1/2-expressing *Xenopus* oocytes and HEK293 cells. Data are presented as mean ± SEM. Current amplitudes in HEK293 cells and neurons were adjusted to 24 mM K^+ (as in oocytes) as described in Methods.

I_{basal} range, pA/pF	corresponding I_{basal} in oocytes	cell type	I_{basal}, pA/pF	I_{evoked}, pA/pF	I_{total}, pA/pF	R_a	n
0.5–3	0.1–0.6 μA	neurons	1.8±0.1	13.5±2.3	15.3±2.3	9.4±1.3	25
		oocytes	1.82±0.1	4.2±0.4	6.0±0.4	3.5±0.3	29
		HEK cells	1.51±0.2	10.5±3	12.03±3	8.3±2	8
3–13	0.6–2.6 μA	neurons	5.8±0.4	19.9±2.3	25.7±2.3	4.8±0.5	29
		oocytes	7.2±0.4	10±0.8	17±0.9	2.5±0.1	74
		HEK cells	6.4±1.1	16±7	22.8±6.7	4.3±1.7	5
13–50	2.6–10 μA	neurons	17.3±2.2	26.1±6.5	43.4±6.2	2.7±0.5	6
		oocytes	28±0.9	15.6±1	43.6±1.3	1.6±0.04	128
		HEK cells	25.7±3.1	34±7	60±9	2.4±0.2	9
>50	>10 μA	neurons	-	-	-	-	-
		oocytes	65.9±2.1	84.5±2.7	84.5±2.7	1.3±0.03	41
		HEK cells	67.6±4.6	96±28	164±26	2.5±0.5	3

doi:10.1371/journal.pcbi.1004598.t004

previously obtained in HEK cells expressing m2R and GIRK1/2 [51] (Table 2), the data from cultured hippocampal neurons (Fig 1), and the data obtained in oocytes, in a uniform manner. To enable direct comparison between the different systems, we arbitrarily segregated all the recordings into 4 groups, based on basal GIRK currents: <3 pA/pF, 3–13 pA/pF, 13–50 pA/pF and > 50 pA/pF (Table 4). For modeling, we needed to estimate channel surface densities, which have not been directly measured in HEK293 cells and neurons. To this end, we used I_{total} to indirectly assess the channel densities. The ratio $I_{\beta\gamma}/I_{total}$ is fairly consistent in oocytes and HEK cells, ranging between 1.6 and 2.2 (Table 1 and ref. [96]). Thus, for each I_{basal} range, we calculated $I_{\beta\gamma}$ from I_{total} assuming $I_{\beta\gamma}/I_{total} = 2$ (Fig 7). Then we calculated densities using Eq 2 and $P_{o,max}$ of 0.105, as measured in oocytes.

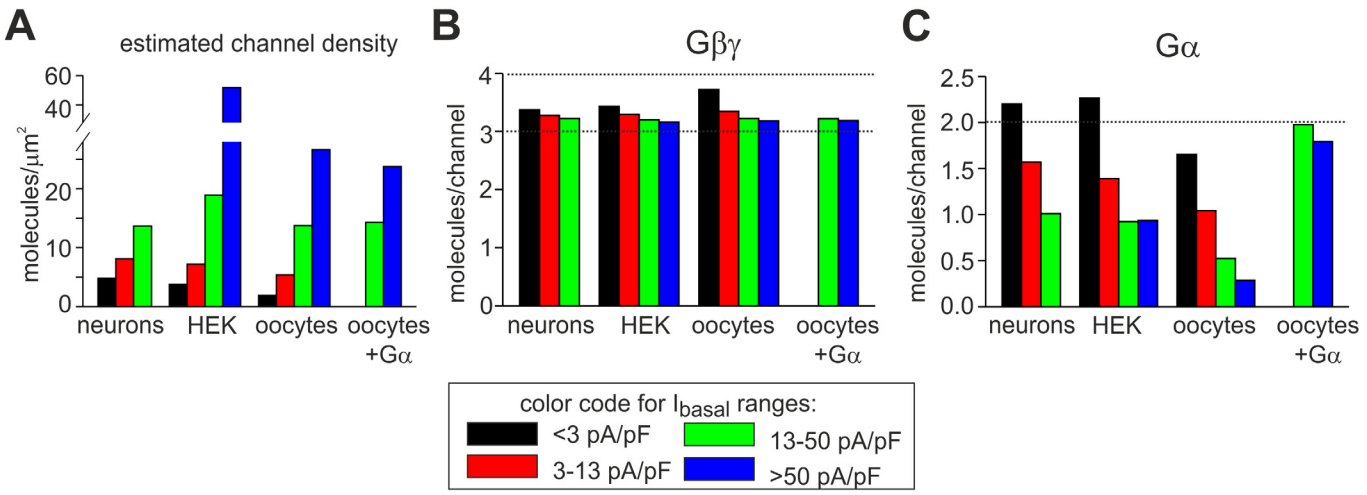

Fig 7. Estimated densities and calculated functional stoichiometries of the GIRK channel, Gβγ and $G\alpha_{i/o}$ in oocytes, HEK293 cells and neurons. Comparison of cultured mouse hippocampal neurons, and in oocytes and HEK293 cells expressing GIRK1/2. **(A)** Cells were subdivided into four groups according to the indicated I_{basal} ranges, and channel densities were estimated assuming $I_{\beta\gamma} = 2I_{total}$ and $P_{o,max} = 0.105$. Densities in Gα expression experiments in oocytes were estimated from I_{total} in control groups of oocytes expressing GIRK1/2 and m2R only. **(B, C)** Estimates of Gβγ and Gα available for GIRK activation in the 4 channel density groups. In oocytes and HEK293 cells I_{evoked} was elicited by ACh via m2R, in neurons—by baclofen acting on $GABA_B$ receptors.

doi:10.1371/journal.pcbi.1004598.g007

The segregation of GIRK activity by I_{basal} yielded relatively similar channel density groups in all cell types; neurons did not appear to express large amounts of GIRK, and the high density group was empty (Fig 7A). Next, using the procedure of Fig 5, we calculated the Gβγ and then Gα available for GIRK in all cases (Fig 7B and 7C). In all three systems, the relationship between G protein subunits and channel density was very similar to that found in oocytes. The most striking result was the persistent, channel density-independent availability of more than 3 Gβγ molecules per channel (Fig 7B). In all cases, the estimated Gα:GIRK ratio was about 2 for the low channel densities, but this number decreased as channel density increased (Fig 7C). Nevertheless, estimates of Gα:GIRK ratio in oocytes were lower than in HEK cells or neurons, indicating that there was a relative shortage of GIRK-associated $G\alpha_{i/o}$ in oocytes. We have therefore reanalyzed the experiments [30] in which Gα was co-expressed in oocytes in 5–10 fold excess (in terms of RNA quantities) over GIRK1/2 (Fig 7, denoted as "oocytes+Gα"). These doses produced the maximal GIRK-specific "priming" effect of $G\alpha_{i3}$: strong reduction in I_{basal} and increase in I_{evoked} without a significant reduction in I_{total} (S1 Table). To note, coexpression of $G\alpha_{i3}$ also produced R_a of ~10 which was comparable to the neurons with the lowest I_{basal} and highest R_a (compare S1 Table and Table 4). Calculation of available Gβγ and Gα showed a robust persistence of Gβγ:GIRK ratio of above 3 (Fig 7B). Expectedly, the estimate of the available Gα greatly increased after $G\alpha_{i3}$ overexpression, but, remarkably, Gα:GIRK ratio did not exceed 2 Gα molecules/channel (Fig 7C).

Variations in $I_{\beta\gamma}/I_{total}$ ratio and $P_{o,max}$ in different cells could bias our estimates of channel density (Eq 2) and thus also estimates of Gβγ and Gα. Therefore, for neurons, we repeated our calculations for a range of $I_{\beta\gamma}/I_{total}$ ratios between 1.5 and 3 (S9A Fig) and $P_{o,max}$ between 0.05 and 0.2 (S9C Fig). For comparison, a similar range of $I_{\beta\gamma}/I_{total}$ ratios was also tested for the oocyte data (S9B Fig). The exact values of Gβγ:GIRK and Gα:GIRK ratios varied, especially with changes in $I_{\beta\gamma}/I_{total}$ ratio. Generally, the lowest channel density is most sensitive to perturbations, and, for $I_{\beta\gamma}/I_{total}$ = 1.5 (the lowest ratio tested), calculated Gβγ:GIRK and Gα:GIRK ratios exceed our usual estimates. However, this ratio is lower than that observed experimentally (Table 1), likely causing an overestimate of the values of Gβγ and Gα. In all, although the absence of direct measurements of channel densities and $P_{o,max}$ in HEK cells and neurons introduces an element of uncertainty, our results support the functional stoichiometry of 3–4 Gβγ and 2 or less Gα molecules per GIRK1/2 channel. Importantly, for a wide range of parameters, the main trends persist: available Gβγ is in excess over Gα; Gβγ:GIRK ratio remains high (>3) whereas Gα:GIRK ratio decreases as I_{basal} increases.

Changes in functional stoichiometry of GIRK, Gβγ and Gα explain the inverse R_a-I_{basal} correlation

The systematic study presented above supports our hypothesis [51] that the inverse R_a-I_{basal} relationship for GIRK1/2 reflects a progressive decline in GIRK1/2-associated Gα relative to Gβγ. We could now test this hypothesis quantitatively, and establish whether the calculated changes in GIRK:Gα:Gβγ functional stoichiometry can fully account for the R_a-I_{basal} relationship shown in Fig 1. To this end, we simulated the changes in R_a as a function of I_{basal} for a range of channel densities. We used channel densities, I_{basal} values and Gβγ:GIRK and Gα:GIRK ratios calculated above (Tables 1 and 3 for oocytes, Table 4 for neurons). No free parameters were allowed. The results are shown in Fig 8, for oocytes (grey circles) and hippocampal neurons (black triangles). At this point, the channel density estimates and thus the simulations for oocytes are more reliable than for neurons.

First, for simplicity, we assumed a constant Gβγ:GIRK ratio at all densities (3.5 in oocytes and 3.4 in neurons; see Fig 7). For further simulations, in order to construct continuous curves,

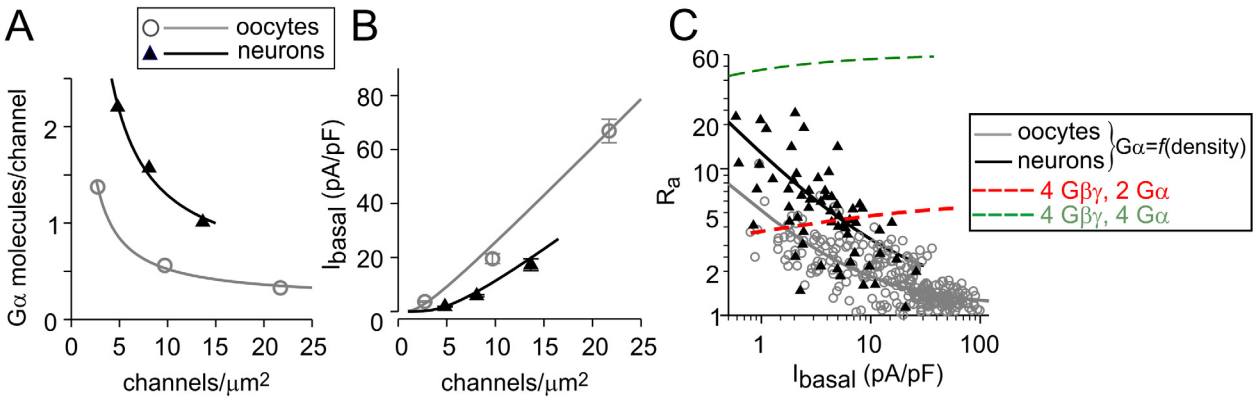

Fig 8. Inverse relation between I_{basal} and R_a arises from the decrease in Gα available for GIRK activation at higher I_{basal}. (A) Gα molecules/channel as a function of channel density. Data for Gα:GIRK and channel density were adopted from Tables 1 and 3 (oocytes) and Table 4 (neurons). To generate a continuous curve, the channel density-Gα relationship was arbitrary fitted with a hyperbolic decay function of the form $G\alpha = Y_o + a/x$, where x is channel density and *a* is a constant. **(B)** Simulated relation between I_{basal} and channel density. We utilized eqs 5–15 and solved them numerically in the 1–30 channels/μm^2 range, using constant values of Gβγ:GIRK ratio (3.5 for oocytes and 3.4 for neurons) and the calculated values of Gα:GIRK from the fitted curves shown in A. **(C)** Simulated relationship of I_{basal} and R_a, with variable Gα:GIRK (from A) and constant Gβγ:GIRK ratios. Simulations with 4 Gβγ and 2 Gα (red line) or 4 Gβγ and 4 Gα (green line) available for one GIRK1/2 channel at all densities did not adequately describe the data.

doi:10.1371/journal.pcbi.1004598.g008

we needed to assign numeric values for Gα:GIRK ratios within the full range of channel densities, based on the individual data points calculated for the "density groups" (Fig 8A). Since the reduction in Gα:GIRK ratio as a function of channel density is a process of unknown nature, the data points were arbitrarily fitted to a hyperbolic function (Fig 8A, solid lines). Next, we simulated the relation between I_{basal} and channel density, by substituting the obtained values of Gα:GIRK into eqs 5–15 (Fig 8B). The simulation gave a good match to data of Table 1 (oocytes) and Table 4 (neurons), indicating that the fitting procedure of Fig 8A was satisfactory. Finally, values of Gα:GIRK from Fig 8A and I_{basal} from Fig 8B were used to simulate the R_a-I_{basal} relationship (Fig 8C, solid black and grey lines), matching well the raw data (triangles and circles). Simulations based on a constant relations of GIRK, Gα and Gβγ at all channel densities (allowing Gβγ and Gα recruitment) could not account for the observed trend in R_a changes. This is exemplified for a 1:4:2 and 1:4:4 GIRK:Gβγ:Gα stoichiometry (Fig 8C, red and green dashed lines, respectively). We conclude that the decrease in Gα available for GIRK activation at higher I_{basal} can fully account for the inverse R_a-I_{basal} relationship in both experimental systems.

Discussion

General summary

In this work we have quantitatively analyzed the GPCR-$G_{i/o}$-GIRK1/2 cascade, focusing on basal (I_{basal}) and agonist-evoked (I_{evoked}) activities, both of which regulate neuronal excitability. We developed a mathematical model which allows quantification and simulation of macroscopic GIRK1/2 currents under steady-state conditions, before and after activation by neurotransmitter or by Gβγ. Our simulations fully rested on experimental data and parameters obtained in this and previous works. The modeling accurately described basal and evoked GIRK1/2 currents in two expression systems and in hippocampal neurons in a wide range of channel's surface densities, correctly predicted the dose-dependent activation of GIRK1/2 by coexpressed Gβγ in *Xenopus* oocytes, and fully accounted for the inverse correlation between I_{basal} and agonist activation index (R_a) previously observed in heterologous systems and, as shown here, also in hippocampal neurons. Our experimental findings and the model lay the

basis for further analysis of the GPCR-$G_{i/o}$-GIRK cascade, for example for GIRKs of different subunit composition, and in different cells.

Importantly, the present quantitative analysis provides novel and often unanticipated insights into the mechanisms of GIRK regulation by G protein subunits, Gβγ and $G\alpha^{GDP}$. It reveals an unequal and, moreover, variable functional GIRK1/2:Gβγ:Gα stoichiometry: 1) Under all conditions tested, between 3 and 4 Gβγ dimers are available for GIRK1/2; 2) Only two or less Gα are available per GIRK1/2 channel; 3) Increase of GIRK1/2 surface density is accompanied by a proportional increase in Gβγ (which is recruited by the channel), but not Gα. The unequal, effector-dependent Gα-Gβγ stoichiometry within the GIRK1/2 signaling cascade is an unexpected departure from classical schemes which usually assume that, prior to GPCR activation, the heterotrimeric G proteins available to the effector exist as stoichiometric complexes of Gα and Gβγ [97]. We propose that the unique functional stoichiometry of GIRK1/2 with G protein subunits, and the cooperative nature of GIRK gating by Gβγ, underlie the complex pattern of basal and agonist-evoked activities and allow GIRK1/2 to act as a sensitive bidirectional detector of both Gβγ and $G\alpha^{GDP}$.

Our conceptual model of GIRK1/2 regulation (Fig 9) rests on the main findings of this study regarding the GIRK1/2:Gβγ:Gα stoichiometry (points 1–3 above) and the notion that, for Gβγ to activate GIRK, it must have its Gα-interacting interface exposed and free to contact GIRK [19,92,98,99]. In the resting state, the channel's environment is enriched in 3–4 molecules of Gβγ and 1–2 Gα. In this scenario, between one and three Gβγ molecules are not associated with $G\alpha^{GDP}$ and can bind and activate GIRK, resulting in a basal activity that is between 1 and 26% of total $P_{o,max}$ (see Fig 2C). Because of the gating cooperativity, occupancy of the first two Gβγ-binding sites yields low I_{basal}. The fewer Gα, the more "free" Gβγ remains to occupy the activation sites at rest, yielding higher I_{basal}. After GPCR-induced separation of $G\alpha^{GTP}$ from Gβγ (lower arm of the scheme), due to gating cooperativity, addition of each Gα-free Gβγ ensures a robust 4–6 fold activation (e.g. going from 2 to 3 or 3 to 4 Gβγ-occupied sites). An even stronger activation takes place with a shift from 2 to 4 Gβγ-occupied sites (×16); and so on. Overexpression of Gβγ "sequesters" Gα and allows full occupancy of all Gβγ binding sites (middle arm of the scheme). Finally, overexpression of GIRK1/2 recruits Gβγ but not Gα, increasing Gβγ/Gα ratio (upper arm of the scheme). The balance between available $G\alpha^{GDP}$ and Gβγ yields a continuum of basal activity magnitudes even on the level of a single channel, and sensitively regulates the extent of activation by the agonist.

The scheme emphasizes the important fact that, given the relatively fixed amount of Gβγ available for GIRK1/2 activation, it is the availability of $G\alpha_{i/o}$ that determines the level of basal activity and, consequently, the extent of activation by agonists (as experimentally observed previously; [30,31]). The imbalance between Gβγ and Gα renders GIRK1/2 with a sizeable I_{basal}, allowing it to act as a bidirectional, servo-like device [51] where its activity can be regulated not only by positive (Gβγ, Na^+, PIP_2) but also negative ($G\alpha^{GDP}$, protein kinase C, $G\alpha_q^{GTP}$, PIP_2 depletion) stimuli.

Surface levels of GIRK and G proteins in *Xenopus* oocytes

Surface levels of endogenous G protein subunits and of heterologously expressed channels and G proteins crucially determine the behavior of the reconstituted signaling cascade, but they have never been quantitatively studied in the past in this common model system. We obtained very close estimates of surface levels of GIRK using two independent approaches: quantitative immunochemistry (which measures all channels in the PM) and electrophysiology (which counts only functional channels) (Fig 4). This indicated that the majority of GIRK1/2 channels in the PM of *Xenopus* oocytes were functional. Further use of GIRK1/2 as a molecular

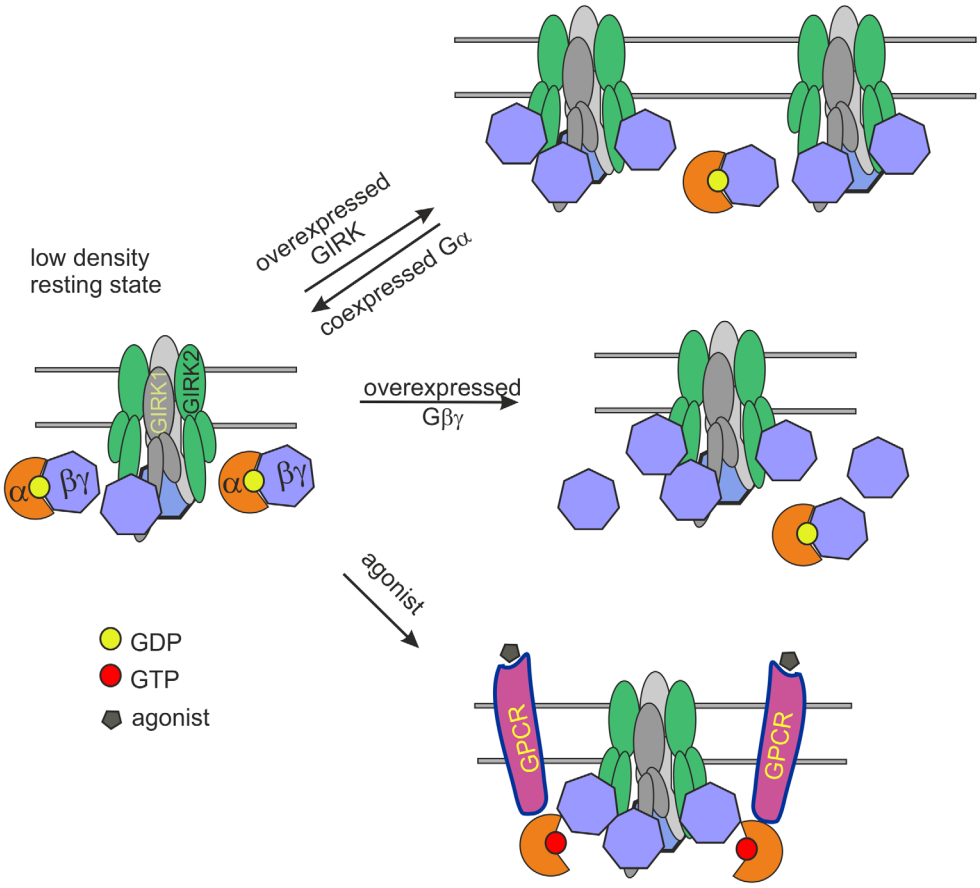

Fig 9. Schematic representation of the GPCR-G-protein-GIRK system. In resting state (no activated GPCR), the GIRK1/2 channel, a heterotetramer of 2 GIRK1 (grey) and 2 GIRK2 (green) subunits, is expected to interact with ~ 3–4 Gβγ subunits, two of which are bound to $G\alpha^{GDP}$ subunits (GDP is shown by a yellow circle). For simplicity, the hypothetical Gβγ anchoring sites (which may be separate or partly overlapping with the Gβγ-activation sites) are not shown. The interaction of GIRK with Gβγ subunits is reversible. $G\alpha^{GDP}$ can release the bound Gβγ in basal state, but since Gβγ-$G\alpha^{GDP}$ interaction is of a high affinity, the probability of GIRK activation due to this process is relatively low. Thus, at any given time the channel is occupied by 2–3 Gβγ molecules (with an open probability of 6–26% of $P_{o,max}$ as shown in Fig 2C). GIRK overexpression leads to a decrease in GIRK:Gα ratio but does not change the GIRK:Gβγ ratio due to the additional recruitment of Gβγ by GIRK1/2, thus effectively increasing the proportion of channels occupied by > 3 Gβγ molecules, leading to an increase in "basal" open probability. The opposite process occurs upon overexpression of Gα, leading to a decrease in free Gβγ available for channel activation. On expression of Gβγ, its availability for channel activation increases, leading to higher fraction of 4 Gβγ-occupied channels with an open probability close to $P_{o,max}$. Activation of G-proteins by an agonist (grey pentagon) via a GPCR (magenta) leads to an exchange of GDP to GTP (red circle) on Gα molecules, and to the subsequent dissociation of the Gαβγ heterotrimer, liberating additional Gβγ for channel activation.

doi:10.1371/journal.pcbi.1004598.g009

fluorescent ruler for Gβγ yielded Gβγ density very close to density estimated from quantitative immunochemistry, affirming the "molecular ruler" procedure with GIRK1/2 and lending additional support to the measurements of GIRK1/2 density.

We estimated total cellular endogenous Gβγ in the oocyte as ~170 nM, similar to other cell types, 200–800 nM [100] and to the recent high-precision mass spectrometry measurement of ~200 nM Gβ in Xenopus eggs [101]. Notably, examination of data reported in the latter work [101] suggests a total concentration of all Gα in *Xenopus* eggs of ~350 nM. Thus, total oocyte's Gβγ is not in excess over Gα, supporting our assumption (S4 Fig) that endogenous heterotrimeric G proteins are in the Gαβγ form before activation by GPCRs or coexpression of GIRK.

Our estimate of 24 molecules/μm^2 of endogenous PM-associated Gβγ, presumably as Gαβγ, is comparable to the ~40 molecules/μm^2 evaluated in HEK cells [102]. In terms of concentration, 24 molecules/μm^2 corresponds to ~4 μM, much higher than the cytosolic level of ~0.2 μM. Such enrichment of G proteins at the PM is expected, because of the lipid modification of both Gα and Gγ [84,103]. It is probable that a substantial fraction of the PM-associated endogenous Gβγ is not available for GIRK activation, being associated with $G\alpha_s$ or $G\alpha_q$ rather than $G\alpha_{i/o}$, or located in separate PM compartments, or associated with other effectors such as adenylyl cyclase [104]. Simulations showed that the main conclusions of our study are not affected by assuming a wide range of endogenous $G_{i/o}$ proteins available for GIRK, from 1 to 24 molecules/μm^2.

In this work, we varied the levels of heterologously expressed GIRK1/2 and Gβγ. For GIRK1/2, the surface densities ranged from about 1 to 30 molecules/μm^2 in oocytes and about 1–60 channels/μm^2 in HEK293 cells (Table 4 and Fig 7). Densities of <20 channels/μm^2 were estimated in cultured hippocampal neurons (Fig 7A). This is comparable to 9–10 channels/μm^2 found in spines of cerebellar Purkinje neurons by quantitative electron microscopy [105]. Thus, the "low" and "intermediate" densities of expressed GIRK1/2 and Gβγ in oocytes and HEK293 cells may be the most physiologically relevant.

Modeling GIRK1/2 regulation by Gβγ in basal and agonist-activated states

For our description of GIRK currents, we have considered several models of GIRK channel gating by Gβγ (Fig 2B): the previously developed "concerted activation" model [58], the"graded contribution" model, and a more general model that includes 4 to 5 closed-open transitions. We were able to show that the latter two models converge to the same form of description of macroscopic steady-state P_o based on fractional contributions of channels occupied by 1 to 4 Gβγ molecules, experimentally demonstrated for GIRK1/4 [13,14] (see Results and Supplemental Discussion S2 Text for a detailed discussion). We have therefore chosen the graded contribution model as our main tool to simulate and predict GIRK1/2 currents. Despite its relative simplicity, this model incorporates several complex properties of GIRK gating, and provides a strong computational tool for the analysis of the G protein-GIRK signaling. First, in this model we implemented the gating cooperativity of GIRK, by including the graded contribution of each bound Gβγ to channel opening (Fig 2C). Second, to our knowledge, this is the first model to describe both basal and agonist-evoked GIRK activity. Third, the model allows to estimate the amount of G protein subunits available for channel activation without any *a priori* assumptions regarding the levels of endogenous Gα or Gβγ; the GIRK-available Gα and Gβγ are calculated from experimental data (Fig 5). Finally, our method of calculating the functional stoichiometry of GIRK and Gβγ applies even if I_{basal} is partly due to the presence of a GPCR activated by low dose of an ambient neurotransmitter. In this case, the available Gα calculated using the method of Fig 5 will represent only that fraction of GIRK-coupled Gα that is still in its GDP-bound form.

In this work we left aside auxiliary/modulatory proteins such as RGS, focusing on the minimal essential composition of the cascade. We also have not addressed the impact of direct GIRK-Gα interaction. We and others did not find significant direct effects of $G\alpha_i^{GDP}$ on GIRK1/2 gating; the main function of $G\alpha^{GDP}$ is the prevention of basal activation of the channel by ambient Gβγ and the release of Gβγ for channel activation by agonist/GPCR [31,34,36,106]. This function is fully implemented in our model. As for $G\alpha_i^{GTP}$, it regulates the kinetics of I_{evoked} of GIRK1/2 but barely affects the steady-state amplitude [29,36]. Our present results suggest that, for GIRK1/2, effects of activated $G\alpha^{GTP}$ on GIRK1/2 current amplitude are negligible,

within a possible ~10% error. These considerations justify the omission of Gα-GIRK binding reactions from model's equations. It remains possible that certain $G\alpha^{GTP}$ may differently regulate GIRK channels of other subunit compositions or under certain conditions [34,107].

Both graded contribution and concerted models showed that I_{basal} and I_{evoked} of the expressed GIRK1/2, and their changes with channel surface density, cannot be accurately described unless there is a recruitment of Gβγ to the PM by the channel. Recruitment of Gα is probably negligible (S4 Fig, Table 3). The prediction of preferential availability of Gβγ over Gα for GIRK1/2 concurs with the experimental findings [25], supporting the model's validity. Further validation came from predicting the system's response to perturbation in the form of dose-dependent response to coexpression of Gβγ, producing a satisfactory simulation of both $I_{\beta\gamma}$ and $R_{\beta\gamma}$ (Fig 6, S7 and S8 Figs). Finally, on the basis of experimental data and the calculated molar ratios of GIRK:Gβγ:Gα for different channel densities, the model fully accounted for the inverse correlation between R_a and I_{basal} in GIRK1/2 (Fig 8), which was the starting point of this endeavor.

We also made the first steps to extend the model to hippocampal neurons. The analysis of GIRK behavior in HEK cells and hippocampal neurons yielded estimates of Gβγ:GIRK and Gα:GIRK ratios close to those obtained in oocytes (3–4 Gβγ and $\leq$ 2 Gα), and a satisfactory simulation of the inverse R_a-I_{basal} relation observed in the neurons (Fig 8). Uncertainties remain, because calculation of channel density in neurons relied on oocyte and partly HEK cell data for $I_{\beta\gamma}/I_{total}$ ratios and $P_{o,max}$. A variety of GIRK compositions and distinct localization and density in cellular compartments further complicate the picture. Future quantitative studies are warranted for a more accurate description of GIRK activity in various neurons.

Functional stoichiometry of GIRK and G protein subunits

Our analysis provides two major insights into functional stoichiometry of GIRK1/2 vs. the G protein subunits. First, the molar ratios are both uneven and can change as a function of channels' density in the PM. The stoichiometry of more than 3 Gβγ per GIRK1/2 is practically invariable, whereas the amount of available $G\alpha_{i/o}$ is lower than Gβγ and further drops sharply as the level of expression of the channel increases. These estimates of Gβγ and Gα availability remained remarkably stable under a wide range of potentially variable parameters, such as K_D of GIRK-Gβγ binding, the extent of Gβγ-independent basal activity, the size of submembrane reaction space, the $I_{total}/I_{\beta\gamma}$ ratio and $P_{o,max}$ in neurons, etc. Second, unexpectedly, the limiting stoichiometry for Gβγ:Gα:GIRK is 4:2:1.

The uneven Gβγ:Gα stoichiometry and the decrease in Gβγ:Gα ratio were suggested by previous qualitative findings [50,51]. Our new results support this hypothesis and provide new insights into the underlying mechanism. Assumptions of pre-assembly of GIRK1/2 with 1, 2, 3 or 4 Gαβγ heterotrimers failed to recapitulate the observed macroscopic currents and R_a (S4 Fig). The decrease in Gα/GIRK ratio as channel's levels increase is consistent with total PM concentration of $G\alpha_{i/o}$ being relatively constant at all GIRK1/2 densities (Table 3). This is in agreement with little or no recruitment of Gα to the PM by GIRK1/2 [25,50]. On the other hand, the total amount of GIRK-available Gβγ in the PM increases as more GIRK1/2 channels are expressed, substantially exceeding the "basal" concentration of Gβγ of the naïve oocytes. The conspicuous persistence of Gβ:GIRK stoichiometry is best demonstrated in the oocytes, where it rests on a full quantitative analysis of experimental data. The identical estimates obtained in HEK cells and neurons (Fig 7B), though based on partial data, provide further support. The ability of GIRK1/2 to sustain a steady Gβγ-enriched environment strongly argues for a strong association between Gβγ and GIRK1/2, in line with the proposed high-affinity "anchoring" and recruitment of Gβγ by GIRK1 [25]. The mechanism of Gβγ recruitment is

unknown but may be due to co-trafficking from the endoplasmic reticulum [22] or "kinetic scaffolding" and similar mechanisms [63,108,109], as discussed in [25]. At present we cannot rule out that the participation of another Gβγ-binding PM protein, such as a GPCR, or unknown scaffolding proteins, is important for the enrichment of Gβγ.

It is widely accepted that the GIRK signaling cascade occurs within signaling complexes of GIRK channels with subunits of $G_{i/o}$ heterotrimeric proteins and some GPCRs (reviewed in [4,61,110,111,112]). The uneven and variable stoichiometry within the GIRK1/2-Gβγ-$G\alpha_i$ signaling complex revealed by this study is compatible with a high-affinity, dynamic complex, where the channel and the G protein subunits are allowed to dissociate and reassociate in the PM [113]. These considerations justify our use of standard kinetic formalism for modeling. Finite affinity and reversibility of GIRK-Gβγ interaction is also supported by the demonstration of competition between two Gβγ effectors, GIRK and voltage-gated calcium channels, for available Gβγ in sympathetic neurons [114], and by recent GIRK2 reconstitution studies in lipid bilayers [106].

In contrast to Gβγ, our present analysis supports the notion [36,51,106] that, at least in heterologous or artificial systems, $G\alpha_{i/o}^{GDP}$ is not an obligatory partner in the complex. Notably, in neurons and HEK cells the calculated Gα:GIRK ratios are higher than in oocytes (Fig 7 and Table 4); thus the higher R_a in these cells. The greater availability of Gα in HEK cells and neurons may reflect the presence of scaffolding or trafficking aids absent in the oocytes. However, the inverse R_a-I_{basal} correlation and the (calculated) reduction in Gα at high channel densities are maintained in neurons and HEK cells, supporting the expendability of Gα.

The apparent limiting stoichiometry of 4 Gβγ molecules per channel is not surprising, since the model explicitly includes 4 Gβγ-binding sites per channel. However, the calculated availability of two or less $G\alpha_{i/o}^{GDP}$, under most conditions examined, was unexpected. The limit of 2 Gα per channel was only slightly exceeded in simulations of lowest channel densities and when allowing substantial deviations from our standard assumptions (S9 Fig). Most conspicuously, overexpression of $G\alpha_{i3}$, which reduced I_{basal} by 75–80% and elevated the activation index R_a to about 10, increased the calculated Gα:GIRK ratio from less than 0.5 to 2—but no more—Gα molecules per channel (Fig 7, S1 Table). Taken together, our results point to a limiting stoichiometry of 2 Gα molecules available for a GIRK1/2 channel. It is not clear what limits the amount of available Gα, but it is tempting to speculate that this limit reflects the maximal number of Gα molecules that can interact with GIRK1/2. The actual stoichiometry of this interaction is unknown, but the NMR study of Shimada and colleagues [115] indicates that the interacting surface of $G\alpha^{GTP}$ requires two GIRK1 subunits of a GIRK1 tetramer for full contact. One GIRK1 subunit interacts with the helical domain of Gα and the other one with the GTPase domain [115].

We emphasize that our conclusions are valid for GIRK1/2 but may not be so for other GIRK channels. Thus, homomeric GIRK2 channels, with their low I_{basal} and very high response to Gβγ, do not recruit Gβγ to the PM [25] and probably do not show pre-association with 3–4 Gβγ, or may have more Gα. Excess of Gβγ over Gα has been observed in the phototransduction cascade [116,117] though it has not been linked to any effector. We speculate that effector-dependent changes in the balance of Gα and Gβγ may take place with effectors other than GIRK, playing a role in their regulation.

Materials and Methods

Ethics statement

All experiments were approved by Tel Aviv University Committee for Animal Use and Care (permits M-08-081 and M-13-002 for *Xenopus* frogs and M-12-061 for mice).

Animals and oocyte culture

Female frogs, maintained at 20±2°C on 10 h light/14 h dark cycle, were anaesthetized in a 0.17% solution of procaine methanesulphonate (MS222), and portions of ovary were removed through a small incision on the abdomen. The incision was sutured, and the animal was held in a separate tank until it had fully recovered from the anesthesia and then returned to the tank. The animals did not show any signs of postoperational distress and were allowed to recover for at least 3 months until the next surgery. Following the final collection of oocytes, anaesthetized frogs were killed by decapitation and double pithing. *Xenopus* oocytes were injected with RNA, and incubated in for 3–4 days at 20–22°C in NDE-96 solution (in mM: 96 NaCl, 2 KCl, 1 $CaCl_2$, 1 $MgCl_2$, 2.5 Na-pyruvate, 50 μg/ml gentamycin, 5 mM HEPES/NaOH, pH 7.5). All experiments with nerve cells derived from newborn mice, that have been analyzed in this paper, have been performed previously [47], and no additional mice have been used.

Antibodies, cDNA constructs, proteins and RNAs

The anti-GIRK1 polyclonal antibody was from Alomone Labs (Jerusalem), #APC-005. This antibody was raised against the distal C-terminal residues 437–501 of mouse GIRK1. 3 μg/mL were used for Western blots. The anti-Gβ polyclonal antibody (T-20, from Santa Cruz. #sc-378) is directed against the last 50 amino acids (a.a.) of mouse Gβ. 0.4 μg/mL were used for Western blots.

Most DNA constructs were as reported previously: bovine $G\beta_1$, bovine $G\gamma_2$, human muscarinic type 2 receptor (M2R), human Gαi3, rat GIRK1, mouse GIRK2, YFP-GIRK1, GIRK2-HA, $G\beta_1$-YFP, $G\gamma_2$-YFP and $G\gamma_2$-CFP [36,51,57]. To compare antibody labeling efficiency of bovine vs. *Xenopus* Gβ, we created the YFP-Gβ-XL construct in which the last 50 amino acids of the C-terminus in bovine Gβ were made identical to those of *Xenopus* $G\beta_1$, by mutating 7 a.a.: V296I, A299C, A302R, D303E, A305V, A309S and D322S by standard PCR protocols. Preparation and storage of $G\beta_1\gamma_2$ and of the GST-fused distal C-terminus of GIRK1, GST-dCT (a.a.365-501) used for calibrations of Fig 4A were done as described previously [69,118]. RNA was synthesized *in vitro* [57]. Amounts of injected RNA are indicated in the text, Tables 1, S1 and in Figure legends.

Confocal imaging and calculation of surface density of Gβγ-YFP

Fluorescence levels of the expressed YFP (yellow fluorescent protein) and cerulean (termed here CFP, cyan fluorescent protein) were measured in intact *Xenopus* oocytes essentially as described [25,32]. Both YFP and CFP carried mutations that increase stability and reduce dimerization [32]. Briefly, oocytes were imaged in ND96 solution in a 0.7 mm glass-bottom dish using Zeiss 510META confocal microscope with a 20× air objective. Images were acquired in the spectral mode. CFP was excited at 405 nm and emission was measured at 481–492 nm. YFP was excited at 514 nm and emission was measured at 535–546 nm. Fluorescent signals were averaged from 3 regions of interest (ROI) using Zeiss LSM Image Browser, and averaged background measured at an area outside the cell was subtracted. The average signal from uninjected oocytes was subtracted for final analysis. Saturation of emission measurement was strictly avoided to ensure that the readout of the confocal microscope was linear within the range of measurement. All measurements were made in the linear range of the recording apparatus.

In calculating Gβγ surface density through comparing fluorescent signals from YFP-GIRK and Gβγ-YFP, the fluorescent intensities of the two proteins were compared directly from oocytes of the same batch on the same day, as described in Fig 4D. No correction for non-fluorescent (improperly folded) YFP [119] was needed (assuming that the percent of misfolding

was similar in all YFP fusion proteins used here), because the ionic current $I_{\beta\gamma}$ (a fluorescence-independent parameter) was used as the basis for GIRK density estimates.

Giant membrane patches of oocyte membrane were prepared and imaged as described [25,95]. For imaging, fixated membranes were immunostained with the anti-Gβ antibody at 1:200 dilution. Cy3-conjugated anti-rabbit secondary antibody (Jackson ImmunoResearch) was used for imaging with the 543 nm laser, and excitation was measured at 566–577 nm. Background fluorescence from an area outside the giant patch was subtracted. For final analysis shown in Fig 6, the signal from uninjected oocytes was subtracted from all groups.

Biochemistry

Manual separation of plasma membranes from the rest of the oocyte ("cytosol") was performed as described [81], with modifications. Plasma membranes together with the vitelline membranes (extracellular collagen-like matrix) were removed manually with fine forceps after a 5–15 min incubation in a low osmolarity solution (5 mM NaCl, 5 mM HEPES, and protease inhibitors (Roche Complete Protease Inhibitors Cocktail, 1 tablet/50 ml), pH = 7.5). The remainder of cell (cytosols) was processed separately. First, the nuclei were separated by centrifuge for 10 min at 700×g at 4°C. Plasma membranes and cytosols were solubilized in 35 μl running buffer (2% SDS, 10% glycerol, 5% β-mercaptoethanol, 0.05% Bromophenol Blue, 62.5 mM Tris-HCl pH 6.8) and heated to 65°C for 5 min. Samples were electrophoresed on 12% polyacrylamide-SDS gel, and transferred to nitrocellulose membranes for Western blotting with the various antisera. The signals were visualized using the SuperSignal kit (Thermo) and quantitated using ImageJ software (National Institutes of Health, USA).

Electrophysiology

Macroscopic current recording in neurons. Raw data from primary cultures of mouse hippocampal neurons used in the analysis of Figs 1 and 7 were from whole-cell patch clamp experiments. A subset of data shown (40 neurons out of 60) had been reported previously [47] but the I_{basal}-I_{evoked} relation has not been analyzed. The batch solution contained the low-K^+ bath solution (in mM: 145 NaCl, 4 KCl, 1.8 $CaCl_2$, 1 $MgCl_2$, 5.5 D-glucose, 5 HEPES/NaOH; pH 7.4), which was replaced to the high-K^+ solution for GIRK current measurement (in mM: 120 NaCl, 25 KCl, 1.8 $CaCl_2$, 1 $MgCl_2$, 5.5 D-glucose, 5 HEPES/NaOH; pH 7.4). Both external solutions contained 0.5 μM TTX and 0.5 mM kynurenic acid. Patch pipettes (3–5 MΩ) were filled with intracellular solution (in mM: 130 K-Gluconate, 0 or 6 NaCl, 1 EGTA, 1 $MgCl_2$, 10 HEPES, 2 MgATP, 0.3 Tris-GTP, 0.01 Tris-GDP, pH 7.3). Baclofen (Sigma) was added at 100 μM, sTertiapin-Q or rTertiapin-Q (TPNQ; Alomone labs, Jerusalem) at 100–120 nM [120]. We refrained from using Ba^{2+} as GIRK blocker in neurons because of its low specificity [1]. Indeed, 1 mM Ba^{2+} blocked a much greater fraction of the total inward current in high-K^+ solution (S1 Fig), confirming that additional Ba^{2+} -sensitive channels contribute to total basal conductance in these cells (e.g. [53]). In contrast, we used Ba^{2+} to block the expressed GIRK channels in *Xenopus* oocytes and HEK293 cells, which have negligible intrinsic (endogenous) Ba^{2+}-sensitive basal currents (S2 Fig) [120,121].

Current measurements in neurons were done at -70 mV. To correct for the difference in K^+ driving force when comparing whole-cell currents from neurons and oocytes (for Fig 7 and Table 4), correction to a holding potential of -80 mV was done assuming E_K = -37 mV in the 25 mM K^+ solution. 4 cells (out of 65) with I_{basal}<0.5 pA/pF were discarded because the recording was deemed unreliable owing to the low signal-to-noise ratio. One cell was found to be outlier by Grubb's test using GraphPad outlier calculator http://graphpad.com/quickcalcs/

Grubbs1.cfm. No correction has been made for the 1 mM difference in $[K]_{out}$ of oocyte's vs. neuronal high-K^+ solution (24 vs. 25 mM).

Macroscopic current recording in Xenopus oocytes. All experiments were done at 20–22°C essentially as described [51]. Data acquisition and analysis were done using pCLAMP (Molecular Devices, Sunnyvale, CA). Whole-cell currents were measured using two electrode voltage clamp in the ND96 (low K^+) solution and in a high K^+ solutions (24 mM K^+, isotonically replacing NaCl in ND96) as shown in S2 Fig. Currents were recorded at −80 mV, filtered at 500 Hz, and sampled at 5 or 10 kHz. Currents in oocytes were converted to densities, in pA/pF, assuming an oocyte's capacitance of 200 nF [88]. For analysis of correlation between I_{evoked} and R_a and for Table 1, new raw data in the low and high GIRK1/2 density groups (total of 41 cells) were combined with raw data collected for our previous publication [30] (20 cells). I_{basal} was measured after blocking all GIRK currents by 5 mM Ba^{2+} [31].

Patch clamp recordings in Xenopus oocytes. Patch clamp experiments were done using Axopatch 200B (Molecular Devices, Sunnyvale, CA). Currents were recorded at -80 mV, routinely filtered at 2 kHz and sampled at 20 kHz. In some patches we also used filtering at 5 kHz. Patch pipettes had resistances of 1.4–3.5 MΩ. Pipette solution contained, in mM: 144 KCl, 2 NaCl, 1 $MgCl_2$, 1 $CaCl_2$, 1 $GdCl_3$, 10 HEPES/KOH, pH 7.5. $GdCl_3$ completely inhibited the stretch-activated channels. The bath solution contained, in mM: 144 KCl, 2 $MgCl_2$, 6 NaCl, 1 EGTA, 10 HEPES/KOH, pH 7.5. To obtain single channel recordings, oocytes were injected with low doses of RNA of GIRK1 (10–50 pg), and RNA of GIRK2 was 1/2 to 1/3 of that (5–17 pg), to avoid the formation of GIRK2 homotetramers. In addition, 50 ng of the antisense oligonucleotide against oocyte's endogenous GIRK5 was injected to prevent the formation of GIRK1/5 channels [122]. Number of channels was estimated from overlaps of openings during the whole time of recording (at least 5 min). Single channel current (I_{single}) was calculated from all-point histograms of the original records [123], and open probability (Po) was obtained from event lists generated using idealization procedure based on 50% crossing criterion [124]. Po was calculated only from records that contained 1, 2 or 3 channels. Each recording lasted for at least 4 min and contained >10,000 openings. Thus, the probability of missing a channel was negligible ($p<10^{-248}$ for 1-channel records). In support, P_o in patches with 2 or 3 channels was similar (0.071±0.02, n = 2, and 0.078±0.021, n = 3, respectively) and even lower than in 1-channel patches (0.15±0.026, n = 3), opposite to what would be expected in the case of underestimation of channel number. GPCR-evoked GIRK1/2 activity was induced via the coexpressed m2R with 2 or 5 μM ACh in the patch pipette. 2 μM ACh is a saturating concentration for GIRK1/2 expressed in *Xenopus* oocytes [62]. Because a slow reduction of activity over several minutes was observed in some patches, ACh-induced P_o was estimated during the first minute of the record. For channels activated by coexpressed Gβγ, there was no decrease in P_o over >4 minutes, and the P_o was averaged from the first 4 minutes of the record.

Macroscopic current recording in HEK293 cells. Most of the data on GIRK1/2 expressed in HEK293 cells transfected with cDNAs of GIRK1 and GIRK2 and m2R (Tables 2 and 4; Fig 7) are from experiments described previously [51]. Data on $I_{\beta\gamma}$ in HEK cells have been obtained in the same series of experiments but have not been reported previously. HEK293 cells were transfected with cDNAs of GIRK1, GIRK2, m2R (0.5 μg each), without or with the edition of DNAs of Gβ1 and $G\alpha_{i3}$ (0.2 μg each). Whole cell recordings were performed at -80 mV with patch pipette solution containing, in mM: 130 KCl, 1 $MgCl_2$, 5 EGTA, 3 MgATP, 10 HEPES. Low-K bath solution contained, in mM: 140 NaCl, 4 KCl, 1.8 $CaCl_2$, 1.2 $MgCl_2$, 11 glucose, 2 $CdCl_2$, 5.5 HEPES. High-K bath solution contained 90 mM KCl and 54 mM NaCl, the rest was as in low-K solution. To compare with data from oocytes (for Fig 7 and Table 4), the correction factor to adjust for current amplitude difference in 90 mM K^+ (HEK293) vs. 24–25 mM K^+ solution (oocytes, neurons) was determined experimentally to be 3.27±0.14 (n = 7; measured in oocytes).

Modeling of Gβγ activation of GIRK1/2

In general, the macroscopic GIRK1/2 current, I, can be calculated utilizing a modified (Eq 1):

$$I = \quad I_{single} \cdot P_o \cdot N/f_{sc} \tag{5}$$

where I_{single} is a unitary current and N is the number of channels [1]. f_{cs} is a solution conversion factor between solutions used for whole-cell (24 mM K^+) and in cell-attached patches (144 mM K^+). f_{sc} was estimated as 4.63±0.26 (n = 6) by measuring GIRK currents in the same oocytes in the two solutions, in whole-cell configuration.

For the graded contribution model, we define P_o as:

$$P_o = P_{o,max} \cdot \sum_{1}^{4} f_{p,x} \cdot \phi_x \tag{6}$$

where $P_{o,max}$ is the maximal open probability, $f_{p,x}$ is the fraction of Po contributed by x Gβγ-occupied channel (x is an integer between 1 and 4), and the ϕ_x is the fraction of channels in the x Gβγ-occupied state and can be calculated according to:

$$\phi_x = \frac{[C_x]}{C_{total}} \tag{7}$$

where $[C_x]$ is the concentration of channels in x Gβγ-occupied state and C_{total} is the total channel concentration in membrane. For the concerted model, Eq 6 is reduced to

$$P_o = P_{o,max} \cdot \phi_4$$

where ϕ_4 is the fraction of channels with four bound molecules of Gβγ [58].

For the graded contribution model, we calculated values of $f_{p,x}$ based on data described by Ivanova-Nikolova et al. (1998)[13] rendering ~ 0.01, 0.06, 0.26 and 1 values corresponding to 1–4 Gβγ occupied states. Based on mass-action law and Fig 2B, GIRK1/2 channel activity can be described by the following system of eqs (8–12):

$$[C_0] \cdot [G\beta\gamma] = \frac{1}{4} K_D \cdot [C_1] \tag{8}$$

$$[C_1] \cdot [G\beta\gamma] = \frac{2}{3} K_D \cdot [C_2] \tag{9}$$

$$[C_2] \cdot [G\beta\gamma] = \frac{3}{2} K_D \cdot [C_3] \tag{10}$$

$$[C_3] \cdot [G\beta\gamma] = 4 \cdot K_D \cdot [C_4] \tag{11}$$

$$[C_0] + [C_1] + [C_2] + [C_3] + [C_4] = C_{total} \tag{12}$$

where the K_D is a dissociation constant of Gβγ and GIRK1/2. For our simulations we routinely used K_D = 50 nM as measured in direct biochemical experiments [90], but a range of other values has also been tested as explained in the Results.

For both concerted and graded contribution models, G protein dissociation reaction required for modeling of GIRK1/2 basal activity according to the schemes described in Fig 2B

is formulated as:

$$k_{on} \cdot [G\beta\gamma] \cdot [G\alpha_{GDP}] = k_{off} \cdot [G\alpha_{GDP}G\beta\gamma] \quad (13)$$

$$G\beta\gamma_{total} = [G\beta\gamma] + [G\alpha_{GDP}\beta\gamma] + [C_1] + 2 \cdot [C_2] + 3 \cdot [C_3] + 4 \cdot [C_4] \quad (14)$$

$$G\alpha_{total} = [G\alpha_{GDP}] + [G\alpha_{GDP}G\beta\gamma] \quad (15)$$

where $G\beta\gamma_{total}$ and $G\alpha_{total}$ are total concentrations of corresponding subunits available for interaction with the channel and k_{on} and k_{off} are association and dissociation constants of G_i protein subunits ($0.7 \bullet 10^6$ M^{-1} s^{-1} and 0.0013 s^{-1}, respectively [56]). Eqs 8–12, combined with Eqs (13–15) is the most general form of description of a system containing GIRK channel and G proteins. For simulation of agonist-evoked activity, with saturating doses of both GPCR and agonist, we assumed a complete dissociation of G- protein heterotrimer [63,64] and thus Eq 14 is changed to:

$$G\beta\gamma_{total} = [G\beta\gamma] + [C_1] + 2[C_2] + 3[C_3] + 4[C_4] \quad (16)$$

Simulations were performed using Matlab and Berkeley Madonna software. Steady-state simulations used in model development and application, as well as in most Figures, were done utilizing Matlab 6.5 function "solve" which is a part of Symbolic Math Toolbox. This function first looks for analytical solution, and if the former is absent, switches to numerical iterative algorithm ("trust region algorithm", "quasi-Newton algorithm"). MATLAB routines for the calculation of Gβγ and Gα available for GIRK with the graded contribution model are shown in Supplemental Methods (S1 Text).

In several cases we tested a range of arguments to produce continuous curves range of changes in GIRK1/2 currents or their ratios (R_a, $R_{\beta\gamma}$) (Fig 6C, S4, S7 and S8 Figs). Here, in order to reduce calculation time, we utilized Berkley Madonna software which implements 4th order Runge-Kutta method for numerical solution of differential equations (see Supplemental Methods, S1 Text). To assure lack of inconsistencies in calculation, we have compared the Matlab and Berkeley Madonna calculation results for a large number of cases and always obtained the same numbers.

Statistics

Imaging data on protein expression have been normalized as described previously [125]. Fluorescence intensity in each oocyte or giant membrane was calculated relative to the average signal in the oocytes of the control group of the same experiment. This procedure yields average normalized intensity as well statistical variability (e.g. SEM) in all treatment groups as well as in the control group. Statistical analysis was performed with SigmaPlot 11 (Systat Software Inc., San Jose, CA, USA). If the data passed the Shapiro-Wilk normality test and the equal variance test, two-group comparisons were performed using t-test. If not, we performed the Mann-Whitney Rank Sum Test. Multiple group comparison was done with one-way ANOVA if the data were normally distributed. ANOVA on ranks was performed whenever the data did not distribute normally. Tukey's post-hoc test was performed for normally distributed data and Dunn's post-hoc test otherwise. Unless specified otherwise, the data in the graphs is presented as mean ± SEM. Correlation between two parameters (such as basal current and R_a) was tested using the Spearman correlation test by running this test on raw data using the statistical module of SigmaPlot 11.

Supporting Information

S1 Text. Supplemental Methods. MATLAB routines for the calculation of Gβγ and Gα available for GIRK with the graded contribution model; Calculations of model predictions for a range of parameters using the Berkeley Madonna software.
(DOCX)

S2 Text. Supplemental Discussion. Conversion from channel densities to concentrations; GIRK1/2 stoichiometry; Estimating steady-state open probability with the "separate gating transitions" model.
(DOCX)

S1 Table. Effect of coexpression of $G\alpha_{i3}$ on GIRK1/2 currents in oocytes. Data are from 2 to 4 experiments, for each group, shown as mean ± SEM. We did not include experiments with extremely large $G\alpha_{i3}$ RNA quantities, as expression of higher doses of $G\alpha_{i3}$ usually reduced I_{total}, indicating a general Gβγ scavenging effect rather than priming.
(DOCX)

S1 Fig. Block of inward currents in cultured hippocampal neurons by TPNQ and Ba^{2+}. (A) Ba^{2+} (1 mM) blocks a greater fraction of the total inward current in high-K^+ solution, compared to TPNQ (120 nM). The experimental protocol was the same as in Fig 1, with the additional step of Ba^{2+} addition after TPNQ. ΔTPN and ΔBa denote the magnitudes (shown by double-speared arrows) of TPNQ- and Ba-blocked currents, respectively. Note that Ba^{2+} blocked a much greater fraction of the total inward current in high-K^+ solution, most probably of the block of additional Ba^{2+} -sensitive channels present in these neurons. **(B)** Comparison of average TPNQ- and Ba^{2+}-blocked currents in 14 cells of one batch of neurons. Statistical significance ($p<0.001$) was determined using Wilcoxon Signed Rank test (the data did not pass normality test).
(TIF)

S2 Fig. GIRK1/2 currents in oocytes. Holding potential was -80 mV, low-K^+ and high-K^+ solutions contained 2 and 24 mM K^+, respectively (K^+ was replaced for Na^+). Net GIRK currents were determined by subtracting the current remaining after the addition of 5 mM $BaCl_2$. (**A**) I_{basal} and I_{evoked} in an oocyte expressing m2R, GIRK1 and GIRK2. Calculation of R_a was done in every cell from its own I_{basal} and I_{evoked}. (**B**) $I_{\beta\gamma}$ in an oocyte expressing m2R, GIRK1, GIRK2 and Gβγ. Note that adding ACh did not evoke a significant additional GIRK current, suggesting full activation by Gβγ. $R_{\beta\gamma}$ was calculated in each cell by dividing its own $I_{\beta\gamma}$ by the average $I_{\beta\gamma}$ from the control group of the same experiment in which no Gβγ was coexpressed. (C) Expression of m2R in a wide range of doses does not affect I_{basal}. 5–8 oocytes have been tested in each group. There were no significant differences between treatments as tested by one-way ANOVA.
(TIF)

S3 Fig. Characterization of YFP-labeled GIRK1 and Gβ. (A, B) Single channel parameters of GIRK1/2 and YFP-GIRK1/2 channels are very similar. **(A)** Cell-attached records of channel activity expressing the channel and Gβγ (5 ng RNA). **(B)** Comparison of average i_{single} and P_o. Data are from oocytes of the same batch, recorded during a two-day experiment. **(C, D)** The anti-Gβ antibody similarly recognizes YFP-labeled bovine and *Xenopus* Gβ subunits in Western blots of manually pealed plasma membranes. Data are from 4 separate experiments. For Western blots, 15 to 20 plasma membranes were pooled. For confocal imaging, groups of 3–16 oocytes were examined, and the average fluorescence level was compared with that of YFP--GIRK1/2 (therefore the statistical significance was calculated using paired t-test). The density

of the latter was calculated from the measurement of currents as explained in the text. In each experiment, both confocal imaging, current measurement and Western blots of manually peeled membranes were done in oocytes of the same donor. There was a good agreement for surface density estimates of YFP-Gβ-XL from confocal "molecular ruler" measurements and from quantitative Western blots, either in absolute terms as molecules/μm^2 (**C**) or in relative terms, normalized to estimates of YFP-Gβ in each experiment (**D**). YFP fluorescence can be safely assumed to be independent of the species of fused Gβ (mammalian or *Xenopus*). Therefore, similar estimates of surface density observed from confocal imaging and Western blots suggest that the Gβ antibody used here recognizes the oocyte's endogenous Gβ in Western blots similarly to the coexpressed mammalian (bovine) $G\beta_1$.
(TIF)

S4 Fig. Simulation of density-dependent changes in whole-cell GIRK1/2 activity. Experimental data (from Table 1) are shown as red circles (mean ± SEM). The simulations of currents and Ra were done using the graded contribution model. **(A)** Testing the hypothesis that the endogenous Gαβγ heterotrimers are the only source of Gβγ for GIRK activation; I_{basal} is due to spontaneous dissociation of Gαβγ into $G\alpha^{GDP}$ and Gβγ (see Fig 2A). Simulations were performed assuming that only part (1 or 10 molecules/μm^2, black and red curves) or all (24 molecules/μm^2, blue curves) endogenous G proteins can donate Gβγ to activate GIRK1/2. Note that no satisfactory description of data can be obtained under any of these conditions. The simulated I_{basal} is too low; for high channel densities, also the full I_{evoked} could not be obtained even assuming that all endogenous Gαβγ (i.e. all 24 molecules/μm^2) could release Gβγ and activate GIRK. **(B)** Testing the hypothesis that the expressed GIRK1/2 recruits additional endogenous G protein subunits to the PM, e.g. from other cellular compartments. Simulations were done assuming that each GIRK1/2 channel recruits from 1 to 4 $G_{i/o}$ heterotrimers. The recruited Gα and Gβγ were added to the pre-existing endogenous plasma membrane-attached Gαβγ before Gβγ expression. **(C)** Testing the hypothesis that the expressed GIRK1/2 recruits additional endogenous Gβγ, but not Gα, to the PM; the rest was done as in B. Calculations in (B) and (C) assumed 24 molecules/μm^2 of endogenous $G_{i/o}$ available for GIRK. Similar results were obtained assuming 10 molecules/μm^2 (data not shown). Simulations as in A-C were also done with the concerted model, yielding similar results (data not shown).
(TIF)

S5 Fig. The concerted activation model supports the unequal stoichiometry estimates of Gβγ and Gα available for GIRK1/2. The plots present the calculated amounts of Gβγ and Gα available for GIRK1/2 using the concerted model for a range of K_D for the GIRK-Gβγ interaction (5–100 nM), for the three channel density groups of Table 1.
(TIF)

S6 Fig. The presence of Gβγ-independent intrinsic activity and the dimensions of submembrane reaction space do not significantly alter the estimates of GIRK1/2-available G proteins subunits. Calculations were done assuming K_D = 50 nM for the GIRK-Gβγ interaction. **(A-C),** the impact of Gβγ-independent basal activity. Calculation were done for Gβγ-independent intrinsic activity of a single channel ranging from 1% to 10% of $P_{o,max}$. Available Gβγ (**A**), Gα (**B**) and the Gβγ-independent fraction of I_{basal} (**C**) were calculated for the three channel density groups of Table 1. **(D, E)** Varying the submembrane space thickness in a wide range, 1–20 nm, does not significantly change the estimates of functional stoichiometry of GIRK1/2-Gβγ-Gα.
(TIF)

S7 Fig. Simulations of the Gβγ dose-response experiment for a range of assumed Gβγ densities. Because in the experiment of Fig 7 the actual density of Gβγ in the PM has not been

directly measured, the calculations of Fig 7C assumed that it was equal to the average density of 30 Gβγ molecules/μm^2 (with 5 ng RNA), as measured in other 4 experiments done during the same time period. Here, we run simulations as in Fig 7C for 20 or 44 molecules Gβγ/μm^2 (**A, C**) and compare the result with that of Fig 7C (shown here again in **B** for a direct comparison). The color codes are as in Fig 7: the blue line presents the simulation using graded contribution model and amounts of Gα and Gβγ (without coexpressed Gβγ) calculated as explained in Fig 7 legend, and red, black and green lines show simulation with endogenous G proteins only and no Gβγ recruitment allowed.
(TIF)

S8 Fig. Another experiment on dose-dependent activation of GIRK1/2 by coexpressed Gβγ. The presentation in similar to that of Fig 7. Gβ was coexpressed with Gγ-YFP in incremental doses, and with a constant amount (1 ng RNA) of wt GIRK1/2. RNA of Gγ-YFP was always half of that of Gβ RNA, by weight. **(A)** Gβγ-YFP fluorescence levels (grey bars, left Y-axis) and GIRK currents (red circles, right Y-axis) are shown on the same plot. GIRK1/2 density, calculated from $I_{\beta\gamma}$ of the 17 ng Gβγ-YFP group, was 13 molecules/μm^2. In addition, we injected YFP-GIRK1/GIRK2 (5 ng GIRK1-YFP) and measured I_{basal} which was 8.4± 1.1 μA (n = 11), comparable to I_{basal} of unlabeled GIRK1/2 (9.4±0.8 μA). Thus, we assumed the same density of ~13 channels/μm^2 for labeled and unlabeled channels. Since the YFP-GIRK1/2 gave a fluorescent signal of 1237 ±221 AU (n = 7), this signal was assumed to correspond to 26 YFP molecules/μm^2. This number was used as the basis of calculations of Gβγ-YFP density for plots shown in B. **(B)** Comparison of measured $I_{\beta\gamma}$ or $R_{\beta\gamma}$ (red circles) and simulated currents or $R_{\beta\gamma}$ (blue curves). The left and right Y-axes are related to $I_{\beta\gamma}$ and $R_{\beta\gamma}$, respectively. Available Gα and Gβγ (before Gβγ coexpression) were estimated from I_{total} and I_{basal}, giving 3.82 and 0.42 molecules/μm^2 of Gβγ and Gα, respectively.
(TIF)

S9 Fig. Estimated stoichiometries of Gα and Gβγ available for GIRK in neurons and oocytes in a range of $I_{\beta\gamma}/I_{total}$ ratios and $P_{o,max}$. Whereas for the oocytes the actual $I_{\beta\gamma}/I_{total}$ ratio and $P_{o,max}$ are known, in neurons these parameters are not known. Both parameters affect the calculated channel density and could affect the estimates of stoichiometry. The calculations shown in this Figure demonstrate the same general trend in stoichiometries of GIRK1/2, Gβγ and Gα as we have found in the previous analysis in the oocytes, in a range of $I_{\beta\gamma}/I_{total}$ ratios (for neurons and oocytes; **A** and **B**) and $P_{o,max}$ (for neurons; **C**). The estimates of Gβγ are around 3-4/channel and relatively independent of I_{basal}, and those of Gα are below 2 and drop sharply with the increase in I_{basal}. Generally, the lowest channel density is most sensitive to perturbations, and, for the lowest simulated $I_{\beta\gamma}/I_{total}$ ratio, calculated Gβγ/channel and Gα/channel exceed our usual estimates.
(TIF)

Acknowledgments

We thank Etay Artzy for contributing the results of an unpublished experiment that he performed in the laboratory in the framework of his M. Sc. thesis work (S2C Fig).

Author Contributions

Conceived and designed the experiments: DY SB UK MR IFT BS TKR CWD ND. Performed the experiments: DY SB UK MR IFT BS TKR ND. Analyzed the data: DY SB UK MR IFT BS TKR ND. Contributed reagents/materials/analysis tools: CWD. Wrote the paper: DY SB UK CWD ND.

References

1. Hille B (2002) Ion Channels of Excitable Membranes. Sunderland: Sinauer.
2. Luscher C, Slesinger PA (2010) Emerging roles for G protein-gated inwardly rectifying potassium (GIRK) channels in health and disease. Nat Rev Neurosci 11: 301–315. doi: 10.1038/nrn2834 PMID: 20389305
3. Yamada K, Iwayama Y, Toyota T, Ohnishi T, Ohba H, et al. (2012) Association study of the KCNJ3 gene as a susceptibility candidate for schizophrenia in the Chinese population. Hum Genet 131: 443–451. doi: 10.1007/s00439-011-1089-3 PMID: 21927946
4. Luján R, Marron Fernandez de Velasco E, Aguado C, Wickman K (2014) New insights into the therapeutic potential of Girk channels. Trends Neurosci 37: 20–29. doi: 10.1016/j.tins.2013.10.006 PMID: 24268819
5. Voigt N, Abu-Taha I, Heijman J, Dobrev D (2014) Constitutive Activity of the Acetylcholine-Activated Potassium Current IK,ACh in Cardiomyocytes. Advances in Pharmacology 70: 393–409. doi: 10.1016/B978-0-12-417197-8.00013-4 PMID: 24931203
6. Williams TA, Monticone S, Mulatero P (2015) KCNJ5 mutations are the most frequent genetic alteration in primary aldosteronism. Hypertension 65: 507–509. doi: 10.1161/HYPERTENSIONAHA.114.04636 PMID: 25624337
7. Logothetis DE, Kurachi Y, Galper J, Neer EJ, Clapham DE (1987) The βγ subunits of GTP-binding proteins activate the muscarinic K^+ channel in heart. Nature 325: 321–326. PMID: 2433589
8. Wickman K, Clapham DE (1995) Ion channel regulation by G proteins. Physiol Rev 75: 865–885. PMID: 7480165
9. Dascal N (1997) Signalling via the G protein-activated K^+ channels. Cell Signal 9: 551–573. PMID: 9429760
10. Inanobe A, Kurachi Y (2014) Membrane channels as integrators of G-protein-mediated signaling. Biochimica et Biophysica Acta (BBA)—Biomembranes 1838: 521–531.
11. Stanfield PR, Nakajima S, Nakajima Y (2003) Constitutively active and G-protein coupled inward rectifier K^+ channels: Kir2.0 and Kir3.0. Rev Physiol Biochem Pharmacol 145: 47–179.
12. Ito H, Tung RT, Sugimoto T, Kobayashi I, Takahashi K, et al. (1992) On the mechanism of G protein βγ subunit activation of the muscarinic K^+ channel in guinea pig atrial cell membrane. Comparison with the ATP-sensitive K^+ channel. J Gen Physiol 99: 961–983. PMID: 1640222
13. Ivanova-Nikolova TT, Nikolov EN, Hansen C, Robishaw JD (1998) Muscarinic K^+ channel in the heart. Modal regulation by G protein βγ subunits. J Gen Physiol 112: 199–210. PMID: 9689027
14. Sadja R, Alagem N, Reuveny E (2002) Graded contribution of the Gβγ binding domains to GIRK channel activation. Proc Natl Acad Sci U S A 99: 10783–10788. PMID: 12124401
15. Krapivinsky G, Gordon EA, Wickman K, Velimirovic B, Krapivinsky L, et al. (1995) The G-protein-gated atrial K^+ channel I_{KACh} is a heteromultimer of two inwardly rectifying K^+-channel proteins. Nature 374: 135–141. PMID: 7877685
16. Corey S, Clapham DE (2001) The stoichiometry of Gβγ binding to G-protein-regulated inwardly rectifying K+ channels (GIRKs). J Biol Chem 276: 11409–11413. PMID: 11148218
17. Yokogawa M, Osawa M, Takeuchi K, Mase Y, Shimada I (2011) NMR analyses of the Gβγ binding and conformational rearrangements of the cytoplasmic pore of G protein-activated inwardly rectifying potassium channel 1 (GIRK1). J Biol Chem 286: 2215–2223. doi: 10.1074/jbc.M110.160754 PMID: 21075842
18. Whorton MR, MacKinnon R (2013) X-ray structure of the mammalian GIRK2-βγ G-protein complex. Nature 498 190–197. doi: 10.1038/nature12241 PMID: 23739333
19. Mahajan R, Ha J, Zhang M, Kawano T, Kozasa T, et al. (2013) A computational model predicts that Gβγ acts at a cleft between channel subunits to activate GIRK1 channels. Sci Signal 6: ra69-. doi: 10.1126/scisignal.2004075 PMID: 23943609
20. Dupre DJ, Robitaille M, Ethier N, Villeneuve LR, Mamarbachi AM, et al. (2006) Seven transmembrane receptor core signalling complexes are assembled prior to plasma membrane trafficking. J Biol Chem 281: 34561–34573. PMID: 16959776
21. Riven I, Iwanir S, Reuveny E (2006) GIRK channel activation involves a local rearrangement of a preformed G protein channel complex. Neuron 51: 561–573. PMID: 16950155
22. Rebois RV, Robitaille M, Gales C, Dupre DJ, Baragli A, et al. (2006) Heterotrimeric G proteins form stable complexes with adenylyl cyclase and Kir3.1 channels in living cells. J Cell Sci 119: 2807–2818. PMID: 16787947

23. David M, Richer M, Mamarbachi AM, Villeneuve LR, Dupre DJ, et al. (2006) Interactions between GABA-B_1 receptors and Kir 3 inwardly rectifying potassium channels. Cell Signal 18: 2172–2181. PMID: 16809021

24. Richard-Lalonde M, Nagi K, Audet N, Sleno R, Amraei M, et al. (2013) Conformational dynamics of Kir3.1/Kir3.2 channel activation via δ-opioid receptors. Mol Pharmacol 83: 416–428. doi: 10.1124/mol.112.081950 PMID: 23175530

25. Kahanovitch U, Tsemakhovich V, Berlin S, Rubinstein M, Styr B, et al. (2014) Recruitment of Gβγ controls the basal activity of GIRK channels: crucial role of distal C-terminus of GIRK1. J Physiol London 592: 5373–5390. doi: 10.1113/jphysiol.2014.283218 PMID: 25384780

26. Dascal N (2001) Ion-channel regulation by G proteins. Trends Endocrinol Metab 12: 391–398. PMID: 11595540

27. Huang CL, Slesinger PA, Casey PJ, Jan YN, Jan LY (1995) Evidence that direct binding of Gβγ to the GIRK1 G protein- gated inwardly rectifying K^+ channel is important for channel activation. Neuron 15: 1133–1143. PMID: 7576656

28. Leaney JL, Milligan G, Tinker A (2000) The G protein α subunit has a key role in determining the specificity of coupling to, but not the activation of, G protein-gated inwardly rectifying K^+ channels. J Biol Chem 275: 921–929. PMID: 10625628

29. Ivanina T, Varon D, Peleg S, Rishal I, Porozov Y, et al. (2004) $G\alpha_{i1}$ and $G\alpha_{i3}$ differentially interact with, and regulate, the G protein-activated K^+ channel. J Biol Chem 279: 17260–17268. PMID: 14963032

30. Peleg S, Varon D, Ivanina T, Dessauer CW, Dascal N (2002) Gαi controls the gating of the G-protein-activated K+ channel, GIRK. Neuron 33: 87–99. PMID: 11779482

31. Rubinstein M, Peleg S, Berlin S, Brass D, Dascal N (2007) $G\alpha_{i3}$ primes the G protein-activated K^+ channels for activation by coexpressed Gβγ in intact *Xenopus* oocytes. J Physiol 581: 17–32. PMID: 17289785

32. Berlin S, Keren-Raifman T, Castel R, Rubinstein M, Dessauer CW, et al. (2010) Gαi and Gβγ jointly regulate the conformations of a Gβγ effector, the the neuronal G-protein activated K+ channel (GIRK). J Biol Chem 285: 6179–6185. doi: 10.1074/jbc.M109.085944 PMID: 20018875

33. Rusinova R, Mirshahi T, Logothetis DE (2007) Specificity of Gβγ signaling to Kir3 channels depends on the helical domain of pertussis toxin-sensitive Gα subunits. J Biol Chem 282: 34019–34030. PMID: 17872944

34. Leal-Pinto E, Gomez-Llorente Y, Sundaram S, Tang Q-Y, Ivanova-Nikolova T, et al. (2010) Gating of a G protein-sensitive mammalian Kir3.1—prokaryotic Kir channel chimera in planar lipid bilayers. J Biol Chem 285: 39790–39800. doi: 10.1074/jbc.M110.151373 PMID: 20937804

35. Fowler CE, Aryal P, Suen KF, Slesinger PA (2006) Evidence for association of $GABA_B$ receptors with Kir3 channels and RGS4 proteins. J Physiol (Lond) 580: 51–65.

36. Berlin S, Tsemakhovich VA, Castel R, Ivanina T, Dessauer CW, et al. (2011) Two distinct aspects of coupling between Gαi and G protein-activated K+ channel (GIRK) revealed by fluorescently-labeled Gαi3 subunits. J Biol Chem 286: 33223–33235. doi: 10.1074/jbc.M111.271056 PMID: 21795707

37. Torrecilla M, Marker CL, Cintora SC, Stoffel M, Williams JT, et al. (2002) G-protein-gated potassium channels containing Kir3.2 and Kir3.3 subunits mediate the acute inhibitory effects of opioids on locus ceruleus neurons. J Neurosci 22: 4328–4334. PMID: 12040038

38. Luscher C, Jan LY, Stoffel M, Malenka RC, Nicoll RA (1997) G protein-coupled inwardly rectifying K+ channels (GIRKs) mediate postsynaptic but not presynaptic transmitter actions in hippocampal neurons. Neuron 19: 687–695. PMID: 9331358

39. Wiser O, Qian X, Ehlers M, Ja WW, Roberts RW, et al. (2006) Modulation of basal and receptor-induced GIRK potassium channel activity and neuronal excitability by the mammalian PINS homolog LGN. Neuron 50: 561–573. PMID: 16701207

40. Chen X, Johnston D (2005) Constitutively active G-protein-gated inwardly rectifying K^+ channels in dendrites of hippocampal CA1 pyramidal neurons. J Neurosci 25: 3787–3792. PMID: 15829630

41. Sanders H, Berends M, Major G, Goldman MS, Lisman JE (2013) NMDA and GABAB (KIR) conductances: the "perfect couple" for bistability. J Neurosci 33: 424–429. doi: 10.1523/JNEUROSCI.1854-12.2013 PMID: 23303922

42. Chung HJ, Qian X, Ehlers M, Jan YN, Jan LY (2009) Neuronal activity regulates phosphorylation-dependent surface delivery of G protein-activated inwardly rectifying potassium channels. Proc Natl Acad Sci U S A 106: 629–634. doi: 10.1073/pnas.0811615106 PMID: 19118198

43. Chung HJ, Ge WP, Qian X, Wiser O, Jan YN, et al. (2009) G protein-activated inwardly rectifying potassium channels mediate depotentiation of long-term potentiation. Proc Natl Acad Sci U S A 106: 635–640. doi: 10.1073/pnas.0811685106 PMID: 19118199

44. Cooper A, Grigoryan G, Guy-David L, Tsoory MM, Chen A, et al. (2012) Trisomy of the G protein-coupled K^+ channel gene, Kcnj6, affects reward mechanisms, cognitive functions, and synaptic plasticity in mice. Proc Natl Acad Sci USA 109: 2642–2647. doi: 10.1073/pnas.1109099109 PMID: 22308328

45. Makara Judit K, Magee Jeffrey C (2013) Variable dendritic integration in hippocampal CA3 pyramidal neurons. Neuron 80: 1438–1450. doi: 10.1016/j.neuron.2013.10.033 PMID: 24360546

46. Voigt N, Maguy A, Yeh Y-H, Qi X, Ravens U, et al. (2008) Changes in $I_{K,ACh}$ single-channel activity with atrial tachycardia remodelling in canine atrial cardiomyocytes. Cardiovasc Res 77: 35–43. PMID: 18006448

47. Farhy Tselnicker I, Tsemakhovich V, Rishal I, Kahanovitch U, Dessauer CW, et al. (2014) Dual regulation of G proteins and the G-protein–activated K^+ channels by lithium. Proc Natl Acad Sci USA 111: 5018–5023. doi: 10.1073/pnas.1316425111 PMID: 24639496

48. He C, Yang X, Zhang H, Mirshahi T, Jin T, et al. (2002) Identification of critical residues controlling GIRK channel activity through interactions with the βγ subunits of G proteins. J Biol Chem 277: 6088–6096. PMID: 11741896

49. Leaney JL, Benians A, Graves FM, Tinker A (2002) A novel strategy to engineer functional fluorescent inhibitory G-protein α subunits. J Biol Chem 277: 28803–28809. PMID: 12048213

50. Rishal I, Porozov Y, Yakubovich D, Varon D, Dascal N (2005) Gβγ-dependent and Gβγ-independent basal activity of G protein-activated K^+ channels. J Biol Chem 280: 16685–16694. PMID: 15728579

51. Rubinstein M, Peleg S, Berlin S, Brass D, Keren-Raifman T, et al. (2009) Divergent regulation of GIRK1 and GIRK2 subunits of the neuronal G protein gated K^+ channel by $G\alpha_i$GDP and Gβγ. J Physiol 587: 3473–3491. doi: 10.1113/jphysiol.2009.173229 PMID: 19470775

52. Sodickson DL, Bean BP (1996) $GABA_B$ receptor-activated inwardly rectifying potassium current in dissociated hippocampal CA3 neurons. J Neurosci 16: 6374–6385. PMID: 8815916

53. Kim CS, Johnston D (2015) A1 adenosine receptor-mediated GIRK channels contributes to the resting conductance of CA1 neurons in the dorsal hippocampus. J Neurophysiol 113: 2511–2523. doi: 10.1152/jn.00951.2014 PMID: 25652929

54. Logothetis DE, Jin T, Lupyan D, Rosenhouse-Dantsker A (2007) Phosphoinositide-mediated gating of inwardly rectifying K^+ channels. Pflugers Arch 455: 83–95. PMID: 17520276

55. Sarvazyan NA, Lim WK, Neubig RR (2002) Fluorescence analysis of receptor-G protein interactions in cell membranes. Biochemistry 41: 12858–12867. PMID: 12379129

56. Sarvazyan NA, Remmers AE, Neubig RR (1998) Determinants of $G_{i1\alpha}$ and βγ binding. Measuring high affinity interactions in a lipid environment using flow cytometry. J Biol Chem 273: 7934–7940. PMID: 9525890

57. Rishal I, Keren-Raifman T, Yakubovich D, Ivanina T, Dessauer CW, et al. (2003) Na^+ promotes the dissociation between Gα-GDP and Gβγ, activating G-protein-gated K^+ channels. J Biol Chem 278: 3840–3845. PMID: 12488455

58. Yakubovich D, Rishal I, Dascal N (2005) Kinetic modeling of Na^+-induced, Gβγ -dependent activation of G-protein-gated K^+ channels. J Mol Neurosci 25: 7–20. PMID: 15781962

59. Gilman AG (1987) G proteins: transducers of receptor-generated signals. Annu Rev Biochem 56: 615–649. PMID: 3113327

60. Neubig RR (1994) Membrane organization in G-protein mechanisms. FASEB J 8: 939–946. PMID: 8088459

61. Lambert NA (2008) Dissociation of heterotrimeric G proteins in cells. Sci Signal 1: re5. doi: 10.1126/scisignal.125re5 PMID: 18577758

62. Ben-Chaim Y, Tour O, Dascal N, Parnas I, Parnas H (2003) The M2 muscarinic G-protein-coupled receptor is voltage sensitive. J Biol Chem 278: 22482–22491. PMID: 12684524

63. Ross EM (2008) Coordinating speed and amplitude in G-protein signaling. Curr Biol 18: R777–R783. doi: 10.1016/j.cub.2008.07.035 PMID: 18786383

64. Bondar A, Lazar J (2013) Dissociated GαGTP and Gβγ subunits are the major activated form of heterotrimeric $G_{i/o}$ proteins. J Biol Chem 289: 1271–1281. doi: 10.1074/jbc.M113.493643 PMID: 24307173

65. Hosoya Y, Yamada M, Ito H, Kurachi Y (1996) A functional model for G protein activation of the muscarinic K^+ channel in guinea pig atrial myocytes. Spectral analysis of the effect of GTP on single-channel kinetics. J Gen Physiol 108: 485–495. PMID: 8972387

66. Kurachi Y, Ishii M (2004) Cell signal control of the G protein-gated potassium channel and its subcellular localization. J Physiol London 554: 285–294. PMID: 12923211

67. Murakami S, Suzuki S, Ishii M, Inanobe A, Kurachi Y (2010) Cellular modelling: experiments and simulation to develop a physiological model of G-protein control of muscarinic K^+ channels in mammalian atrial cells. Phil Trans R Soc A 368: 2983–3000. doi: 10.1098/rsta.2010.0093 PMID: 20478917

68. Ivanova-Nikolova TT, Breitwieser GE (1997) Effector contributions to Gβγ-mediated signaling as revealed by muscarinic potassium channel gating. J Gen Physiol 109: 245–253. PMID: 9041452

69. Yakubovich D, Pastushenko V, Bitler A, Dessauer CW, Dascal N (2000) Slow modal gating of single G protein-activated K^+ channels expressed in *Xenopus* oocytes. J Physiol London 524: 737–755. PMID: 10790155

70. Nemec J, Wickman K, Clapham DE (1999) Gβγ binding increases the open time of I_{KACh}: kinetic evidence for multiple Gβγ binding sites. Biophys J 76: 246–252. PMID: 9876138

71. Grigg JJ, Kozasa T, Nakajima Y, Nakajima S (1996) Single-channel properties of a G-protein-coupled inward rectifier potassium channel in brain neurons. J Neurophysiol 75: 318–328. PMID: 8822560

72. Kofuji P, Davidson N, Lester HA (1995) Evidence that neuronal G-protein-gated inwardly rectifying K^+ channels are activated by Gβγ subunits and function as heteromultimers. Proc Natl Acad Sci U S A 92: 6542–6546. PMID: 7604029

73. Falkenburger BH, Jensen JB, Hille B (2010) Kinetics of PIP_2 metabolism and KCNQ2/3 channel regulation studied with a voltage-sensitive phosphatase in living cells. J Gen Physiol 135: 99–114. doi: 10.1085/jgp.200910345 PMID: 20100891

74. Falkenburger BH, Jensen JB, Hille B (2010) Kinetics of M1 muscarinic receptor and G protein signaling to phospholipase C in living cells. J Gen Physiol 135: 81–97. doi: 10.1085/jgp.200910344 PMID: 20100890

75. Linderman JJ (2009) Modeling of G-protein-coupled receptor signaling pathways. J Biol Chem 284: 5427–5431. doi: 10.1074/jbc.R800028200 PMID: 18940812

76. Rangamani P, Iyengar R (2008) Modelling cellular signalling systems. Essays Biochem 45: 83–94. doi: 10.1042/BSE0450083 PMID: 18793125

77. Arshavsky VY, Lamb TD, Pugh EN Jr. (2002) G proteins and phototransduction. Annu Rev Physiol 64: 153–187. PMID: 11826267

78. Vorobiov D, Bera AK, Keren-Raifman T, Barzilai R, Dascal N (2000) Coupling of the muscarinic m2 receptor to G protein-activated K+ channels via Gαz and a receptor-Gαz fusion protein. Fusion between the receptor and Gαz eliminates catalytic (collision) coupling. J Biol Chem 275: 4166–4170. PMID: 10660578

79. Wydeven N, Young D, Mirkovic K, Wickman K (2012) Structural elements in the Girk1 subunit that potentiate G protein–gated potassium channel activity. Proc Natl Acad Sci USA 109: 21492–21497. doi: 10.1073/pnas.1212019110 PMID: 23236146

80. Sadler SE, Maller JL (1981) Progesterone inhibits adenylate cyclase in Xenopus oocytes. Action on the guanine nucleotide regulatory protein. J Biol Chem 256: 6368–6373. PMID: 7240211

81. Ivanina T, Perets T, Thornhill WB, Levin G, Dascal N, et al. (1994) Phosphorylation by protein kinase A of RCK1 K^+ channels expressed in *Xenopus* oocytes. Biochemistry 33: 8786–8792. PMID: 8038169

82. Kennedy ME, Nemec J, Corey S, Wickman K, Clapham DE (1999) GIRK4 confers appropriate processing and cell surface localization to G- protein-gated potassium channels. J Biol Chem 274: 2571–2582. PMID: 9891030

83. Pabon A, Chan KW, Sui JL, Wu X, Logothetis DE, et al. (2000) Glycosylation of GIRK1 at Asn119 and ROMK1 at Asn117 has different consequences in potassium channel function. J Biol Chem 275: 30677–30682. PMID: 10889209

84. Ross EM (1995) Protein modification: palmitoylation in G-protein signaling pathways. Curr Biol 5: 107–109. PMID: 7743169

85. Lauffenburger D, Linderman JJ (1996) Receptors: Models for Binding, Trafficking, and Signaling. New York: Oxford University Press.

86. Runnels LW, Scarlata SF (1998) Regulation of the rate and extent of phospholipase Cβ2 effector activation by the βγ subunits of heterotrimeric G proteins. Biochemistry 37: 15563–15574. PMID: 9799521

87. Runnels LW, Scarlata SF (1999) Determination of the affinities between heterotrimeric G protein subunits and their phospholipase Cβ effectors. Biochemistry 38: 1488–1496. PMID: 9931014

88. Dascal N (1987) The use of Xenopus oocytes for the study of ion channels. CRC Crit Rev Biochem 22: 317–387. PMID: 2449311

89. Silverman SK, Lester HA, Dougherty DA (1996) Subunit stoichiometry of a heteromultimeric G protein-coupled inward- rectifier K^+ channel. J Biol Chem 271: 30524–30528. PMID: 8940021

90. Krapivinsky G, Krapivinsky L, Wickman K, Clapham DE (1995) Gβγ binds directly to the G protein-gated K^+ channel, I_{KACh}. J Biol Chem 270: 29059–29062. PMID: 7493925

91. Luchian T, Dascal N, Dessauer C, Platzer D, Davidson N, et al. (1997) A C-terminal peptide of the GIRK1 subunit directly blocks the G protein- activated K+ channel (GIRK) expressed in Xenopus oocytes. J Physiol (Lond) 505: 13–22.

92. Albsoul-Younes AM, Sternweis PM, Zhao P, Nakata H, Nakajima S, et al. (2001) Interaction sites of the G protein β subunit with brain G protein-coupled inward rectifier K^+ channel. J Biol Chem 276: 12712–12717. PMID: 11278861

93. Jelacic TM, Sims SM, Clapham DE (1999) Functional expression and characterization of G-protein-gated inwardly rectifying K+ channels containing GIRK3. J Membr Biol 169: 123–129. PMID: 10341034

94. Kienitz M-C, Mintert-Jancke E, Hertel F, Pott L (2014) Differential effects of genetically-encoded Gβγ scavengers on receptor-activated and basal Kir3.1/Kir3.4 channel current in rat atrial myocytes. Cell Signal 26: 1182–1192. doi: 10.1016/j.cellsig.2014.02.007 PMID: 24576551

95. Singer-Lahat D, Dascal N, Mittelman L, Peleg S, Lotan I (2000) Imaging plasma membrane proteins in large membrane patches of *Xenopus* oocytes. Pflugers Arch—Eur J Physiol 440: 627–633.

96. Wydeven N, Fernandez de Velasco EM, Du Y, Benneyworth MA, Hearing MC, et al. (2014) Mechanisms underlying the activation of G-protein–gated inwardly rectifying K+ (GIRK) channels by the novel anxiolytic drug, ML297. Proc Natl Acad Sci USA 111: 10755–10760. doi: 10.1073/pnas.1405190111 PMID: 25002517

97. Oldham WM, Hamm HE (2008) Heterotrimeric G protein activation by G-protein-coupled receptors. Nat Rev Mol Cell Biol 9: 60–71. PMID: 18043707

98. Ford CE, Skiba NP, Bae H, Daaka Y, Reuveny E, et al. (1998) Molecular basis for interactions of G protein betagamma subunits with effectors. Science 280: 1271–1274. PMID: 9596582

99. Mirshahi T, Mittal V, Zhang H, Linder ME, Logothetis DE (2002) Distinct sites on G protein βγ subunits regulate different effector functions. J Biol Chem 277: 36345–36350. PMID: 12124391

100. Katanaev VL, Chornomorets M (2007) Kinetic diversity in G-protein-coupled receptor signalling. Biochem J 401: 485–495. PMID: 16989639

101. Wühr M, Freeman Robert M Jr., Presler M, Horb Marko E, Peshkin L, et al. (2014) Deep proteomics of the Xenopus laevis egg using an mRNA-derived reference database. Curr Biol 24: 1467–1475. doi: 10.1016/j.cub.2014.05.044 PMID: 24954049

102. Hille B, Dickson E, Kruse M, Falkenburger B (2014) Dynamic Metabolic Control of an Ion Channel. Progress in Molecular Biology and Translational Science 123: 219–247. doi: 10.1016/B978-0-12-397897-4.00008-5 PMID: 24560147

103. Clapham DE, Neer EJ (1997) G protein βγ subunits. Annu Rev Pharmacol Toxicol 37: 167–203. PMID: 9131251

104. Sadana R, Dascal N, Dessauer CW (2009) N-terminus of type 5 adenylyl cyclase scaffolds Gs heterotrimer. Mol Pharmacol 76: 1256–1264. doi: 10.1124/mol.109.058370 PMID: 19783621

105. Fernandez-Alacid L, Watanabe M, Molnar E, Wickman K, Lujan R (2011) Developmental regulation of G protein-gated inwardly-rectifying K+ (GIRK/Kir3) channel subunits in the brain. Eur J Neurosci 34: 1724–1736. doi: 10.1111/j.1460-9568.2011.07886.x PMID: 22098295

106. Wang W, Whorton MR, MacKinnon R (2014) Quantitative analysis of mammalian GIRK2 channel regulation by G proteins, PIP2 and Na+ in a reconstituted system. Elife (Cambridge): e03671.

107. Schreibmayer W, Dessauer CW, Vorobiov D, Gilman AG, Lester HA, et al. (1996) Inhibition of an inwardly rectifying K channel by G-protein α- subunits. Nature 380: 624–627. PMID: 8602262

108. Zhong H, Wade SM, Woolf PJ, Linderman JJ, Traynor JR, et al. (2003) A spatial focusing model for G protein signals. Regulator of G protein signaling (RGS) protein-mediated kinetic scaffolding. J Biol Chem 278: 7278–7284. PMID: 12446706

109. Mori MX, Erickson MG, Yue DT (2004) Functional stoichiometry and local enrichment of calmodulin interacting with Ca^{2+} channels. Science 304: 432–435. PMID: 15087548

110. Zylbergold P, Ramakrishnan N, Hebert T (2010) The role of G proteins in assembly and function of Kir3 inwardly rectifying potassium channels. Channels 4: 411–421. doi: 10.4161/chan.4.5.13327 PMID: 20855978

111. Raveh A, Riven I, Reuveny E (2009) Elucidating the gating of the GIRK channel using spectroscopic approach. J Physiol 587: 5331–5335. doi: 10.1113/jphysiol.2009.180158 PMID: 19752111

112. Nagi K, Pineyro G (2014) Kir3 channel signaling complexes: focus on opioid receptor signaling. Front Cell Neurosci 8: 186. doi: 10.3389/fncel.2014.00186 PMID: 25071446

113. Doupnik CA (2008) GPCR-Kir channel signaling complexes: defining rules of engagement. J Recept Signal Transduct Res 28: 83–91. doi: 10.1080/10799890801941970 PMID: 18437632

114. Ruiz-Velasco V, Ikeda SR (1998) Heterologous expression and coupling of G protein-gated inwardly rectifying K+ channels in adult rat sympathetic neurons. J Physiol (Lond) 513: 761–773.

115. Mase Y, Yokogawa M, Osawa M, Shimada I (2012) Structural basis for the modulation of the gating property of G protein-gated inwardly rectifying potassium ion channel (GIRK) by the i/o-family G protein α subunit (Gαi/o). J Biol Chem 287: 19537–19549. doi: 10.1074/jbc.M112.353888 PMID: 22511772

116. Elia N, Frechter S, Gedi Y, Minke B, Selinger Z (2005) Excess of $G\beta_e$ over $Gq\alpha_e$ in vivo prevents dark, spontaneous activity of Drosophila photoreceptors. J Cell Biol 171: 517–526. PMID: 16260498

117. Clack JW, Springmeyer ML, Clark CR, Witzmann FA (2006) Transducin subunit stoichiometry and cellular distribution in rod outer segments. Cell Biol Int 30: 829–835. PMID: 16895762

118. Ivanina T, Rishal I, Varon D, Mullner C, Frohnwieser-Steinecke B, et al. (2003) Mapping the Gβγ-binding sites in GIRK1 and GIRK2 subunits of the G protein-activated K^+ channel. J Biol Chem 278: 29174–29183. PMID: 12743112

119. Takanishi CL, Bykova EA, Cheng W, Zheng J (2006) GFP-based FRET analysis in live cells. Brain Res 1091: 132–139. PMID: 16529720

120. Dascal N, Lim NF, Schreibmayer W, Wang W, Davidson N, et al. (1993) Expression of an atrial G-protein-activated potassium channel in Xenopus oocytes. Proc Natl Acad Sci U S A 90: 6596–6600. PMID: 8341673

121. Hommers LG, Lohse MJ, Bunemann M (2003) Regulation of the inward rectifying properties of GIRK channels by Gβγ subunits. J Biol Chem 278: 1037–1043. PMID: 12403784

122. Hedin KE, Lim NF, Clapham DE (1996) Cloning of a *Xenopus laevis* inwardly rectifying K^+ channel subunit that permits GIRK1 expression of I_{KACh} currents in oocytes. Neuron 16: 423–429. PMID: 8789957

123. Yakubovich D, Rishal I, Dessauer CW, Dascal N (2009) Amplitude histogram-based method of analysis of patch clamp recordings that involve extreme changes in channel activity levels. J Mol Neurosci 37: 201–211. doi: 10.1007/s12031-008-9117-z PMID: 18622586

124. Sakmann B, Neher E (1995) Single-Channel Recording. New York. 700 p.

125. Kanevsky N, Dascal N (2006) Regulation of maximal open probability is a separable function of Cavβ subunit in L-type Ca2+ channel, dependent on NH2 terminus of α1C (Cav1.2α). J Gen Physiol 128: 15–36. PMID: 16801381

Supporting Information.

Supplemental Methods.

MATLAB routines for the calculation of Gβγ and Gα available for GIRK with the graded contribution model

Template for the calculation of $G\beta\gamma_{total}$

[c0,c1,c2,c3,c4, cf,gbg,gbgt]=

solve ('4*c0*gbg= K_D*c1', '3*c1*gbg=2* K_D *c2', '2*c2*gbg=3 *K_D *c3',

'c3*gbg=4* K_D *c4','c0+c1+c2+c3+c4=n*166e-9 ',

'gbg+c1+2*c2+3*c3+4*c4=m',

'.013*c1+.065*c2+.26*c3+c4=cf',

'cf=p /(72836285*.105)')

% Copy the system to worksheet

% Enter the following:

% n – number of channels per μm^2

% p – current in μA (I_{total})

% gbgt - $G\beta\gamma_{total}$

Template for the calculation of $G\alpha_{total}$

[c0, c1, c2, c3, c4, cf, ga, gagbg, gat, gbg]=

solve ('c0*gbg= 4*K_D*c1', '3*c1*gbg=2* K_D*c2' , '2*c2*gbg=3 *K_D *c3',

'c3*gbg=4* K_D*c4', 'c0+c1+c2+c3+c4=n*166e-9',

'gbg+gagbg+c1+2*c2+3*c3+4*c4=m', 'ga+gagbg=gat', '0.0013*gagbg=0.7e6*ga*gbg '

'.013*c1+.065*c2+.26*c3+c4=cf',

'cf=q /(72836285*.105)')

% Copy the system to worksheet

% Enter the following:

% n – number of channels per μm^2

% q – current in μA (I_{basal})

% m - $G\beta\gamma_{total}$

% gat - $G\alpha_{total}$

Template for the simulation of a Gβγ overexpression experiment

[c0, c1, c2, c3, c4, cf, curr, ga, gagbg, gat, gbg]=

solve ('c0*gbg= 4*K_D*c1', '3*c1*gbg=2* K_D*c2' , '2*c2*gbg=3 *K_D *c3',

'c3*gbg=4* K_D*c4', 'c0+c1+c2+c3+c4=n*166e-9',

'gbg+gagbg+c1+2*c2+3*c3+4*c4=m', 'ga+gagbg=gat', '0.0013*gagbg=0.7e6*ga*gbg '

'.013*c1+.065*c2+.26*c3+c4=cf',

'curr=cf*(72836285*.105)')

% Copy the system to worksheet

% Enter the following:

% n – number of channels per μm^2

% curr – current in μA

% m - $G\beta\gamma_{total}$

% gat - $G\alpha_{total}$

All results are in M

Calculations of model predictions for a range of parameters using the Berkeley Madonna software.

To simulate macroscopic GIRK1/2 currents or their ratios (R_a, $R_{\beta\gamma}$) for a range of arguments in order to produce continuous curves (Figs. 5, 7C, S4, S7, S8), we utilized Berkley Madonna software which implements 4th order Runge-Kutta method for numerical solution of differential equations. In these calculations, channel activation process by Gβγ was described by following system of differential equations:

$$d(G\beta\gamma)/dt = k_{off}\bullet G\alpha GDPG\beta\gamma + k_{-1}\bullet C_1 + 2\bullet k_{-1}\bullet C_2 + 3\bullet k_{-1}\bullet C_3 + 4\bullet k_{-1}\bullet C_4 -$$
$$-G\beta\gamma\bullet(k_{on}\bullet G\alpha GDP + 4\bullet k_1\bullet C_0 + 3\bullet k_1\bullet C_1 + 2\bullet k_1\bullet C_2 + k_1\bullet C_3)$$
$$d(G\alpha GDP)/dt = k_{off}\bullet G\alpha GDPG\beta\gamma - k_{on}\bullet G\alpha GDP\bullet G\beta\gamma$$
$$d(C_0)/dt = k_{-1}\bullet C_1 - 4\bullet k1\bullet C_0\bullet G\beta\gamma$$
$$d(C_1)/dt = 2\bullet k_{-1}\bullet C_2 + 4\bullet k_1\bullet C_0\bullet G\beta\gamma - C_1\bullet(k_{-1} + 3\bullet k_1\bullet G\beta\gamma)$$
$$d(C_2)/dt = 3\bullet k_{-1}\bullet C_3 + 3\bullet k_1\bullet C_1\bullet G\beta\gamma - C_2\bullet(2\bullet k_{-1} + 2\bullet k_1\bullet G\beta\gamma)$$
$$d(C_3)/dt = 4\bullet k_{-1}\bullet C_4 + 2\bullet k_1\bullet C_2\bullet G\beta\gamma - C_3\bullet(3\bullet k_{-1} + k_1\bullet G\beta\gamma)$$
$$d(C_4)/dt = k_1\bullet C_3\bullet G\beta\gamma - 4\bullet k_{-1}\bullet C_4$$

,

where all symbols are defined as in the main text of the paper, and k_1 and k_{-1} are forward and reverse rate constants of GIRK-Gβγ interaction, respectively. We used $k_1 = 10^7$ $M^{-1}s^{-1}$ and $k_{-1} = 0.5$ s^{-1}. These rate constants of Gβγ and GIRK channel interaction are unknown, but these values are in Smoluchowski limit [1] and render K_D = 50 nM which we used in main calculations of our model.

The rate constants of interaction between Gβγ and $G\alpha_i$ were k_{off} = 0.0013 s^{-1} and k_{on} = 0.7×10^6 $M^{-1}s^{-1}$ [2].

Supplemental discussion

Conversion from channel densities to concentrations.

There is no consensus about the way the reaction rates are changed by the reduction of dimensionality [3,4,5]. Nevertheless, for proteins that interact in the submembrane cytosolic space conversion from two-dimensional rate constants and densities into three-dimensional rate constants and concentrations is a well-accepted paradigm. This is particularly useful, and has been used in the past, in calculations involving GPCRs and G proteins or effectors and G proteins (e.g. [6,7,8,9]).

GIRK1/2 stoichiometry.

Silverman et al. [10] have shown that GIRK1/4 channels with 2:2 stoichiometry are preferentially expressed in oocytes and contribute the majority of the macroscopic current, but 3:1 or 1:3 stoichiometry is viable (see also [11]). No such data are available for GIRK1/2. Generally speaking, for macroscopic currents, the exact subunit stoichiometry does not matter, because for a constant RNA ratio as used here (equal amounts of RNAs for both subunits), a relatively constant composition of channel population (in terms of stoichiometry) is expected, subject to natural variability. We cannot exclude the possibility that, in some single-channel recordings, we observed channels of unequal stoichiometry. Nevertheless, since simulations are based on average i_{single} and $P_{o,max}$ from a rather large sample of patches (since the closing of data collection for this paper, we have recorded more single GIRK1/2 channels and always obtain a similar $P_{o,max}$ around 0.11; data not shown), we posit that the average values of $P_{o,max}$ and i_{single} faithfully represent the population of channels seen in our macroscopic recordings.

Estimating steady-state open probability with the "separate gating transitions" model.

For clarity, here we present the separate gating transitions model from Fig. 2B using the notation which will be utilized in the following equations.

$$\begin{array}{ccccccccc} C_0^c & \Leftrightarrow & C_1^c & \Leftrightarrow & C_2^c & \Leftrightarrow & C_3^c & \Leftrightarrow & C_4^c \\ \Updownarrow & & \Updownarrow & & \Updownarrow & & \Updownarrow & & \Updownarrow \\ C_0^o & \Leftrightarrow & C_1^o & \Leftrightarrow & C_2^o & \Leftrightarrow & C_3^o & \Leftrightarrow & C_4^o \end{array}$$

where C_x^c denotes concentration of channels occupied by x Gβγ molecules in closed state and C_x^o is is the concentration of channels occupied by x Gβγ molecules in open state.

The open probability for the above scheme can be calculated according to:

$$P_o = \frac{\sum_{x=0}^{x=4} C_x^o}{\sum_{x=0}^{x=4} C_x^c + \sum_{x=0}^{x=4} C_x^o} \qquad \text{(S1)}$$

The equilibrium constant K_x between C_x^c and C_x^o is

$K_x = C_x^o / C_x^c$ (S2)

and $P_{o,x}$ is the open probability of x Gβγ molecules occupied channel and can be defined as

$$P_{o,x} = \frac{C_x^o}{C_x^o + C_x^c} = \frac{K_x}{1+K_x} \qquad \text{(S3)}$$

If C_x is the concentration of channels occupied by x Gβγ molecules, then

$C_x = C_x^c + C_x^o$ (S4)

and if C_{total} is total channel concentration, then

$$C_{total} = \sum_{x=0}^{x=4} C_x = \sum_{x=0}^{x=4} C_x^c + \sum_{x=0}^{x=4} C_x^o \qquad \text{(S5)}$$

Thus (S1) can be rearranged

$$P_o = \frac{\sum_{x=0}^{x=4} C_x^o}{C_{total}} \qquad \text{(S6)}$$

Solving (S2) and (S4) for C_x^o renders

$$C_x^o = \frac{K_x}{(1+K_x)} \cdot C_x \qquad \text{(S7)}$$

Substituting (S3) into (S7) renders

$$C_x^o = P_{o,x} \cdot C_x \qquad \text{(S8)}$$

Substituting (S8) into (S6) renders

$$P_o = \frac{\sum_{x=0}^{x=4} P_{o,x} \cdot C_x}{C_{total}} \qquad \text{(S9)}$$

If $f_{p,x}$ is the fraction of $P_{o,max}$ (maximal observable P_o) and is defined as $f_{p,x} = P_{o,x}/P_{o.max}$ and ϕ_x is the fraction of channels occupied by x Gβγ molecules (defined as $\phi_x = C_x/C_{total}$), then substitution of definitions of $f_{p,x}$ and ϕ_x to (S9) will render

$$P_o = P_{o,\max} \cdot \sum_{x=0}^{x=4} f_{p,x} \cdot \phi_x \qquad \text{(S10)}$$

This equation is identical to Equation 6 (Methods).

The graded contribution model and the more elaborated independent gating transitions model will predict distinct single channel behavior of GIRK1/2, which may need to be investigated in detail to distinguish between the two models. Nevertheless, as shown above, the description of steady-state P_o by the two models converges to Equation 6 (Methods), suggesting that this is a general equation which can describe GIRK1/2 macroscopic gating for any number of open states. As a consequence, the two models should produce identical fractional macroscopic steady-state currents ($P_o/P_{o,max}$, where $P_{o,max}$ is equivalent to $I/I_{\beta\gamma}$, where I is either I_{basal}, I_{total} or I_{evoked}) once the channel is occupied by x Gβγ. In other words, for steady state description of macroscopic currents that we present in our study, the results are expected to be the similar both for the graded contribution model as well as for the more elaborated independent gating transitions model.

Supplemental References

1. Berg OG, von Hippel PH (1985) Diffusion-controlled macromolecular interactions. Annu Rev Biophys Biophys Chem 14: 131-160.
2. Sarvazyan NA, Remmers AE, Neubig RR (1998) Determinants of $G_{i1}\alpha$ and $\beta\gamma$ binding. Measuring high affinity interactions in a lipid environment using flow cytometry. J Biol Chem 273: 7934-7940.
3. Axelrod D, Wang MD (1994) Reduction-of-dimensionality kinetics at reaction-limited cell surface receptors. Biophys J 66: 588-600.
4. Kholodenko BN, Hoek JB, Westerhoff HV (2000) Why cytoplasmic signalling proteins should be recruited to cell membranes. Trends Cell Biol 10: 173-178.

5. Shoup D, Lipari G, Szabo A (1981) Diffusion-controlled bimolecular reaction rates. The effect of rotational diffusion and orientation constraints. Biophys J 36: 697-714.

6. Lauffenburger D, Linderman JJ (1996) Receptors: Models for Binding, Trafficking, and Signaling. New York: Oxford University Press.

7. Runnels LW, Scarlata SF (1998) Regulation of the rate and extent of phospholipase Cβ2 effector activation by the βγ subunits of heterotrimeric G proteins. Biochemistry 37: 15563-15574.

8. Runnels LW, Scarlata SF (1999) Determination of the affinities between heterotrimeric G protein subunits and their phospholipase Cβ effectors. Biochemistry 38: 1488-1496.

9. Yakubovich D, Rishal I, Dascal N (2005) Kinetic modeling of Na^+-induced, Gβγ -dependent activation of G-protein-gated K^+ channels. J Mol Neurosci 25: 7-20.

10. Silverman SK, Lester HA, Dougherty DA (1996) Subunit stoichiometry of a heteromultimeric G protein-coupled inward- rectifier K^+ channel. J Biol Chem 271: 30524-30528.

11. Grasser E, Steinecker B, Ahammer H, Schreibmayer W (2008) Subunit stoichiometry of heterologously expressed G-protein activated inwardly rectifying potassium channels analysed by fluorescence intensity ratio measurement. Pflugers Arch 455: 1017-1024.

Supplemental Table 1

Table S1. Effect of coexpression of $G\alpha_{i3}$ on GIRK1/2 currents in oocytes. Data are from 2 to 4 experiments, for each group, shown as mean ± SEM. We did not include experiments with extremely large $G\alpha_{i3}$ RNA quantities, as expression of higher doses of $G\alpha_{i3}$ usually reduced I_{total}, indicating a general Gβγ scavenging effect rather than priming [12,13].

50-200 pg GIRK1/2 (n=10)				**50-200 pg GIRK1/2+0.5-2 ng Gαi3 (n=10)**			
I_{basal} (μA)	I_{evoked} (μA)	I_{total} (μA)	R_a	I_{basal} (μA)	I_{evoked} (μA)	I_{total} (μA)	R_a
4.8±0.42	4.2±0.76	9.1±1	1.9±0.14	1.2±0.2	6.8±0.9	8.0±0.7	10.5±2.7
0.5-1 ng GIRK1/2 (n=27)				**0.5-1 ng GIRK1/2 + 5-10 ng Gαi3 (n=16)**			
I_{basal} (μA)	I_{evoked} (μA)	I_{total} (μA)	R_a	I_{basal} (μA)	I_{evoked} (μA)	I_{total} (μA)	R_a
12.6±0.7	2.5±0.3	15.1±0.8	1.2±0.03	2.4±0.6	11.5±0.8	13.9±1.2	10.4±1.7

Supporting Figures

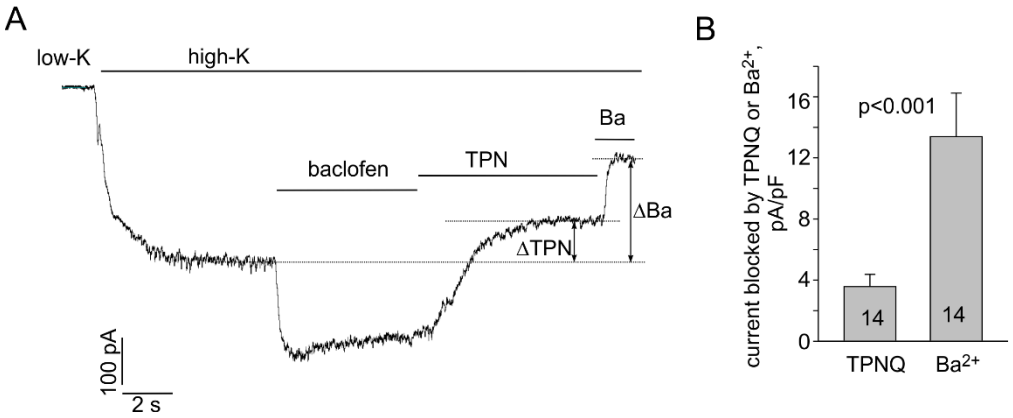

Fig. S1. Block of inward currents in cultured hippocampal neurons by TPNQ and Ba^{2+}. (A) Ba^{2+} (1 mM) blocks a greater fraction of the total inward current in high-K^+ solution, compared to TPNQ (120 nM). The experimental protocol was the same as in Fig. 1, with the additional step of Ba^{2+} addition after TPNQ. ΔTPN and ΔBa denote the magnitudes (shown by double-speared arrows) of TPNQ- and Ba-blocked currents, respectively. Note that Ba^{2+} blocked a much greater fraction of the total inward current in high-K^+ solution, most probably of the block of additional Ba^{2+} -sensitive channels present in these neurons. **(B)** Comparison of average TPNQ- and Ba^{2+}-blocked currents in 14 cells of one batch of neurons. Statistical significance ($p<0.001$) was determined using Wilcoxon Signed Rank test (the data did not pass normality test).

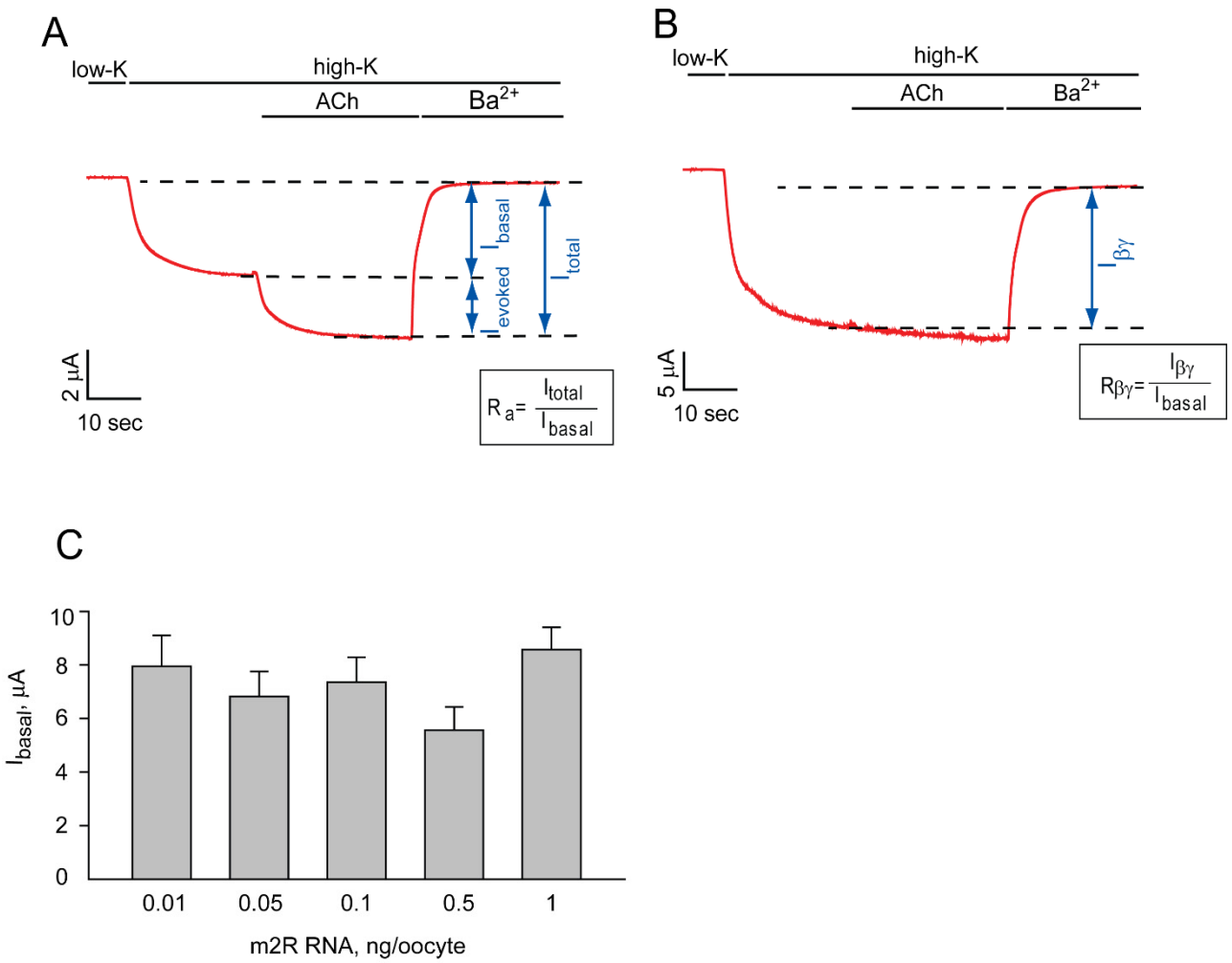

Fig. S2. GIRK1/2 currents in oocytes. Holding potential was -80 mV, low-K^+ and high-K^+ solutions contained 2 and 24 mM K^+, respectively (K^+ was replaced for Na^+). Net GIRK currents were determined by subtracting the current remaining after the addition of 5 mM $BaCl_2$. (**A**) I_{basal} and I_{evoked} in an oocyte expressing m2R, GIRK1 and GIRK2. Calculation of R_a was done in every cell from its own I_{basal} and I_{evoked}. (**B**) $I_{\beta\gamma}$ in an oocyte expressing m2R, GIRK1, GIRK2 and Gβγ. Note that adding ACh did not evoke a significant additional GIRK current, suggesting full activation by Gβγ. $R_{\beta\gamma}$ was calculated in each cell by dividing its own $I_{\beta\gamma}$ by the average $I_{\beta\gamma}$ from the control group of the same experiment in which no Gβγ was coexpressed. **(C)** Expression of m2R in a wide range of doses does not affect I_{basal}. 5-8 oocytes have been tested in each group. There were no significant differences between treatments as tested by one-way ANOVA.

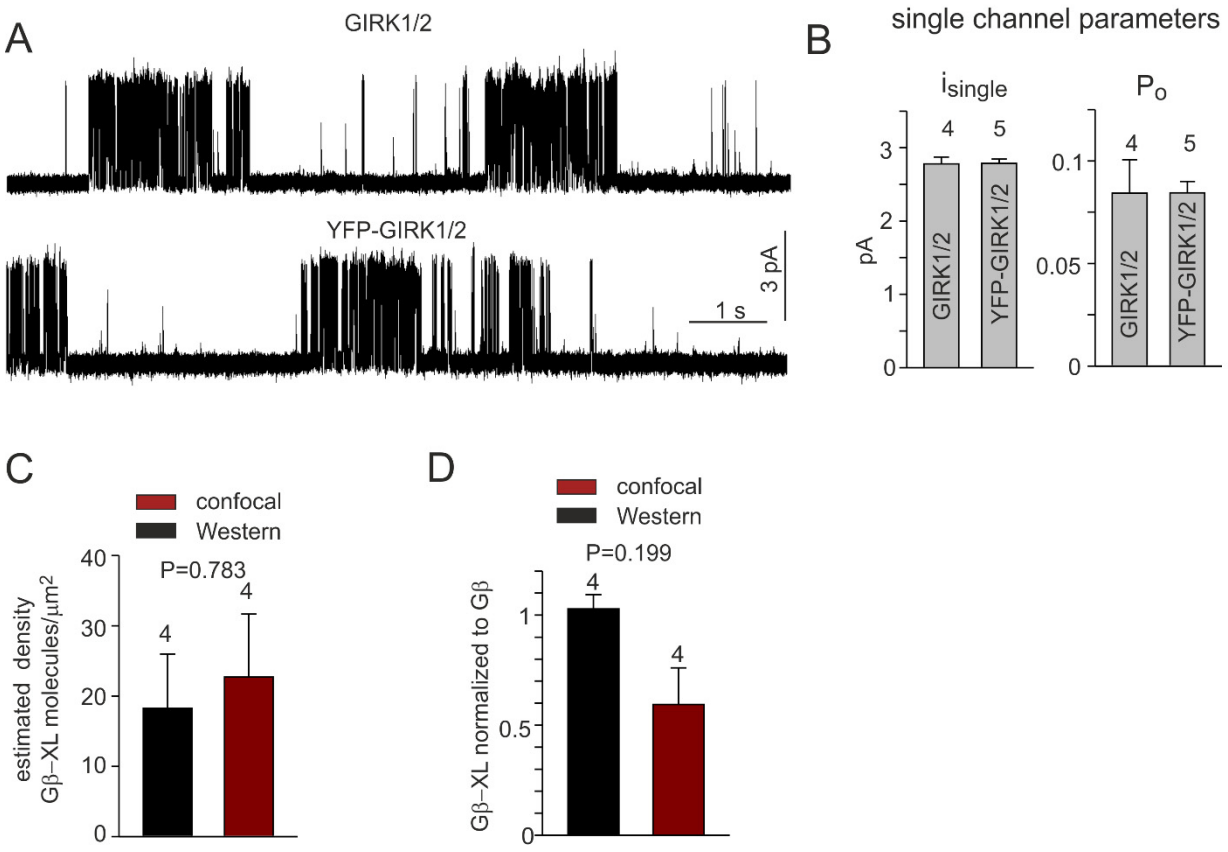

Fig. S3. Characterization of YFP-labeled GIRK1 and Gβ. (A, B) Single channel parameters of GIRK1/2 and YFP-GIRK1/2 channels are very similar. **(A)** Cell-attached records of channel activity expressing the channel and Gβγ (5 ng RNA). **(B)** Comparison of average i_{single} and P_o. Data are from oocytes of the same batch, recorded during a two-day experiment. **(C, D)** The anti-Gβ antibody similarly recognizes YFP-labeled bovine and *Xenopus* Gβ subunits in Western blots of manually pealed plasma membranes. Data are from 4 separate experiments. For Western blots, 15 to 20 plasma membranes were pooled. For confocal imaging, groups of 3-16 oocytes were examined, and the average fluorescence level was compared with that of YFP-GIRK1/2 (therefore the statistical significance was calculated using paired t-test). The density of the latter was calculated from the measurement of currents as explained in the text. In each experiment, both confocal imaging, current measurement and Western blots of manually peeled membranes were done in oocytes of the same donor. There was a good agreement for surface density estimates of YFP-Gβ-XL from confocal "molecular ruler" measurements and from quantitative Western blots, either in absolute terms as molecules/μm^2 (**C**) or in relative terms, normalized to estimates of YFP-Gβ in each experiment (**D**). YFP fluorescence can be safely assumed to be independent of the species of fused Gβ (mammalian or *Xenopus*). Therefore, similar estimates of surface density observed from confocal imaging and Western blots suggest that the Gβ antibody used here recognizes the oocyte's endogenous Gβ in Western blots similarly to the coexpressed mammalian (bovine) $G\beta_1$.

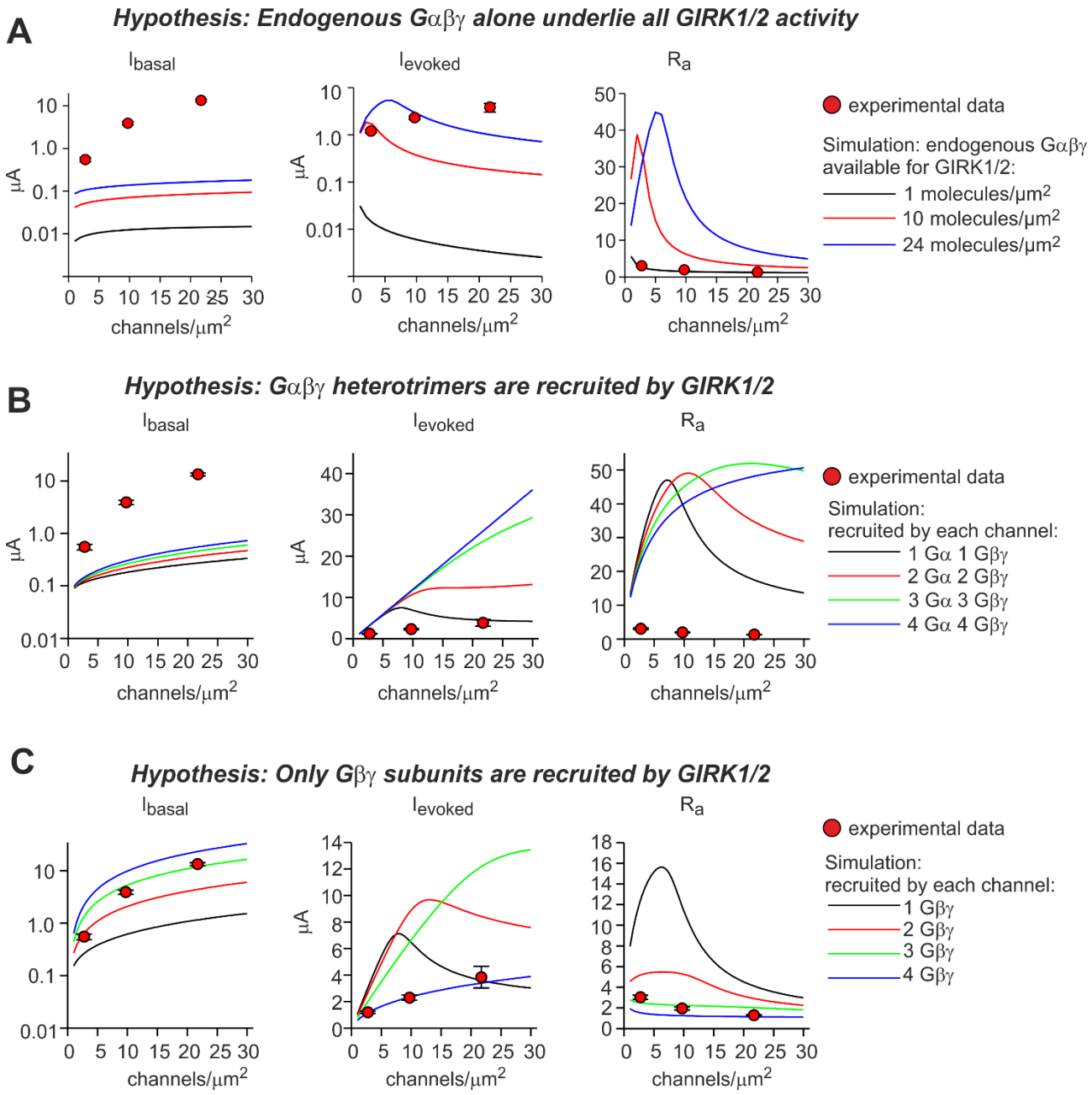

Fig. S4. Simulation of density-dependent changes in whole-cell GIRK1/2 activity. Experimental data (from Table 1) are shown as red circles (mean ± SEM). The simulations of currents and Ra were done using the graded contribution model. **(A)** Testing the hypothesis that the endogenous Gαβγ heterotrimers are the only source of Gβγ for GIRK activation; I_{basal} is due to spontaneous dissociation of Gαβγ into $G\alpha^{GDP}$ and Gβγ (see Fig. 2A). Simulations were performed assuming that only part (1 or 10 molecules/μm^2, black and red curves) or all (24 molecules/μm^2, blue curves) endogenous G proteins can donate Gβγ to activate GIRK1/2. Note that no satisfactory description of data can be obtained under any of these conditions. The simulated I_{basal} is too low; for high channel densities, also the full I_{evoked} could not be obtained even assuming that all endogenous Gαβγ (i.e. all 24 molecules/μm^2) could release Gβγ and activate GIRK. **(B)** Testing the hypothesis that the expressed GIRK1/2 recruits additional endogenous G protein subunits to the PM, e.g.

from other cellular compartments. Simulations were done assuming that each GIRK1/2 channel recruits from 1 to 4 $G_{i/o}$ heterotrimers. The recruited Gα and Gβγ were added to the pre-existing endogenous plasma membrane-attached Gαβγ before Gβγ expression. **(C)** Testing the hypothesis that the expressed GIRK1/2 recruits additional endogenous Gβγ, but not Gα, to the PM; the rest was done as in B. Calculations in (B) and (C) assumed 24 molecules/μm^2 of endogenous $G_{i/o}$ available for GIRK. Similar results were obtained assuming 10 molecules/μm^2 (data not shown). Simulations as in A-C were also done with the concerted model, yielding similar results (data not shown).

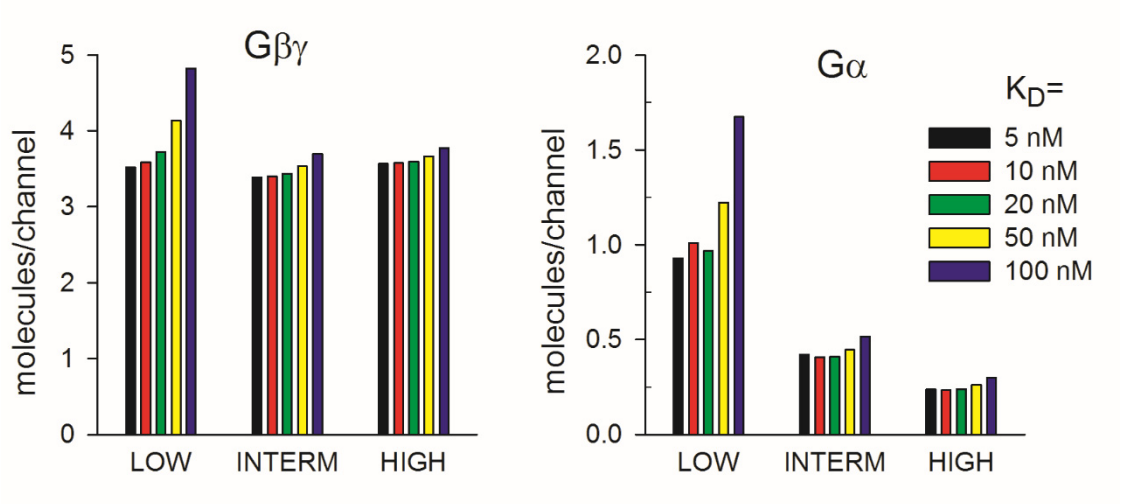

Fig. S5. The concerted activation model supports the unequal stoichiometry estimates of Gβγ and Gα available for GIRK1/2. The plots present the calculated amounts of Gβγ and Gα available for GIRK1/2 using the concerted model for a range of K_D for the GIRK-Gβγ interaction (5-100 nM), for the three channel density groups of Table 1.

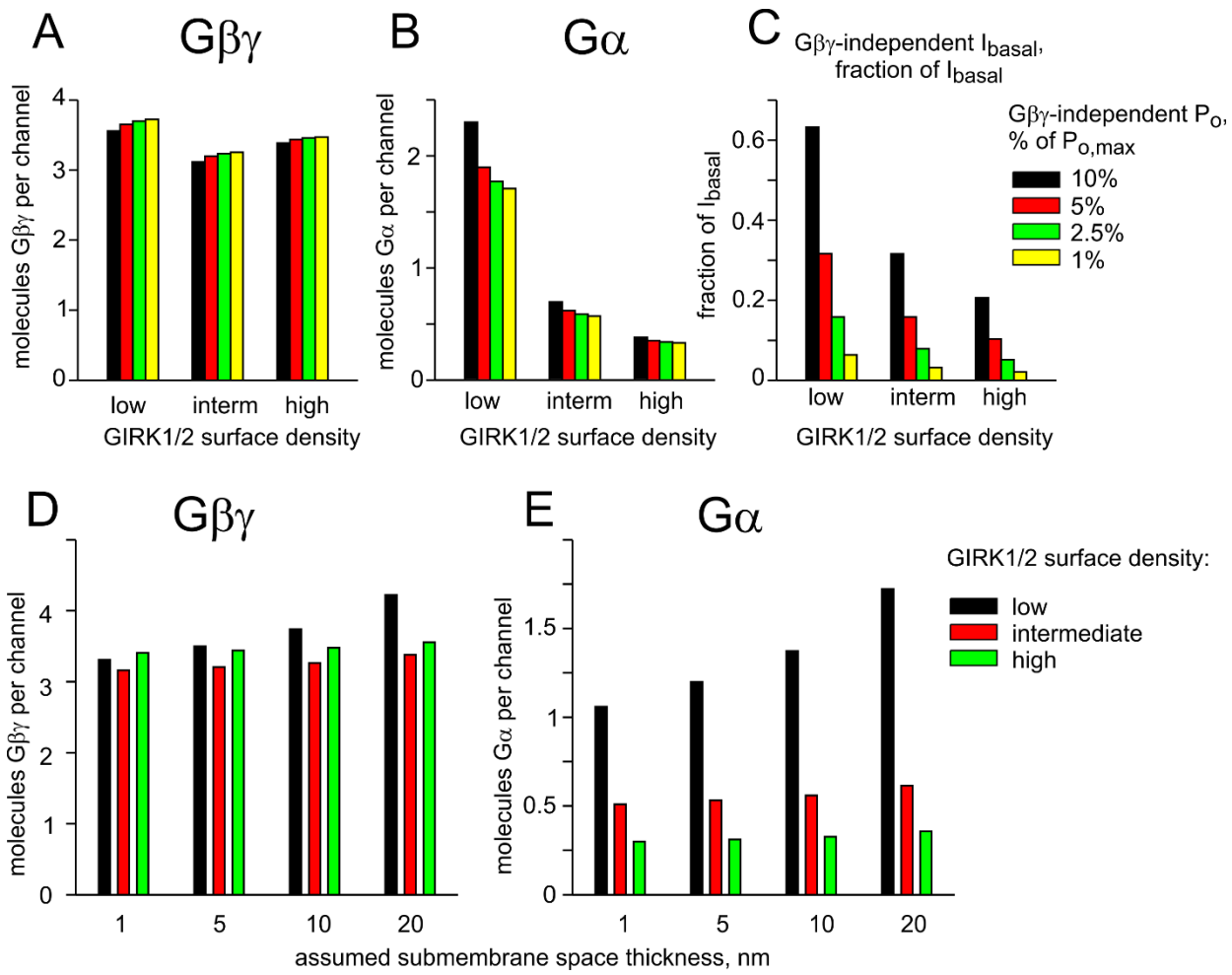

Fig. S6. The presence of Gβγ-independent intrinsic activity and the dimensions of submembrane reaction space do not significantly alter the estimates of GIRK1/2-available G proteins subunits. Calculations were done assuming K_D=50 nM for the GIRK-Gβγ interaction. **(A-C),** the impact of Gβγ-independent basal activity. Calculation were done for Gβγ-independent intrinsic activity of a single channel ranging from 1% to 10% of $P_{o,max}$. Available Gβγ (**A**), Gα (**B**) and the Gβγ-independent fraction of I_{basal} (**C**) were calculated for the three channel density groups of Table 1. **(D, E)** Varying the submembrane space thickness in a wide range, 1-20 nm, does not significantly change the estimates of functional stoichiometry of GIRK1/2-Gβγ-Gα.

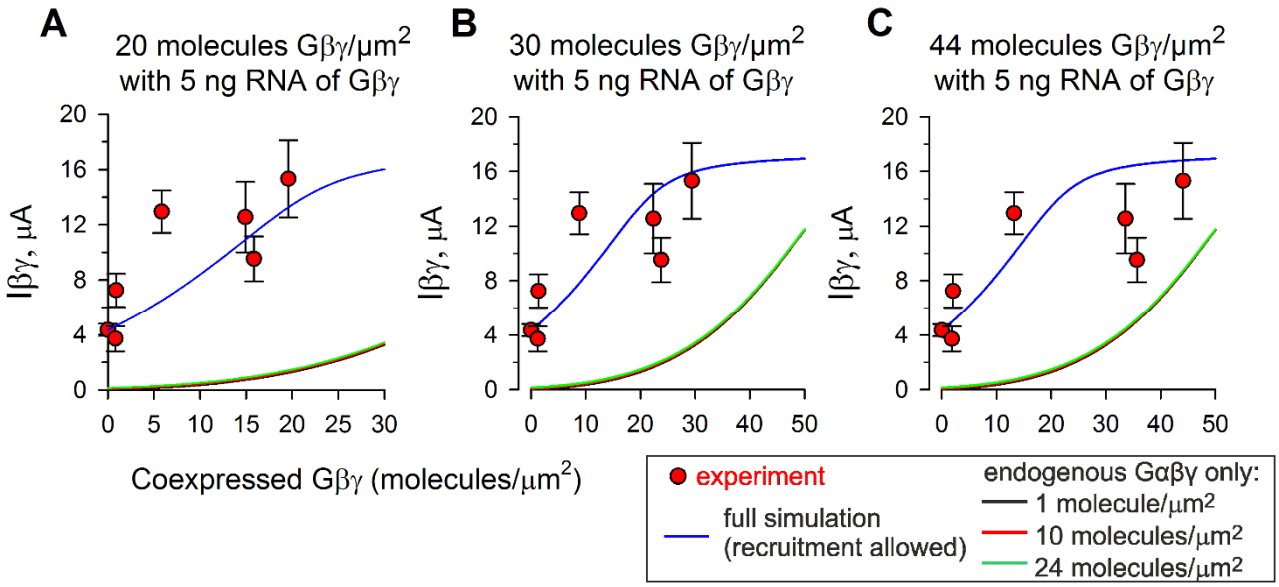

Fig. S7. Simulations of the Gβγ dose-response experiment for a range of assumed Gβγ densities. Because in the experiment of Fig. 7 the actual density of Gβγ in the PM has not been directly measured, the calculations of Fig. 7C assumed that it was equal to the average density of 30 Gβγ molecules/μm^2 (with 5 ng RNA), as measured in other 4 experiments done during the same time period. Here, we run simulations as in Fig. 7C for 20 or 44 molecules Gβγ/μm^2 (**A, C**) and compare the result with that of Fig. 7C (shown here again in **B** for a direct comparison). The color codes are as in Fig. 7: the blue line presents the simulation using graded contribution model and amounts of Gα and Gβγ (without coexpressed Gβγ) calculated as explained in Fig. 7 legend, and red, black and green lines show simulation with endogenous G proteins only and no Gβγ recruitment allowed.

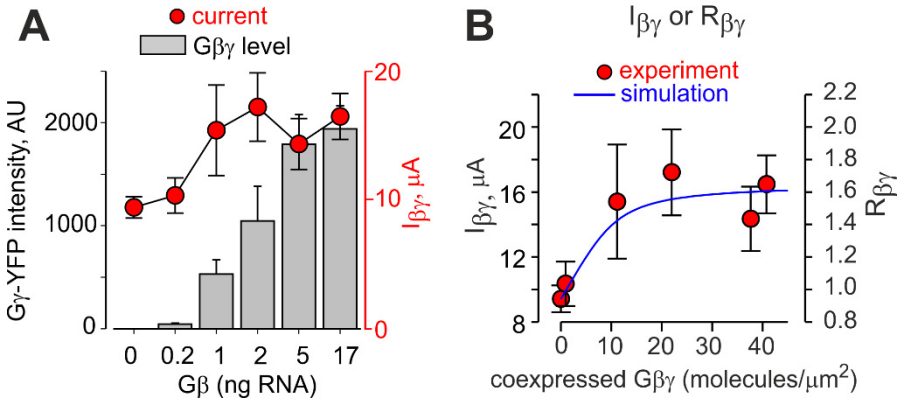

Fig. S8. Another experiment on dose-dependent activation of GIRK1/2 by coexpressed Gβγ. The presentation in similar to that of Fig. 7. Gβ was coexpressed with Gγ-YFP in incremental doses, and with a constant amount (1 ng RNA) of wt GIRK1/2. RNA of Gγ-YFP was always half of that of Gβ RNA, by weight. **(A)** Gβγ-YFP fluorescence levels (grey bars, left Y-axis) and GIRK currents (red circles, right Y-axis) are shown on the same plot. GIRK1/2 density, calculated from $I_{\beta\gamma}$ of the 17 ng Gβγ-YFP group, was 13 molecules/μm^2. In addition, we injected YFP-GIRK1/GIRK2 (5 ng GIRK1-YFP) and measured I_{basal} which was 8.4± 1.1 μA (n=11), comparable to I_{basal} of unlabeled GIRK1/2 (9.4±0.8 μA). Thus, we assumed the same density of ~13 channels/μm^2 for labeled and unlabeled channels. Since the YFP-GIRK1/2 gave a fluorescent signal of 1237 ±221 AU (n=7), this signal was assumed to correspond to 26 YFP molecules/μm^2. This number was used as the basis of calculations of Gβγ-YFP density for plots shown in B. **(B)** Comparison of measured $I_{\beta\gamma}$ or $R_{\beta\gamma}$ (red circles) and simulated currents or $R_{\beta\gamma}$ (blue curves). The left and right Y-axes are related to $I_{\beta\gamma}$ and $R_{\beta\gamma}$, respectively. Available Gα and Gβγ (before Gβγ coexpression) were estimated from I_{total} and I_{basal}, giving 3.82 and 0.42 molecules/μm^2 of Gβγ and Gα, respectively.

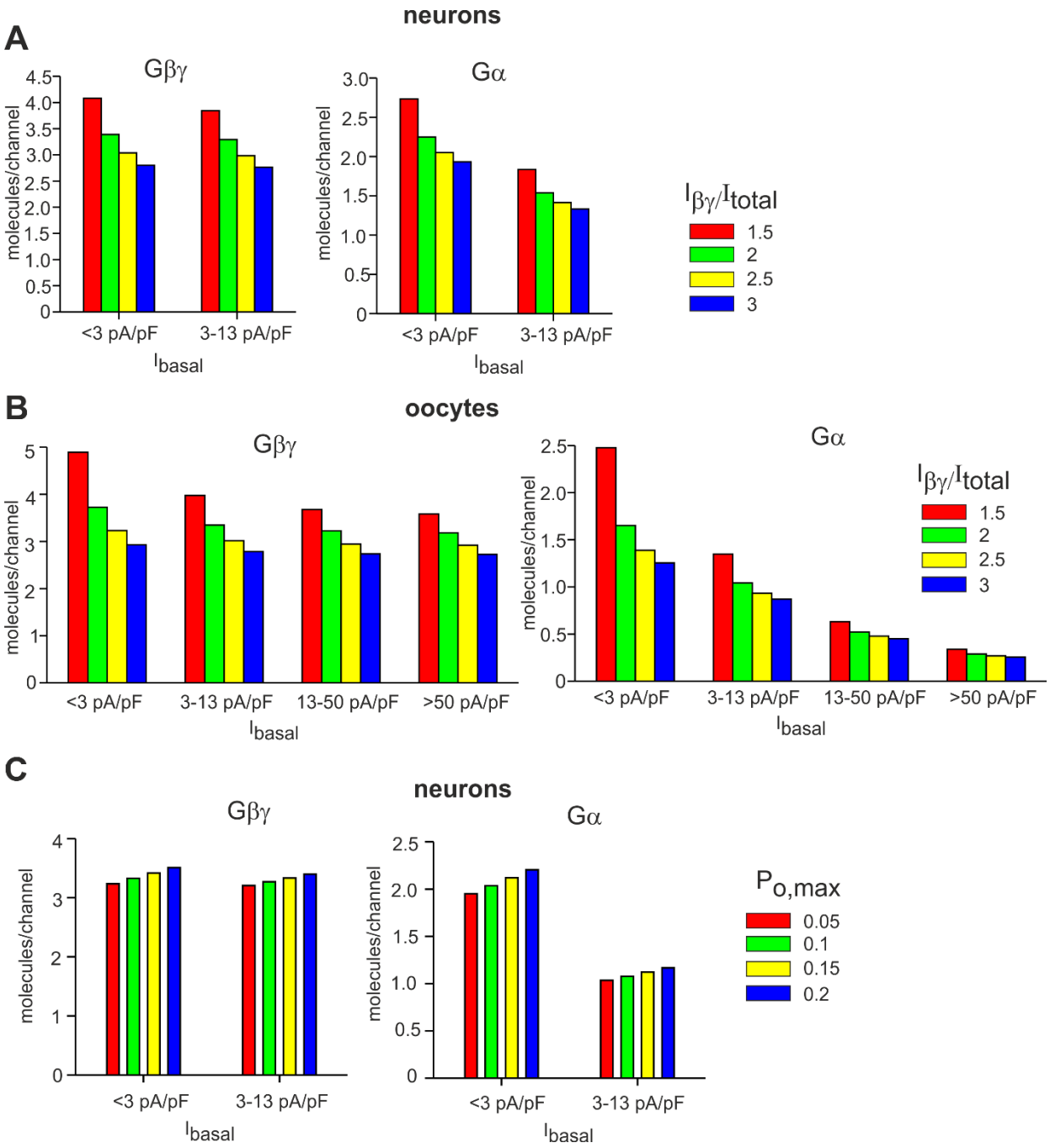

Fig. S9. Estimated stoichiometries of Gα and Gβγ available for GIRK in neurons and oocytes in a range of $I_{\beta\gamma}/I_{total}$ ratios and $P_{o,max}$. Whereas for the oocytes the actual $I_{\beta\gamma}/I_{total}$ ratio and $P_{o,max}$ are known, in neurons these parameters are not known. Both parameters affect the calculated channel density and could affect the estimates of stoichiometry. The calculations shown in this Figure demonstrate the same general trend in stoichiometries of GIRK1/2, Gβγ and Gα as we have found in the previous analysis in the oocytes, in a range of $I_{\beta\gamma}/I_{total}$ ratios (for neurons and oocytes; **A** and **B**) and $P_{o,max}$ (for neurons; **C**). The estimates of Gβγ are around 3-4/channel and relatively independent of I_{basal}, and those of Gα are below 2 and drop sharply with the increase in I_{basal}. Generally, the lowest channel density is most sensitive to perturbations, and, for the lowest simulated $I_{\beta\gamma}/I_{total}$ ratio, calculated Gβγ/channel and Gα/channel exceed our usual estimates.